UNIVERSITY *of* LIMERICK

OLLSCOIL LUIMNIGH

RESONANT OVER-REFLECTION OF WAVES BY JETS

By

Vladimir Nikolaevich Lapin

SUBMITTED IN FULFILLMENT OF THE
REQUIREMENTS FOR THE DEGREE OF
DOCTOR OF PHILOSOPHY
AT
UNIVERSITY OF LIMERICK
LIMERICK, IRELAND
MAY 2011

UNIVERSITY OF LIMERICK
DEPARTMENT OF
MATHEMATICS AND STATISTICS

The undersigned hereby certify that they have read and recommend to the Faculty of Informatics and Electronics for acceptance a thesis entitled "**Resonant over-reflection of waves by jets**" by **Vladimir Nikolaevich Lapin** in fulfillment of the requirements for the degree of **Doctor of Philosophy**.

Dated: May 2011

External Examiner: _____
Prof. Victor I. Shrira

Research Supervisor: _____
Prof. Eugene S. Benilov

Internal Examiner: _____
Dr. William Lee

UNIVERSITY OF LIMERICK

Date: **May 2011**

Author: **Vladimir Nikolaevich Lapin**

Title: **Resonant over-reflection of waves by jets**

Department: **Mathematics and Statistics**

Degree: **Ph.D.** Convocation: **September** Year: **2011**

I hereby declare that this thesis is entirely my own work and that it has not been submitted for any other academic award.

Signature of Author

Table of Contents

Abstract

The present thesis studies the problem of scattering of large-scale waves by surface currents in the ocean. It has been known for more than a century that corresponding linear equations governing propagation of small amplitude waves across the shear flow contain *critical layer* singularities (Rayleigh [74]). And more than 40 years ago it was established that propagating waves can effectively interact with the mean flow at such points. As the result, the waves can be partly absorbed (Booker & Bretherton [8]) or *over-reflected* (*i.e.* amplified) (Jones [40]). A special case of this phenomenon, when amplification is infinitely strong, is traditionally referred to as *resonant over-reflection*. Physically the latter corresponds to spontaneous emission of waves by the current. Resonant over-reflection was poorly studied in the past with only a few cases reported in the literature. The aim of this study is to fill this gap and clarify the nature of the phenomenon.

We examine scattering of inertia-gravity gravity waves by zonal currents within the reduced gravity rotating shallow water model and Rossby-wave scattering by "two-jet" currents on the quasi-geostrophic β-plane. In both cases reflection and transmission coefficients were calculated numerically for the case when mean flow velocity profiles are approximated by Bickley jets.

Resonant over-reflection was found to occur within these two models. We proposed a plausible physical interpretation of the phenomenon as a "resonance" of a wave trapped between two containing potential barriers. It is further demonstrated that, generally, resonantly over-reflected waves are always marginal to radiating instabilities, and hence, indicate when unstable shear flows can generate temporally growing propagating waves that carry energy into the far field. The importance of the obtained results is connected to investigation of sources and distribution of waves in the ocean and atmosphere.

Acknowledgements

My Ph.D. studies took place in the Department of Mathematics and Statistics in the University of Limerick, Ireland. The work of the present thesis has been carried out as a part of the three-year project "Stability of vortices in fluids" headed by my supervisor Prof. Eugene S. Benilov to whom I am extremely thankful for his relentless support, scientific guidance and warm advice. I have benefitted enormously from our many discussions and his engagement in the work of his students.

During these years, from September 2008 to August 2011, within the department I have enjoyed the friendly atmosphere and have daily received help from many people I wish to thank here. I would like to express my appreciation to Prof. Stephen B.G. O'Brien, director of MACSI group, for hosting me. I would like to express my gratitude to Dr. Michael Vynnycky (the expert on the Comsol finite element software) and Dr. Andrei Korobeinikov, whom I often approached with scientific questions. Their advice and stimulating discussions were greatly rewarding.

Also, I would like to thank all the members of MACSI who welcomed me as a part of the group and helped with my research-related and general-life queries and problems. A special thanks goes to the fellow PhD students Vladimir Zubkov, Roman Sedakov and Ana-Maria Magdalina; and to my office mates Niall Ryan and Joseph Lynch and many-many others who have given me invaluable scientific and moral support throughout the project. Finally, I would like to thank my close friends and family for their caring, warm encouragement and support.

I would like to thank the referees of this thesis Prof. Victor Shrira and Dr. William Lee for their useful comments during the review stage, which greatly improved the manuscript.

I gratefully acknowledge the financial support of the Science Foundation Ireland delivered through RFP Grant 08/RFP/MTH1476 and MACSI (Mathematical Applications Consortium for Science and Industry).

List of Symbols

$\vec{r}$	Radius Vector	33
t	Time	33
r, θ, φ	Spherical coordinates	33
x, y, z	Cartesian coordinates	35
$\vec{v} = (u, v, w)$	Velocity and its components	33

ρ	Fluid density	7
g	Acceleration due to gravity	7
$\vec{\Omega}, \Omega$	Angular velocity and speed of the Earth's rotation	8
p	Pressure	33

L, D	Horizontal and vertical scales of motion	4
U, W	Horizontal and vertical scales of velocity	4
ϱ_0	Characteristic value of the density	7
g_r	Reduced gravity	7
N	Buoyancy frequency	8
r_0	Radius of the earth	9
θ_0	Central latitude	9
f, f_0	Coriolis parameter and its value at the central latitude	8
β	Northward gradient of the Coriolis parameter	9
$\delta = \frac{D}{L}$	Ratio of vertical to horizontal scales	11
$\Delta = \frac{L}{r_0}$	Ratio of horizontal scale to the Earth's radius	11
$Ro = \frac{U}{fL}$	Rossby number	11
$Fr = \frac{U}{\sqrt{g_r D}}$	Froude number	13
$Bu = \frac{\sqrt{g_r D}}{fL}$	Burger number	13
$R_d = \frac{\sqrt{gD}}{f}$	Rossby deformation radius	13

List of Acronyms

GFD geophysical fluid dynamics 2

PDE partial differential equation 2

IGW internal gravity wave 5

QG quasi-geostrophic 10

RGRSW reduced gravity rotating shallow water 10

RSW rotating shallow water 14

OR over-reflection 18

ROR resonant over-reflection (or hyper-reflection) 20

PV potential vorticity 58

Chapter 1

Introduction

An ocean traveler has even more vividly the impression that the ocean is made of waves than that it is made of water.

The Nature of the Physical World, Cambridge (1929)
Arthur S. Eddington, English astronomer and physicist

Atmospheric winds and ocean currents directly impact many human activities as they shape the environment we exist in. For instance, winds move air and drag clouds along. And obviously, understanding these motions is the essential to be able to forecast weather and climate which makes up the general motivation for this study. In addition, accurate information on atmospheric and ocean circulation is necessary for safe and cost effective aviation, shipping and fishing services.

More indirectly, but no less importantly, ocean currents influence atmospheric processes and Earth's environmental system in general. The main mechanism is redistribution of heat contained within the vast amounts of moving water. For instance, the presence of the Gulf Stream makes British Isles, Central Europe and Scandinavia much warmer and humid place than it would be otherwise. If it ever stopped flowing, Ireland, known as the Emerald Isle, would have weather conditions similar to these in Iceland and Canada.

The goal of this work is to make a contribution to the over century-long mathematical studies of the extremely complex ocean-atmosphere system. The problem at hand addresses some aspects of wave-mean flow interaction with application to eastward (westward)-flowing ocean surface currents, such as, for example, the eastward Gulf Stream extension, Kuroshio extension and Antarctic Circumpolar Current. New general analytical findings as well as numerical results for specific problems were obtained.

Heavy geophysical specificity of the problem obliges the author to present a brief review of the subject before giving an outline of the considered problem, major results and thesis structure. This includes discussion of such objects as currents, winds, waves and mechanisms of their interaction. We also describe some classical geophysical models which we used in our study. The reader already familiar with the abbreviation *GFD* and fundamentals of the science can skip the next section (§1.1) with no damage to reading experience.

1.1 Background of the study

The atmosphere and ocean has so many common features that it is reasonable to study them together. Mathematically both can be perceived as a thin layer of stratified fluid on a rotating sphere. Hence, many models of geophysical fluid dynamics (GFD) can be applied to study motions in both the ocean and atmosphere. And even though the problems considered here are formulated in oceanological context the results can be directly extended to the case of atmosphere.

Generally speaking, GFD is the science of all types of fluid motion naturally occurring on the planet on all space and time scales. However, it is most useful to studies of *large-scale* phenomena in the ocean and atmosphere, such as the circulating currents or cyclonic/anticyclonic vortices. And exactly in these cases the similarities in the ocean and atmosphere dynamics are the most striking.

The focus of GFD is to examine the general physical mechanisms behind the observed motions rather than to model in details each specific phenomena. Hence, to avoid complications various approximate models that retain only essential parameters in the governing partial differential equations (PDEs) are derived and employed. If needed these models can be adjusted to include additional parameters (*e.g.* moist convection) to meet the requirements of weather and climate forecasting, weather hazards prediction and oceanographic services.

Some basic ocean-atmospheric observed phenomena, cornerstone premises and classical models of GFD which provide necessary physical background for this work will be discussed in this chapter.

1.1.1 Surface ocean currents and atmospheric winds

Surface currents in the open ocean, far from the influence of land, constitute one of the central objects of this study. Here their origin is explained; and also, major surface currents found on the Earth and their typical characteristics are described.

Ocean currents are primarily driven by two mechanisms: ground level winds and density gradients. The latter give rise to deep slow currents which we do not consider here. Prevailing winds, on the other hand, constitute the fundamental forcing for the faster surface ocean currents. This fact accounts for the observed similarity of the maps of winds in the lower atmosphere and surface ocean currents at a global scale.

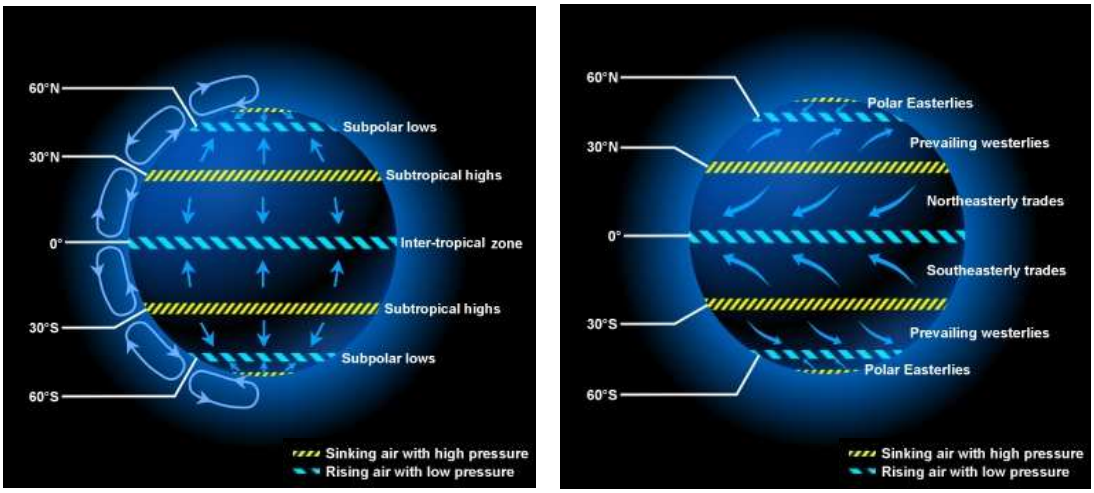

(a) Without the Earth's rotation.

(b) With the Coriolis effect due to the Earth's rotation.

Figure 1.1: Convective loops and prevailing winds in the lower atmosphere. Source [91].

The winds are formed and shaped by two primary forces: solar radiation and the Earth's rotation. Uneven heating of the Earth's surface results in atmospheric convection which is the root cause of all winds on the planet. Observations show that three circulation cells exist between the equator and each pole (Fig. 1.1a).

The Coriolis effect tilts winds from their intended South-North direction: any horizontal flow gets deflected to the right in the northern hemisphere and to the left in the southern hemisphere. Combining the convective motion with the Coriolis effect we discover the trade winds at tropical latitudes, and westerlies at mid latitudes which agree with observations (Fig. 1.1b). These winds entrain via friction ocean water and drive surface currents in the ocean.

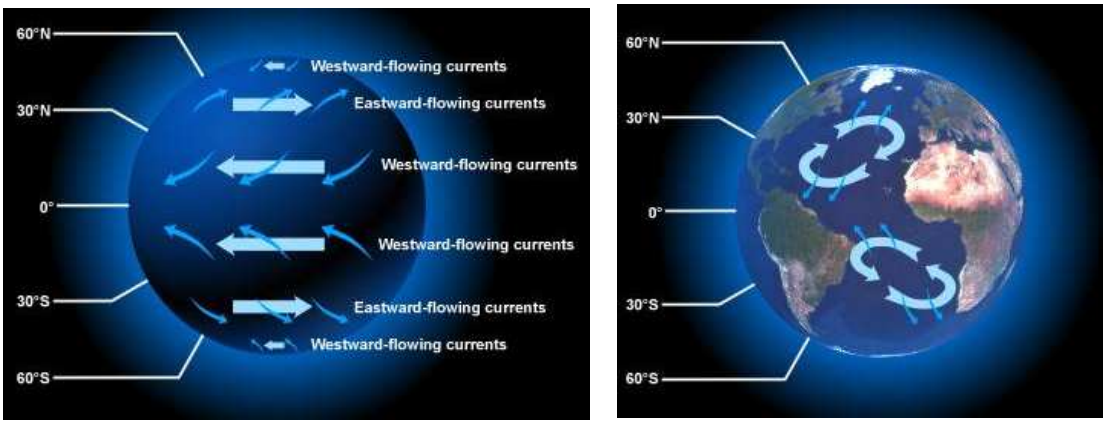

Figure 1.2: Idealized surface currents and real subtropical gyres. Source [91].

In their turn surface currents are again deflected due to the Coriolis effect. Hence, we develop westward-flowing equatorial currents and eastward-flowing currents at mid latitudes. On the real-life Earth these currents run into continents and are forced to close the loop, forming so-called *gyres* (Fig. 1.2). Each gyre comprises of approximately two *zonal* currents: a westward-flowing equatorial and an eastward-flowing current in mid-latitudes; and two *meridional* coastal currents: one poleward-flowing at the western boundary and one at the eastern boundary, flowing towards the equator. Note that throughout this work the case of zonal surface currents will be considered even though the surface gyres can be assumed to flow zonally *(i.e.* from west to east or vice versa) only on a part of their path.

Although the winds strongly affect the surface layer, their influence usually does not extend deeply. Typically, speed of a surface current decays with depth so that motion below 1000 m is negligible. The fastest currents, such as the Gulf Stream and Kuroshio Current, have maximum speeds up to 2.5 $^{\mathrm{m}}/_{\mathrm{s}}$ and their width is of order 100 km.

Major surface ocean currents are shown on Fig. 1.3. The degree of their intensity and importance is illustrated by the fact that the Gulf Stream and the Antarctic circumpolar current carry about 5000 times more water than the Mississippi River. Some typical parameter values are presented in Tab. 1.1. The provided information is presented in numerous journal papers (for references see [98], [99]) and is based on velocity and hydrographic observations, drifting buoy and satellite altimeter data and numerical simulations.

These observations suggest the following typical scales for wind-driven currents: the

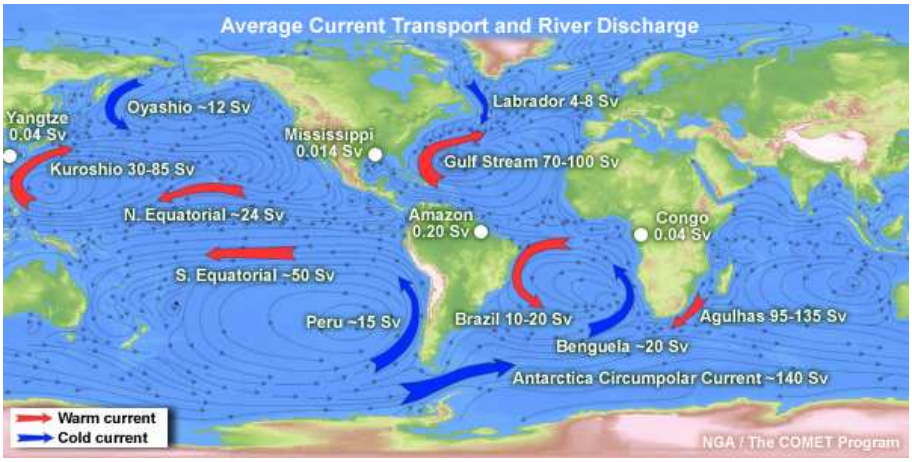

Figure 1.3: Major ocean currents and their volume transport (in sverdrups, where $1\,\mathrm{Sv} = 10^6\,\mathrm{m^3/s}$). Source [91].

Table 1.1: Seasonally averaged characteristics of major ocean surface currents. Source [98], [99] (scientific websites devoted to ocean currents).

Parameter	Gulf Stream	Kuroshio Current	Antarctic CP Current
L: Width	150 km	100 km	up to 2000 km
D: Depth	800 m	500 m	2000-4000 m
U: Max Speed	2 m/s	1.5 m/s	0.5 m/s
M: Magnitude	30-150 Sv	20-80 Sv	$\sim$ 130 Sv

vertical length scale $D \sim 500\,\mathrm{m}$, velocity $U \sim 1\,\mathrm{m/s}$ and horizontal scale $L \sim 50\,\mathrm{km}$ (half-width of the jet) if we wish to model fast currents such as the Gulf Stream or Kuroshio; or $D \sim 2000\,\mathrm{m}$, $U \sim 0.2\,\mathrm{m/s}$ and $L \sim 1000\,\mathrm{km}$ for the Antarctic Circumpolar Current.

1.1.2 Waves in the ocean and atmosphere

Many types of waves exist in the ocean and atmosphere as various restoring forces of different nature are present in the system. It can be the surface tension, buoyancy or something more exotic, like variation of the local components of the Earth's rotation with latitude. Hence, characteristics of the resulting waves (wavelengths and frequencies) are also very different. A good review on waves in the ocean, mechanisms of their generation and dissipation is provided in the book by LeBlond and Mysak [50]. In this thesis only so-called *internal gravity waves (IGWs)* and *Rossby waves* are considered, for which a brief overview is provided.

Stratification & internal gravity waves

Uneven heating of the Earth's surface influences the ocean stratification via changes in its temperature and salinity. A schematic of the vertical profiles of temperature, salinity and density is presented on Fig. 1.4. Thin upper layer ($\sim 100\,\mathrm{m}$) of the ocean is well mixed by the surface waves and is nearly uniform in z-direction. Below this mixed layer lie the so-called main *thermo-*, *halo-* and *pycnoclines* which correspond to the region of rapid decrease of water temperature, salinity and, as the result, sharp increase in density over about $1000\,\mathrm{m}$. These profiles undergo considerable seasonal changes but are qualitatively similar and the resulting stratification is usually gravitationally stable (heavier fluid underlies lighter). One important consequence of the stable stratification is that vertical motions are constrained and horizontal motions are favoured.

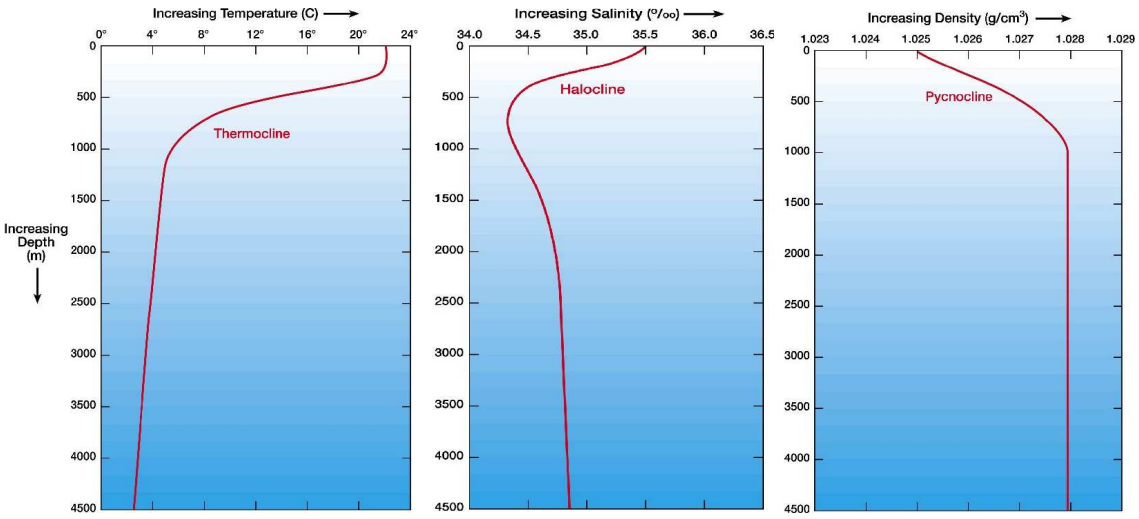

Figure 1.4: Typical ocean stratification: temperature, salinity and density profiles. Source [93].

Stable stratification supports internal gravity wave (IGW). If a fluid element is displaced into a region with different density, gravity tries to restore the equilibrium resulting in oscillations which constitute IGWs. They are similar to usual surface waves which all of us daily observe on the free water surfaces. However, IGWs propagate within the fluid, rather than on the air-water interface.

Wave clouds are often created in the atmosphere by ubiquitous IGWs (Fig. 1.5a). As such disturbance propagates, the air rises up and cools at the crests of waves. If the layer is humid enough the vapour condenses. And when air falls down to the wave trough, the clouds evaporate. Resulting patterns can be observed with the naked eye in virtually any

point on the globe.

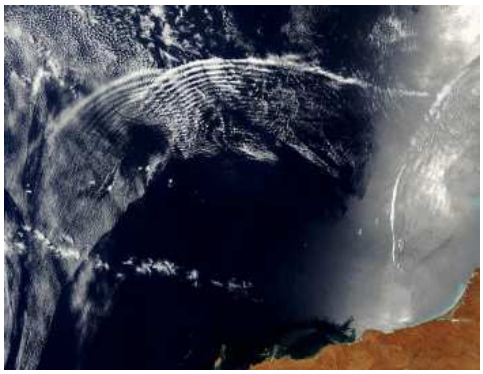

(a) In the atmosphere (visualised by the clouds). Source [94].

(b) In the ocean (visible due to reflection of sunlight). Source [95].

Figure 1.5: Satelite images of IGWs.

Clearly, IGWs in the ocean depths cannot be observed directly. However, when propagating they induce motion on the free ocean surface as the water above flows down the crests and sinks into the troughs. This process creates regions of calm water directly above the wave crests and rough water above the troughs. On the satellite image (Fig. 1.5b) the latter appear as, respectively, brighter and darker stripes.

Note that these waves have much lower frequencies but larger wavelengths and amplitudes than their surface counterparts because the corresponding restoring force (buoyancy) is weaker. Typical registered wavelengths of IGWs are ~ 0.1-$5\,\mathrm{km}$; phase speeds are $\sim 1\,\mathrm{m/s}$. Their amplitudes can be as large as $100\,\mathrm{m}$ in the deep ocean layers (LeBlond and Mysak [50]).

Accelerations due to buoyancy in stratified fluid can be estimated with help of so-called *reduced gravity*

$$g_r = g\frac{\Delta\rho}{\varrho_0}, \tag{1.1}$$

where ϱ_0 is a characteristic value of the density ρ and $\Delta\rho$ is its variation over the vertical scale D; g is the acceleration due to gravity. For the simplest case of two homogeneous layers separated by a sharp interface (1.1) becomes

$$g_r = g\frac{\rho_1 - \rho_2}{\rho_1}, \tag{1.2}$$

where ρ_1 and ρ_2 are densities below and above the interface ($\rho_1 > \rho_2$). Then the characteristic frequency of the IGWs is given with

$$N_0 = \sqrt{\frac{g_r}{D}}. \tag{1.3}$$

In a continuously stratified fluid no clear interface between stratum exists and IGWs can propagate vertically as well as horizontally. Formula (1.3) can be extended for this case as

$$N = \sqrt{-\frac{g}{\rho}\frac{d\rho}{dz}}, \tag{1.4}$$

where by convention z points upwards ($-\frac{d\rho}{dz} > 0$). Note that Eq. (1.4) is the definition of the *Brunt–Väisälä frequency* N (or *buoyancy frequency*) which is a *local* characteristic of stratification. One can show (see [34]) that it gives the upper boundary for the range of frequencies of the internal gravity waves in absence of rotation.

Typically, variations in density of ocean water in the main pycnocline are of order 0.1% over 100 m (see Fig. 1.4). Consequently, we obtain the following characteristic values

$$g_r \sim 0.01\,\mathrm{m/s^2}, \qquad N \sim 0.01\,\mathrm{1/s}. \tag{1.5}$$

The corresponding period of oscillations is about 10 min which, hence, gives the lower bound for IGWs periods.

Slow IGWs (with low frequencies $\sim 10^{-4}\,\mathrm{1/s}$ and large wavelengths $\sim 10\,\mathrm{km}$) are significantly modified by the Coriolis effect. These waves are traditionally referred to as *inertia-gravity waves* (same abbreviation IGWs will be used) or *Poincaré waves* (see Gill [27]). They will be a subject of more detailed discussion in Chapter 4.

β-effect & Rossby waves

Another important type of waves we will touch upon in this work is Rossby waves. The emergence of these peculiar planetary-scale waves is due to variation with latitude θ of the local vertical component Ω_n of the Earth's angular velocity $\vec{\Omega}$. The Coriolis force in the horizontal (which is the restoring force supporting the oscillations) depends on the magnitude of so-called *Coriolis parameter*

$$f = 2\Omega_n = 2\Omega \sin\theta. \tag{1.6}$$

The angular speed of the Earth's rotation $\Omega = \left|\vec{\Omega}\right|$ is about $7.29 \times 10^{-5}\,\mathrm{rad/s}$. Then, for example, within a region around the central latitude $\theta_0 \sim 45^\circ$ (Europe, Northern America) $f \sim 10^{-4}\,1/\mathrm{s}$.

While for some problems variation of the Coriolis parameter can be neglected, for motions on longer length scales L (comparable to the Earth's radius r_0) it is important. This phenomena is referred to as *β-effect* because the linear approximation of (1.6) is traditionally written as

$$f = f_0 + \beta y, \tag{1.7}$$

where

$$f_0 = 2\Omega \sin\theta_0, \qquad \beta = \left(\frac{1}{r_0}\frac{\mathrm{d}f}{\mathrm{d}\theta}\right)_{\theta=\theta_0} = \frac{2\Omega}{r_0}\cos\theta_0, \qquad y = (\theta - \theta_0)\, r_0. \tag{1.8}$$

Typical values of the constant β (also known as the *Rossby parameter*) are $\sim 10^{-11}\,1/\mathrm{m\,s}$ in mid-latitudes. The extreme smallness of this parameter results in Rossby waves having wavelengths $\gtrsim 500\,\mathrm{km}$ (even larger for the atmosphere) and periods $\sim 200\,\mathrm{d}$ (corresponding frequencies $\ll \Omega$) (see Gill [27]). Another important characteristic is that they always travel from East to West.

Rossby waves can be easily observed in the atmosphere as large-scale meanders of the otherwise zonal jet streams (Fig. 1.6a). When the undulation become very pronounced, they detach the masses of cold or warm air that become cyclones and anticyclones. In this way Rossby waves often determine the weather conditions at mid-latitudes.

The situation is different for the case of Rossby waves in the ocean where they exhibit large (up to hundreds meters) displacements of isopycnal surfaces (*i.e.* surfaces separating layers of equal density). These large variations of temperature in the upper ocean on the scale of years and decades are thought to influence climatic variations on Earth.

However, the amplitudes of induced oscillations in the surface height are very small ($\lesssim 10\,\mathrm{cm}$) (Fig. 1.6b). Moreover, the horizontal length scales are huge and propagation speeds are slow ($\lesssim 10\,\mathrm{cm/s}$ or, equivalently, $\lesssim 20\,\mathrm{km/d}$). All this makes oceanic Rossby waves extremely difficult to observe with direct contact measurements (see the review [42] of the evidence collected during 1970 through 1987).

Very little relyable data was available untill the recent emergence of satellite altimetry (Chelton and Schlax [15]). For example, TOPEX/Poseidon satellites launched as a joint mission between NASA and CNES were capable of measuring the height of the sea surface to a precision of few centimeters (a malfunction ended normal satellite operations

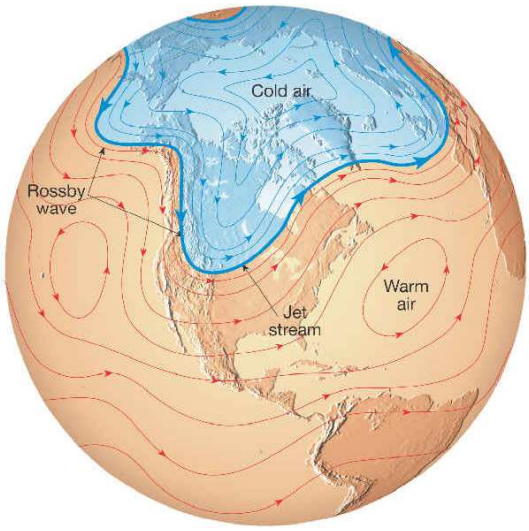

(a) In the atmosphere. Source [97].

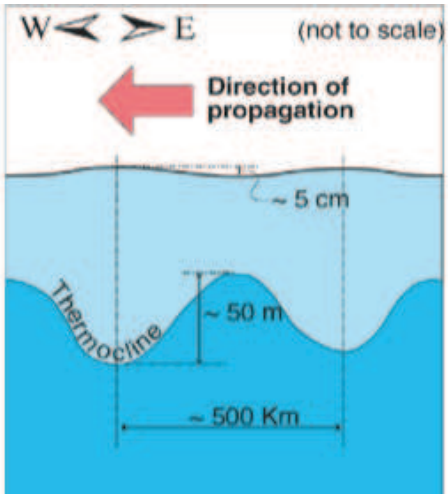

(b) In the ocean. Source [96].

Figure 1.6: A schematic of Rossby waves

in January 2006). The planetary-scale oscillations are revealed when Sea Surface Height Anomalies (the height as seen by the spacecraft minus the long-term average and tides) are plotted for one zonal section as a function of longitude and time (Fig. 1.7).

1.1.3 Theoretical framework

In this section, some fundamental non-dimensional parameters that appear in GFD problems are introduced. The smallness of some of them allows the governing equations to be considerably simplified. We discuss in layman terms origination of of such two basic models: reduced gravity rotating shallow water (RGRSW) model on an f-plane and quasi-geostrophic (QG) β-plane model. These models respectively support IGWs and Rossby waves. Essentially, this section is an informal overview of what is done in Chapter 3 rigorously.

Length scales and plane approximation

Ocean motions we are interested in (surface currents, gravity and Rossby waves) have horizontal scales L within the range $10 \sim 1000\,\mathrm{km}$ (so-called *mesoscales*). When compared with the typical vertical scale D and the Earth's radius one notices

$$D \ll L \ll r_0. \tag{1.9}$$

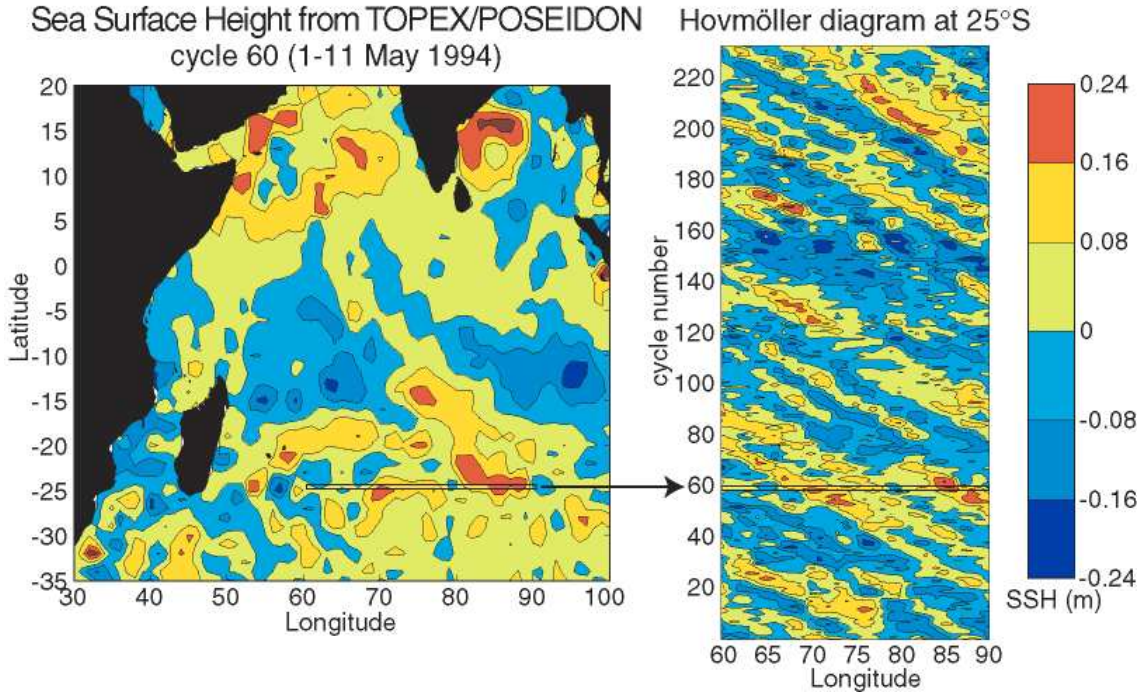

Figure 1.7: Sea Surface Height and Hovmöller diagram. The diagonal (*i.e.* going from bottom right to top left) alignments of crests and troughs correspond to Rossby waves propagating to the west with time. Source [96].

Hence, two small parameters δ and Δ representing the ratios of the length-scales can be introduced

$$\delta = \frac{D}{L} \ll 1, \qquad \Delta = \frac{L}{r_0} \ll 1. \tag{1.10}$$

Consequently, the fragment of the ocean under consideration can be described as a *nearly plane* and *shallow* layer of stratified fluid. As the result, sphericity of the domain can be neglected and the vertical momentum equation can be approximated with the hydrostatic equation. Within these approximations, motions are largely horizontal and the corresponding pressure gradients are due to the surface elevation or density gradients.

Rossby number and geostrophy

As stated above, GFD studies "large-scale" phenomena in the ocean and atmosphere. But how can one define what scale is sufficiently large? This term is usually attributed to motions which are significantly influenced by the Earth's rotation.

In a rotating coordinate frame "frozen" into the planet, the fictitious Coriolis force appears. Its importance can be assessed with help of *Rossby number Ro* which compares

the period of rotation of the earth and the time it takes for a fluid element moving with speed U to cover the distance L

$$Ro = \frac{U}{f_0 L}, \tag{1.11}$$

where f_0 is the local value of the Coriolis parameter. By definition, a large-scale motion has the Rossby number $Ro \lesssim 1$.

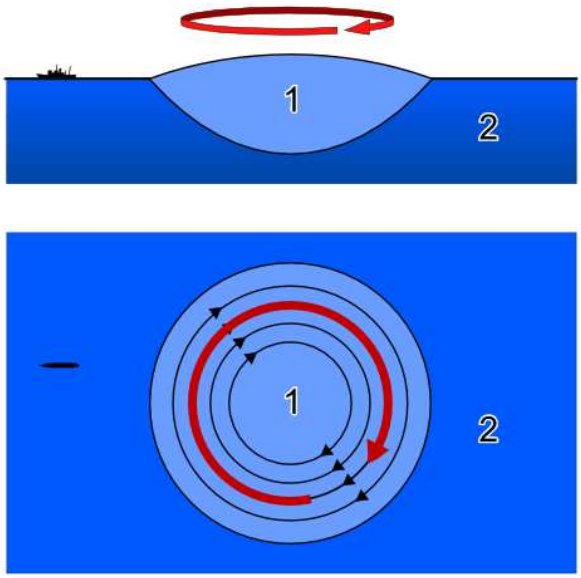

Figure 1.8: A geostrophic current in the ocean in Northern hemisphere. 1. Hot and light water 2. Cold and heavy water. Source [92].

In the horizontal equation of motion the Rossby number estimates the ratio of the inertial $\frac{\mathrm{D}\vec{v}}{\mathrm{D}t}$ and Coriolis forces $2\left[\vec{\Omega}, \vec{v}\right]$ acting on a fluid particle. Hence, when it is small accelerations of fluid particles are negligible (the leading order approximation). The simplified equations represent the equilibrium between the Coriolis force and horizontal pressure gradients. This is the case of so-called *geostrophic balance* and resulting velocity field is *geostrophic*. Note that this approximation is inconsistent in the equatorial regions where horizontal component of the Coriolis force vanishes.

In the ocean the horizontal pressure gradients appear due to swelling of the ocean surface which in its turn is controlled by changes in water density (read temperature and salinity). They drive the water downslope and the resulting motion is being deflected by the Coriolis force. When Coriolis force and pressure gradient balance each other a geostrophic current is formed in which water runs along and not across the lines of constant pressure (Fig. 1.8).

Burger number and Rossby radii

We prepare to investigate a system in which both currents (winds) and waves are present. In classical fluid mechanics it is the *Froude number* defined as the ratio of a characteristic flow velocity to a wave propagation velocity that is typically used to measure the importance of wave effects. When buoyancy (internal gravity) waves are considered the formula becomes as follows:

$$Fr = \frac{U}{\sqrt{g_r D}}. \tag{1.12}$$

Then, the Froude number can alternatively be perceived as a measure of inertia forces when compared to buoyancy forces and, hence, characterize the strength of the density stratification.

However, as mentioned above, the large scales of GFD phenomena motivate researchers to gauge the magnitude of the vertical stratification against the Coriolis effect in the horizontal. Their relative importance is given by the *Burger number*

$$Bu = \frac{\sqrt{g_r D}}{f_0 L} = \frac{Ro}{Fr}. \tag{1.13}$$

Note that an alternative definition of the Froude and Burger numbers is used sometimes in which the terms on the right of (1.12) and (1.13) have been squared.

Now observe that the Burger number can also be written as

$$Bu = \frac{R_d^i}{L}, \tag{1.14}$$

where so-called *internal (or baroclinic) Rossby deformation radius* is introduced

$$R_d^i = \frac{\sqrt{g_r D}}{f_0}. \tag{1.15}$$

It thus represents the scale at which rotational and buoyancy effects are of equal importance ($Bu = 1$). According to (1.14) comparing the internal Rossby radius of deformation and the horizontal length-scale of motion we can estimate the strength of buoyancy effects.

Similar reasoning leads to the introduction of the *(barotropic) Rossby deformation radius*

$$R_d = \frac{\sqrt{gD}}{f_0} \tag{1.16}$$

that characterizes the scale at which motion is equally affected by gravity (*i.e.* the influence of free surface elevation) and rotation. Generally, the term "*barotropic*" is associated

with depth-independent motions of a homogeneous fluid layer. While "*baroclinic*" processes include non-trivial stratification and depend on the z-coordinate. Note, that these two lengths (1.15) and (1.16) will later be used as characteristic length scales in non-dimensionalization.

Table 1.2: Secondary parameters of ocean surface currents specified in Tab. 1.1.

Parameter	Gulf Stream	Kuroshio Current	Antarctic CP Current
δ	~ 0.01	~ 0.01	~ 0.004
Δ	~ 0.01	~ 0.007	~ 0.15
Ro: Rossby number	~ 0.25	~ 0.3	~ 0.01
Bu: Burger number	~ 0.4	~ 0.45	~ 0.1
R_d: Barotropic radius	$\sim 900\,\mathrm{km}$	$\sim 700\,\mathrm{km}$	$\sim 1600\,\mathrm{km}$
R_d^i: Baroclinic radius	$\sim 30\,\mathrm{km}$	$\sim 20\,\mathrm{km}$	$\sim 50\,\mathrm{km}$

Rough estimates for the values of the introduced parameters are presented in Tab. 1.2 for problems considering currents from Tab. 1.1. Observe two typical situations:

- Fast and narrow surface currents, such as the Gulf Stream and Kuroshio. Bu is of order unity and $L \sim R_d^i$. Hence, stratification (and related effects, such as IGWs) should be taken into account. Although, β-effect (1.7) (and Rossby waves) are unimportant.

- Slow and wide surface currents, such as the Antarctic Circumpolar Current. In this case buoyancy-effects can be neglected ($Bu \ll 1$ and IGWs are ruled out). Although, $L \sim R_d$ and is of order of wavelengths of Rossby waves (also, $Ro \ll 1$). Hence, β-effect should be retained in the governing model.

Naturally, these two cases should be examined within two different models. Rigorous derivations of these models they will be done in Chapter 3. The data presented in Tab. 1.1 and 1.2 justifies their validity and applicability.

Rotating shallow water model

In the first model actual density profile of the ocean is approximated with two homogeneous layers via vertical averaging. Then so-called *rotating shallow water (RSW)* equation can be obtained for the case of two layers which supports IGWs on the interface. Under assumption that fluid moves much slower in the bottom layer (below the main thermocline) than in the active top layer, this model simplifies to the *reduced gravity rotating shallow*

water (RGRSW). The Coriolis parameter is assumed constant everywhere in the domain $f \equiv f_0$. This approximation which ignores the variation of the Coriolis parameter is referred to as an f-plane. RGRSW equations will be used in Chapter 4 to examine the interaction between IGWs and a surface zonal jet.

Although, a model which treats the actual stratification as a piecewise constant function may look crude it is complicated enough to describe important aspects of atmospheric and oceanic motions. Multi-layered RSW models are widely used to simulate the wind-driven circulation in the ocean and structure of the main thermocline. Their main advantage is allowing large displacements of isopycnal surfaces. For example, the quasi-geostrophic model with its underlying assumptions of small Rossby number and surface displacement would be inapplicable.

Quasi-geostrophic model

Here we discuss a model appropriate in the second case (planetary scales; $Bu,\ Ro \ll 1$). Condition $Bu \ll 1$ allows us to neglect stratification and consider only barotropic motions. Then one-layer RSW equation on a β-plane can be used in this case. And when the Coriolis parameter f is given by (1.7) it supports Rossby waves which are inhibited within the f-plane.

Smallness of the Rossby number prompts us to use the geostrophic approximation. Although extremely useful and appealing in its simplicity, it is only a diagnostic relationship. It does not compose a closed system of equations. Simply put, geostrophic approximation is degenerate as any pressure field can yield a consistent geostrophic velocity and there is no way to distinguish the correct one.

To resolve this difficulty a higher order approximation is necessary. This so-called *quasi-geostrophic (QG)* approximation can be derived from the RSW equations on the β-plane when the solution is expanded in asymptotic series in Rossby number. As expected, the leading order approximation coincides with the geostrophic approximation. The next order system yields a PDE for the surface elevation (*i.e.* pressure). Once the equation is resolved and the pressure is determined, the velocity field is found from the geostrophic relation. Quasi-geostrophic theory is relatively accurate for synoptic-scale atmospheric motions in which the Rossby number is less than unity.

Motions observed in the ocean or atmosphere are never exactly in geostrophic balance. The difference between the real flows and flows obtained from a quasi-geostrophic model is called *ageostrophic* flow. It arises due to a multitude of effects including baroclinic, viscous

and diffusive forces. These deviations will not be discussed in the work directly but it is important to mention that flow dynamic within the RSW model can be ageostrophic.

1.1.4 Wave-current interaction

Two most prominent phenomena in the ocean and atmosphere are global currents and ubiquitous wave disturbances. Different kinds of restoring mechanisms that exist in the geophysical system create different types of waves. For example, latitudinal variation in rotation, density stratification and compressibility allows, respectively, Rossby, internal-gravity and sound waves to appear in the ocean and atmosphere.

In general, waves can interact with the mean motion in following ways:

1. mean fluid motion can influence propagation of incoming waves (wave scattering)
2. and even generate new waves (spontaneous emission of waves)
3. but in their turn waves can affect the mean flow (collective effect of waves)

In this thesis two linear scattering problems are examined and some new results related to points 1 and 2 are obtained. The propagation of small-amplitude IGWs and Rossby waves through dynamical barriers such as zonal jets is considered, respectively, within the framework of the RGRSW and QG models for the rotating ocean. In addition, we attempted to model the collective effect of stochastic wave fields (wave turbulence) but some fundamental difficulties turned us away from pursuing this investigation.

Problems of wave-mean flow interaction arise in industrial as well as geophysical fluid dynamics and some general results of this work might be extended to address them too.

Wave scattering by a variable medium

Mean motion has a profound effect on propagating waves. Even in the simple case of a small-amplitude waves penetrating a shear flow, the relevant processes include not only conservative scattering (reflection and transmission) but also dissipation and amplification of waves.

This problem falls into the broad category of wave propagation in a slowly variable medium. Within the framework of linear theory it can be described with help of the classical *D'Alembert wave equation* (Vladimirov [86])

$$\frac{\partial^2 U}{\partial t^2} - \nabla \cdot \left(c^2 \, \nabla U \right) = 0, \tag{1.17}$$

where U is a certain scalar function and the propagation speed of waves c can vary spatially. This equation governs propagation of acoustic, electromagnetic, elastic, fluid waves and even quantum particles and, hence, is well studied.

If we look for a one-dimensional harmonic wave solution $U(x,t) = u(x)\exp(i\omega t)$ then Eq. (1.17) simplifies to

$$\frac{\mathrm{d}}{\mathrm{d}x}\left(c^2(x)\frac{\mathrm{d}u}{\mathrm{d}x}\right) + \omega^2 u = 0. \tag{1.18}$$

If $c(x)$ never turns zero then the transformation

$$X = \int_{x_0}^{x} \frac{\mathrm{d}\breve{x}}{c(\breve{x})}, \qquad \psi(X) = \sqrt{c(x)}u(x), \tag{1.19}$$

can be applied so that Eq. (1.18) becomes

$$\frac{\mathrm{d}^2\psi}{\mathrm{d}X^2} + \omega^2\psi = Q(X)\psi, \tag{1.20}$$

where

$$Q = \frac{1}{2c}\frac{\mathrm{d}^2 c}{\mathrm{d}X^2} - \frac{1}{4c^2}\left(\frac{\mathrm{d}c}{\mathrm{d}X}\right)^2.$$

The argumentation in this thesis will be largely guided by a well-known analogy between scattering of quantum particles and waves. Note that Eq. (1.20) is equivalent to the time-independent 1D *Schrödinger equation* for a quantum particle (Landau and Lifshitz [48])

$$E\psi = -\frac{\hbar^2}{2m}\frac{\mathrm{d}^2\psi}{\mathrm{d}X^2} + V(X)\psi, \tag{1.21}$$

when $\frac{2m}{\hbar^2}E = \omega^2$ and $\frac{2m}{\hbar^2}V = Q$; here m is the particle's mass, $\hbar$ is the reduced Planck constant, E is the total energy and V is the potential energy.

The equation has an important property worth being mentioned here. Schrödinger equation in the form (1.21) is known to conserve the *probability flux* (or *wave energy flux* in case of the wave scattering interpretation)

$$\tau(x) = \mathrm{Im}\left(\frac{\mathrm{d}\psi}{\mathrm{d}x}\psi^*\right) = \mathsf{const}. \tag{1.22}$$

where the asterisk denotes complex conjugate.

If function Q (potential V) tends to 0 as $X \to \pm\infty$ then Eqs. (1.20), (1.21) have

oscillatory solutions there. Hence, supplemented with the boundary conditions

$$\left.\begin{array}{rrr} \psi \to \exp(\mathrm{i}\omega X) + r\exp(-\mathrm{i}\omega X) & \text{at} & X \to -\infty \\ \psi \to t\exp(\mathrm{i}\omega X) & \text{at} & X \to +\infty \end{array}\right\} \tag{1.23}$$

the problem represents a free wave (particle) coming from $-\infty$ and propagating through a potential energy barrier. The incident wave (particle) gives rise to a transmitted and reflected waves (particles) with amplitudes t and r (the probabilities for the particle to pass the barrier or be reflected).

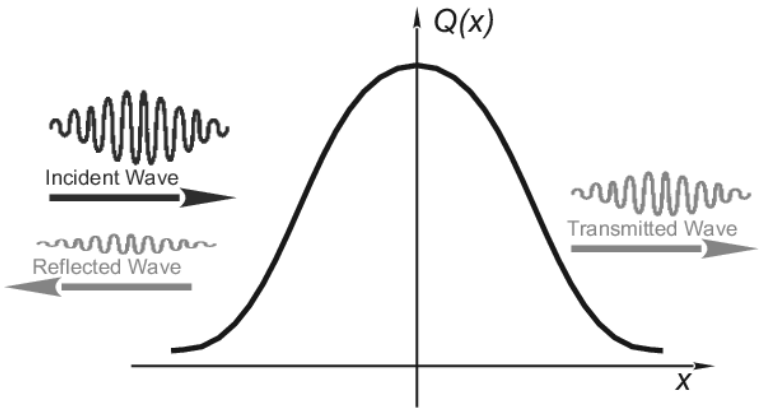

Figure 1.9: Wave scattering by a potential barrier.

Then, so-called *unitarity condition* can be obtained as a consequence. Substitution of the boundary conditions at $X \to \pm\infty$ (1.23) into Eq.(1.22) yields

$$|t|^2 + |r|^2 = 1. \tag{1.24}$$

Hence, the probability to find the particle on either side of the barrier is 1. Or for the wave problem the condition states conservation of wave energy, *i.e.* energy flux of the incident wave is distributed between its transmitted and reflected counterparts.

Note that condition (1.24) is derived under assumption that potential is a smooth real-valued function. If the potential is analytical but *complex-valued* or it has *singularities* (typically, so-called *critical layer* singularities) then the joint energy flux of the reflected and transmitted waves may differ from that of the incident one, which corresponds to *absorption* or *amplification* of the incoming wave. The latter effect is usually referred to as *over-reflection (OR)*. Although, strictly speaking, the term over-reflection

(over-transmission) implies that the amplitude of the reflected (transmitted) wave is (separately!) greater than that of the incident wave. Nevertheless, in this work we use the term "over-reflection" as long as $|t|^2 + |r|^2 > 1$.

Emission of waves by currents

A number of sources starting from topography and finishing with thunderstorms can generate waves in the atmosphere and ocean. But many authors recognize emission of waves by *unstable* currents and vortices as the main mechanism. In particular, according to Shakina [79] unstable shear winds are the primal source of IGWs in the atmosphere. In case of the oceans, observations of the spatial distribution of wave energy around intense currents like the Gulf Stream also confirm this idea [12] (see Fig. 1.10).

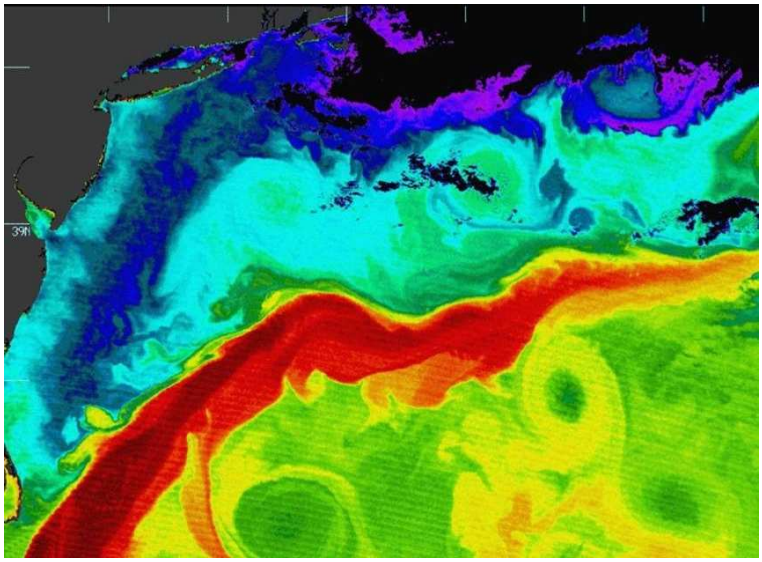

Figure 1.10: Satellite image depicting the surface temperature around the east coast of America (red = warm, blue = cold). The Gulf stream is believed to be the cause of intense wave and eddy fields in the otherwise relatively quiescent regions south and north of the current.

Nevertheless, the mechanism of wave generation is not obvious. According to observations, wave energy decays too slowly away from the jet's core to be explained by the classical instabilities, localized to the seat of shear flow. Arguably, the penetration of waves into the far-field is the manifestation of so-called *radiating instabilities*. These are also present within the linear stability analysis and essentially are "wavy" normal modes with long decay scales. Many analytical and numerical studies estimated characteristics

of disturbances generated by an unstable shear flow and were able to bring the results into correlation with the observations (see Chapter 2).

A special case of radiating instabilities is so-called *resonant over-reflection (or hyper-reflection) (ROR).* In the linear picture it describes an outgoing neutral disturbance being spontaneously generated by the shear layer. Such solutions were discovered sporadically in several problems (Lindzen [54], Maslowe [61] and Lott, Kelder & Teitelbaum [57]). The phenomena is poorly studied and is hardly known to people working in the broad field of scattering and instability problems. Originally, we also were surprised to discover that this phenomena is present in our models but subsequently made it the central topic of the study.

Finally, even thought the fastest growing modes dominate the evolution of unstable flows, radiating instabilities and resonant over-reflection in particular are of great interest as well. The modeling of wave radiation by ocean currents is important for complete understanding of the mechanisms of energy transfer and generation of wave turbulence in calm regions of the ocean (clear air turbulence in the atmosphere). They can also have an important role in early development of unstable flows.

Effect of waves upon the mean flow

Although, persistent mean motions in the ocean and atmosphere described in §1.1.1 appear to be largely stationary their position and intensity varies over a wide range of time scales. Some of the changes can be directly related to the seasonal variation in distribution of solar radiation. But some phenomena such as El Niño, North Atlantic Oscillation and Pacific Decadal Oscillation occur with time scales of decades (climatic phenomena). The cause of such variations is extremely hard to identify as the ocean-atmosphere system behaves fairly chaotically due to its complexity and built-in instabilities. Several mechanisms have been proposed to account for these existence of the oscillations. But most of them directly acknowledge the influence of waves on the dynamics via contribution of momentum and energy to the large-scale motions. Some assign waves only a role of a trigger mechanism. For instance, the onset of an El Niño is often linked to an eastward propagating equatorial Kelvin wave as the latter usually precede the start of an El Niño cycle (McPhaden and Yu [64]).

It will be discussed that waves can interact with the flow and exchange momentum and energy at the critical layers. Although, influence of a single small amplitude wave is certainly negligible, a persistent ensemble of waves can have significant effect on the mean

motion. Hence, the results of the scattering problem described in §1.1.4 can be used in modeling the effect that a prescribed stochastic wave field has on the evolution of currents and winds.

For example, Rossby waves in the ocean are recognized to intensify and alter the western boundary currents. Theoretically this has been discovered and studied by Killworth and McIntyre [43], Benilov *et al.* [5], and references therein. Later Jacobs *et. al.* [38] presented evidence that planetary-scale oceanic waves generated during the 1982-83 El Niño caused northward re-routing of the Kuroshio Extension a decade later when they have crossed the North Pacific.

Note that downward propagating IGWs also can transfer momentum into the depths of the ocean without significant mixing (Muller [67], [68]). Based on this fact Lindzen and Holton [53] were first to conjecture that the Quasi-Biennial Oscillation is a result of zonal winds interacting with vertically propagating IGWs in the atmosphere. Overall, while some theories remain speculative the influence of large-scale waves is universally recognized.

1.2 Thesis outline

After the fundamental objects of the GFD prerequisite for the study are discussed and the necessary terminology is introduced, the outline of the thesis can be clearly stated. We examine linear scattering of IGWs by ageostrophic jets within the reduced gravity rotating shallow water (RGRSW) model and Rossby-wave scattering by a two-jet configuration on the QG β-plane. It is shown that infinitely strong amplification of waves (*resonant over-reflection*) can occur. It is further demonstrated that, generally, a resonantly over-reflected wave is always marginal to instability, *i.e.* either an increase or a decrease of its wavenumber transforms it into a localized unstable mode.

The specific content of the chapters is as follows.

- **Chapter 2: Literature Review.** We set forth the previous work on over-reflection, resonant over-reflection and their connection to instabilities in GFD.
- **Chapter 3: Mathematical Models of Mesoscale Dynamics.** We lay out the general mathematical formulation of GFD problems and non-dimensionalize the equations. With help of traditional approximations we obtain two sets of governing equations used to model scattering of IGWs and Rossby waves respectively. These are the RGRSW model on an f-plane and QG β-plane model.

- **Chapter 4: Gravity Wave Scattering by an Ageostrophic Jet on f-plane.** We examine scattering of small-amplitude IGWs by zonal surface currents within the framework of the RGRSW model. Singularities of the governing equation were studied analytically. That gave insight into the mechanism of energy exchange between the waves and mean flow and ensured reliable numerical simulations. Numerical solutions allow to find the coefficients of reflection and transmission as functions of wavenumber. Amplification and absorption of IGWs occurs in full agreement with the theoretical predictions. We show that the mean flow can spontaneously "emit" the reflected and transmitted waves without the incoming counterpart wave present (resonant over-reflection) and give a physical explanation for the generation mechanism.

- **Chapter 5: Rossby Wave Scattering by a Geostrophic Jet on beta-plane.** In this chapter we put the hypothesized mechanism of resonant over-reflection under test. For this sake we consider a toy problem of scattering of barotropic Rossby waves by a two-jet configuration on the QG β-plane. We solve the problem numerically and, as expected, find resonantly over-reflected waves. The corresponding scattering coefficients of each individual jet satisfy the condition implied by the proposed generation mechanism.

- **Chapter 6: Resonant over-reflection as a marginally stable disturbance.** We investigate the connection between the resonantly over-reflected waves and unstable normal modes both of which are solutions of the equations governing the dynamics of small perturbations. We derive a general conclusion that resonant over-reflection can be perceived as a borderline case of (radiating) instabilities. Hence, we argue that when resonant over-reflection (and, hence, spontaneous emission of waves) is present, the mean flow is unstable.

- **Chapter 7: Conclusions.** In this chapter we summarize the work of the present thesis and discuss the results. Some possible improvements and directions for future work are suggested.

1.3 Publications during the Ph.D. studies

The result of my research within the 3 years of Ph.D. studies is presented in 3 peer reviewed research papers and several contributed talks. The work was carried out jointly with and

under supervision of Eugene Benilov, my scientific advisor.

Publications from work based on this Ph.D.

- Benilov, E. S. & Lapin, V. N. On resonant over-reflection of waves by jets. *Submitted to Phys. Fluids.*

Publications from other work carried out during this Ph.D.

- Benilov, E. S. & Lapin, V. N. Viscous flows down an inclined plate. *Phys. Rev. E.* **83**, 066321.

- Benilov, E. S., Lapin, V. N. & O'Brien S. B. G. On rimming flows with shocks. *To appear in J. Eng. Math.*

- Benilov, E. S. & Lapin, V. N. Coating and rimming flows beyond the lubrication approximation. *In preparation.*

Conference talks

1. `December 2009` – "*Radiating instabilities and hyper-reflection of waves by jets in a rotating ocean*", MACSI colloquium, UL, Limerick, Ireland.

2. `July 2010` – "*Radiating instabilities of jets in a rotating ocean*", ECMI 2010, Bergische Universität, Wuppertal, Germany.

3. `August 2010` – *Same title as in 2*, SIAM Conference on Nonlinear Waves and Coherent Structures, Philadelphia, USA.

4. `April 2011` – "*Shocks in coating flows within a rotating horizontal cylinder*", BAMC 2011, University of Birmingham, Birmingham, UK.

5. `April 2011` – "*Resonant over-reflection of waves as a marginally stable solution*", The 4rd Meeting of the Wave-Flow Interactions Network, University of Cambridge, Cambridge, UK.

6. `April 2011` – *Same title as in 4*, MACSI colloquium, UL, Limerick, Ireland.

Chapter 2

Literature Review

2.1 Wave over-reflection and instability

Linearized equations for a wave disturbance superimposed upon a plane-parallel flow $U(y)$ commonly appear in the linear stability and wave propagation problems. Various models give rise to scattering equations of the type (1.20) but the coefficients look quite different. However, the presence of a *critical layer* singularity at y_c where the velocity of the mean flow matches the corresponding component of the wave's phase speed $U(y_c) = c_{ph}$ is their common characteristic.

Phase speeds of IGWs in the ocean are typically about $1\,\mathrm{m/s}$ (see §1.1.2) which is of the same order as velocities of the fast surface currents like the Gulf Stream 1-2 $\mathrm{m/s}$ (see §1.1.1). Hence, it seems plausible that critical levels will occur fairly frequently when random IGWs propagate through the jet. Observe, that similar situation occurs with regards to Rossby waves ($c_{ph} \lesssim 0.1\,\mathrm{m/s}$) and slower currents like the Antarctic circumpolar current which speeds are $\lesssim 0.5\,\mathrm{m/s}$.

Since the pioneering works by Lin [52] and Miles [66] critical layer singularities were regularized by introducing infinitesimal viscosity. Mathematically this is equivalent to fixing a branch of the multivalent solution. Although, this viscous regularization is not unique and the solution can be made regular if, say, nonlinear effect are taken into account (Killworth and McIntyre [43]). However, both regularization procedures lead to the same magnitude of the jump in the wave energy flux (defined as in (1.22)) across critical layers. Physically this suggests that a wave propagating across the mean flow can interact with it in its critical layers resulting in either absorption or amplification of the wave energy by the mean flow. The latter is traditionally referred to as *over-reflection*.

Historically scattering of waves by shear background flows containing a critical level

was extensively studied within two following set-ups:

1. Propagation of IGWs through a steady plane-parallel flow with vertical shear $U(z)$ in an infinite layer of continuously stratified fluid, is typically studied using the *Boussinesq model*. The corresponding scattering problem is governed by *Taylor-Goldstein equation*. This model is not considered in this work but the corresponding literature will be discussed as it is gives valuable insight. Exactly within this model scattering of waves in presence of critical layers has been studied for the first time by Booker & Bretherton [8].

   They found the reflection and transmission properties of IGWs to be strongly dependent on the value of *Richardson number* ($Ri = \left(\frac{N}{U'}\right)^2$) at the critical layers. Booker & Bretherton [8] have shown that, for Richardson numbers greater than $\frac{1}{4}$, the wave is absorbed by the flow. The case when Richardson number is smaller than $\frac{1}{4}$ has been later discussed by several authors, *e.g.* Jones [40], McKenzie [63], Eltayeb & McKenzie [25], Acheson [1] and van Duin & Kelder [85]. They found that this condition can yield over-reflection/over-transmission.

2. Scattering of barotropic Rossby waves by plane-parallel jets $U(y)$ is traditionally examined within the QG β-plane model. The governing equation is referred to as the *Rayleigh-Kuo equation* [45] and is a simple generalization of the classical Rayleigh's equation arising in the problem of stability of an inviscid parallel shear flow [74]. Rossby-wave scattering by a specific two-jet configuration within this model will be considered in Chapter 5.

   Necessary and sufficient conditions for over-reflection and absorption were derived by Lindzen and Tung [55] and later by Yamada and Okamura [89]. These authors have shown that the scattering of Rossby waves depends on the sign of $\beta - U''$ at the critical layers. In particular, when the condition $\beta - U'' > 0$ holds there the wave energy is absorbed and, on the contrary, when $\beta - U'' < 0$ over-reflection occurs. The time-dependent propagation of a Rossby-wave in a zonal jet was studied by Dickinson [19] where the results were confirmed.

The two above-mentioned models received a lot of attention but are rather simplified. IGW scattering within the model 1 does not take into account neither Earth's rotation nor horizontal structure of the flow while model 2 for barotropic Rossby waves completely neglects stratification. Some authors endeavoured to examine wave scattering in more

complex models. Propagation of IGWs in a stratified ocean with a shear flow in the form $U(y,z)$ has been addressed in theoretical studies [37], [4]. Jones [39] and Grimshaw [29] included rotation into model 1. Nevertheless, all of those models rule out effects of baroclinicity. As discussed in §1.1.3 the simplest model to include rotation, stratification and baroclinicity effects is the reduced gravity rotating shallow water (RGRSW) model. Scattering properties of zonal flows within this model will be examined in Chapter 4.

3. Up to the author's knowledge the problem most similar to the one we study in Chapter 4 was recently examined by Ollers *et al.* [69]. These authors studied scattering of IGWs by a horizontal shear flow $U(y)$ in uniformly stratified fluid on an f-plane. Their scattering Eq. (10) is similar to our Eq. (4.21) except we acknowledge variability of the layer's depth $H(y)$ (baroclinicity) and Ollers' formulation has an extra term due to constant stratification. Ollers *et al.* found that the sign of $-\frac{U''}{U'}$ at the critical layer determines whether over-reflection or absorption occurs.

   The mean flow was taken as a hyperbolic tangent profile with intention to represent the Antarctic circumpolar current. The problem was solved numerically using a straightforward method of introducing a small Rayleigh damping in order to regularize the singularities in the scattering equation. In this thesis a superior method is implemented but that one was used for too for testing purposes.

It is intuitively clear that, since over-reflection transfers energy from jets to waves, it is conducive to the jet's instability. This fact prompted researchers to investigate the connection between the stability and scattering properties of the mean flow. Moreover, In case of the aforementioned models 1 and 2, the necessary conditions for instability coincide with the conditions for over-reflection.

- In case of the Taylor-Goldstein equation (model 1) Miles [66] and later Howard [35] have shown that the flow is stable when the minimum Richardson number is everywhere greater than $\frac{1}{4}$. A necessary condition for instabilities requires the minimum Richardson number to be less than $\frac{1}{4}$ somewhere in the flow (Drazin [21]).

- For the Rayleigh-Kuo equation (model 2) the sufficient stability condition is $\beta - U_{yy} > 0$ everywhere in the flow (Kuo [45], Lin [52]). The condition $\beta - U_{yy} < 0$ must be met somewhere in the flow for it to be potentially unstable.

- For the model 3, Ollers *et al.* [69] also tried to relate the results of the scattering problem with the condition for a zonal shear flow on the f-plane to be *inertially*

unstable: $f\,(U_y - f) > 0$ is fulfilled somewhere in the flow (see Holton [34]). They found that when this condition is satisfied at the critical layer of the incident wave, then over-reflection is favoured although absorption is possible too. The overall situation is similar to that in the scattering problem examined in Chapter 4.

Hence, stable shear flows absorb waves while appearance of over-reflection favours instabilities. Although, generally the correspondence is not clear especially when a precise stability criterion is not present. We will show that, in general, the relation between over-reflection and instability is more subtle than suggested by the two previous examples.

2.2 Radiating instabilities and emission of waves

Generally, the eigenfunctions of the instability problem may display the behavior at infinity that is more "oscillatory" than exponentially decaying. Such unstable *radiating modes* (unlike the conventional *non-radiating normal modes* which rapidly decay to 0 at infinities and, hence, are trapped in space) are those that look "nearly" like free waves in the far-field (their decay is slow). They represent waves being radiated away from the seat of instability. For this to hold the real part of the phase speed of these modes must match the phase speed of some freely propagating wave with the same horizontal wavelength. This natural requirement constitute so-called *phase speed condition* (McIntyre and Weissman [62]). Unstable normal modes spatially decay in the outer regions of instability. Hence, the arising question of how to assess the extent to which instabilities penetrate into the far-field regions has been debated in the literature [62], [84]. As the result, penetration ratio (*i.e.* the ratio of the oscillation scale to the decay scale) is adopted as the gauge of radiation effectiveness of an instability (see [84], [82], [41], [46]).

The concepts of radiating instabilities have been usually considered in the literature within the 3 following models:

1. The case of IGW radiation by unstable shear flows in inviscid Boussinesq fluid (Taylor-Goldstein equation) was investigated in [82], [46] (this model is not a subject of the thesis so citation is limited).

2. Dickinson and Clare [20], Talley [84], Malanotte-Rizzoli [59] and Maslowe [61] examined radiating instabilities within the framework of QG β-plane model (Rayleigh-Kuo equation). Unstable westward jets were found to radiate energy into the far-field [20]. In their turn, their eastward counterparts only support trapped instabilities and cannot radiate (see [84], [59]). The difference is explained by the phase-speed condition:

the instability's phase speed must match a Rossby wave phase speed in the far-field (which is always directed westwardly).

An analytical approach was uses by Talley in [84] where the velocity profile of the background flow was approximated with piecewise quadratic functions. Fantini and Tung [26], Kamenkovich and Pedlosky [41], Pedlosky [72] and Hristova *et al.* [36] extended Talley's work to address non-zonal jets as all real-life currents are not always, and never exactly, zonal. Western and eastern boundary currents were examined within one- and two-layer QG β-plane models in [26], [72] and [36]. The purely meridional velocity profiles were approximated with step-functions. More general nonzonality in the mean flow was considered in [41]. The authors demonstrated the destabilizing effect of the tilt on a zonal flow. The currents were found to generate radiating modes propagating energy away into the far-field in all the cases.

3. Radiating instabilities (and over-reflection of IGWs) within RSW considered by Satomura [77], Takehiro and Hayashi [83], Knessl and Keller [44] and Balmforth [3]. Numerical solutions of the linear stability problem are presented in these papers. Although, rotational effects are usually not included in the models and other simplifying assumptions (like linear velocity profile) are taken so the governing equations are quite different from what we examine in Chapter 4.

Note that conventional stability analysis usually only look for non-radiating modes. Notably, linear stability of a zonal jet on an f-plane with RGRSW model was investigated by Paldor and Ghil [70] (the corresponding scattering problem is examined in Chapter 4). Generation of waves propagating away from the shear zone was explicitly ruled out there by the choice of boundary conditions.

In all the above-mentioned cases radiating instabilities were found to coexist with trapped instabilities (also referred to as Kelvin-Helmholtz modes). Although, the growth rates of the former generally remain much smaller than that for the most unstable non-radiating mode their influence extends much further as they propagate energy far away from the seat of instability.

Hence, radiating instabilities may be responsible (at least, partially) for observed emission of waves by fast (and in fact *unstable*) ocean currents and atmospheric winds (see Schmitz *et al.* [78], Bower and Hogg [12], Romanova and Yakushkin [75] for the review of observational data). So, they may be important for a more complete understanding of phenomena of clear air turbulence in the atmosphere and wave turbulence in calm regions

of the ocean away from major currents and other special regions.

Some recent numerical and experimental studies give strong evidence supporting this idea. In their 3D simulations Viúdez & Dritschel [87] (see references therein for simpler models) discovered that balanced but unstable jets in a rotating stratified fluid emits bursts of IGWs which propagate far from the jet (where other instabilities would not "reach").

Generation of IGWs by balanced flows was observed in laboratory experiments by Lovegrove, Read & Richards [58] and by Williams, Haine & Read [88] in a rotating two-layer annulus experiment and in a single-layer experiment by Afanasyev *et al.* [2]. The exact source of wave radiation is not established but the authors refer to baroclinic instability as the candidate as all usual sources (physical obstructions, the geostrophic adjustment) are filtered out.

One mechanism of how over-reflected gravity waves can cause instability is when the transmitted wave is repeatedly reflected back towards the critical level by a rigid wall (the ground/bottom in atmosphere/ocean) or a turning point beyond which the medium is not transparent. This "*over-reflection hypothesis*" was suggested and developed by a number of authors (Lalas and Einaudi [47], Davis and Peltier [17], [18] and Rosenthal and Lindzen [76]). In a series of works Lindzen and coauthors successfully explained several types of instabilities in geophysical flows with help of this mechanism (see a review paper [56]).

2.3 Resonant over-reflection

The prime goal of the present work is to investigate the phenomena of "*resonant over-reflection*". It describes the singular case of over-reflection where, according to linear theory, the reflected and transmitted waves are *infinitely* strong – which can be interpreted as spontaneous emission of outgoing "reflected" and "transmitted" waves by the flow in the absence of the incident wave. We shall, also, refer to "resonant over-reflection" with a more succinct term, "*hyper-reflection*", which emphasises that this effect is stronger than over-reflection – which is, in turn, stronger than the usual reflection. Also note, that the phenomena, if present, can be thought of as the limiting case of the radiating modes as the growth rate tends to 0.

Occasionally the term "resonant over-reflection" was used incorrectly to describe the aforementioned "wave self-excitation" instabilities (*e.g.* papers by Davis [17], [18]). And it should be emphasised that those two cases should not be confused. The growing modes connected to Lindzen's "over-reflection hypothesis" exist *only* in presence of a reflecting boundary or a turning point.

The phenomenon of resonant over-reflection was introduced in GFD by McKenzie in 1972 [63]. However, since then it was found in just a few cases (despite all the efforts the author has only foundy another two) and and remained poorly studied.

1. McKenzie [63] and Lindzen [54] investigated stability of a Helmholtz velocity profile (also referred to as *vortex-sheet*, see Fig. 2.1) in Boussinesq fluid with constant Brunt–Väisälä frequency N. The shear flow was found to have neutral radiating modes (resonantly over-reflected IGWs) propagating away from the current whenever the horizontal wavenumber is less than $\frac{N}{\sqrt{2}U}$ (where $2U$ is the mean velocity discontinuity). McIntyre & Weissman [62] clarified the energy budget of wave-flow interaction in this problem. Grimshaw [31], [32] examined its weakly nonlinear extension. An equation governing the evolution of the amplitude of the interface displacement was derived but still the solution was found to develop a singularity in a finite time. Hence, Grimshaw confirmed the existence of resonant over-reflection even within the weakly nonlinear theory.

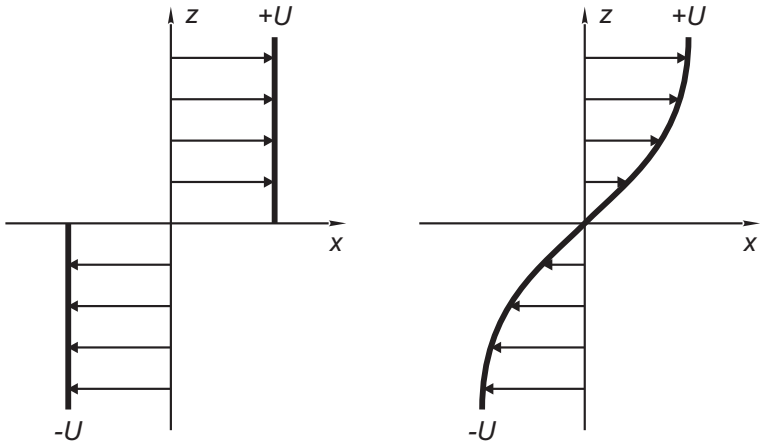

Figure 2.1: A Helmholtz velocity and hyperbolic tangent profiles $U(y) = U_0 \tanh(z/d)$.

It is known (Jones [40], Eltayeb & McKenzie [25]) that discontinuities in the velocity profile and its derivatives are known to give rise to extra reflected energy when a scattering problem is considered. Hence, the assumption of Helmholtz velocity profile is crude and its smooth analogue should be considered (Fig. 2.1). The corresponding scattering problem where the basic flow is a hyperbolic tangent profile was examined numerically by Mied & Dugan [65] and analytically by Grimshaw [30] and van Duin and Kelder [85]. Van Duin and Kelder transformed the governing equation into Heun's equation, obtained the solution in

hypergeometric functions and, as a result, showed that resonant over-reflection is ruled out. Hence, one may suppose that smooth velocity profiles inhibits this "nonphysical" phenomenon.

2. However, Lott, Kelder & Teitelbaum in their analytical study [57] demonstrated that resonant over-reflection can exist with smooth coefficients in the scattering equations. The basic velocity was again $U = U_0 \tanh(z/d)$ but stratification was non-uniform in this case $N^2 = N_1^2 + N_2^2 |\tanh(z/d)|^\alpha$. The authors found that for $\alpha > 2$ the mean flow resonantly over-reflects IGWs of a particular wavenumber (rather than for a range of wavenumbers as in [54]). Hence, this study indicates that if stratification is small at the shear layer the mean flow can support spontaneous generation of IGWs.

3. Neutral radiating modes (resonantly over-reflected Rossby wave) were also found within the QG β-plane model by Maslowe [61], provided the critical level is located at the jet's maximum $c = U_{\max}$.

It can be checked that settings 2 and 3 are described by Sturm–Liouville-kind problems, with coefficients involving *second*-order poles located at the critical level. Setting 1, in turn, is a limiting case of setting 2 (with the width of the velocity "step" and the variation of the Brunt–Väisälä frequency both tending to zero) – thus, it effectively involves a second-order pole multiplied by a discontinuous coefficient.

In this thesis, we shall demonstrate numerically that resonant over-reflection can also occur for IGWs within RGRSW (and RSW) on f-plane (Chapter 4) and Rossby waves on the β-plane (Chapter 5), which both involve *first*-order poles. We shall also examine hyper-reflection in a general formulation, concentrating on its connections with instability (Chapter 6).

Notably, resonant over-reflection was not found by Ollers *et al.* in [69] even though their scattering problem is similar to the one we study in Chapter 4 (and we observe the phenomenon there). We attribute this to the fact that Ollers *et al.* did not carry out numerical calculation of the scattering coefficients as functions of the zonal and meridional wavenumbers (k and $l_{-\infty}$) but varied only one parameter $\beta = \frac{k}{l_{-\infty}}$ (referred to as the angle of incidence) while $l_{-\infty}$ was fixed. Moreover, Figure (6) in [69] shows a sharp jump in values of $|R|$ and $|T|$. Hence, we hypothesize that corresponding point in the parameter space may be close to the point $\left(k^r, l^r_{-\infty}\right)$ at which resonant over-reflection occurs which was missed out.

Chapter 3

Mathematical Models of Mesoscale Dynamics

The ultimate goal of this chapter is to accurately rederive two classical models of geophysical fluid dynamics (GFD): quasi-geostrophic (QG) β-plane model and reduced gravity rotating shallow water (RGRSW) model on an f-plane. In what follows, the Euler's equations of fluid dynamics are non-dimensionalized using some preconceived characteristic scales for motions in the ocean and atmosphere introduced in §1.1. In order to simplify the original equations governing fluid motion on the spinning Earth we use asymptotic analysis with respect to the non-dimensional parameters and vertical averaging. Two models under consideration represent two particular limiting cases. The corresponding equations are much simpler but do retain the essential dynamical features. The clarity of our derivations allows us to have better understanding of the limitations of the models and the boundaries of their applicability.

The content of this chapter, obviously, is not new. Nevertheless, the presented general way of obtaining the RGRSW (§3.4.4) and QG β-plane models (§3.5.2) was developed by the author independently. The following sources were taken as the foundation: Pedlosky [71], Holton [34], Gill [27] and lecture notes by Vladimir Zeitlin presented at the workshop on the mathematics of weather and climate prediction, Met Office, Exeter, 2009.

3.1 Euler's equations

The fundamental approach to mathematical modeling of ocean and atmosphere dynamics resides in application of the hydrodynamic equations for inviscid, incompressible, stratified

fluid (Euler's equations) in a uniformly rotating coordinate frame. The closed system consists of 5 equations for 5 unknowns: fluid velocity $\vec{v}\left(\vec{r},t\right) \equiv \left(u\left(\vec{r},t\right), v\left(\vec{r},t\right), w\left(\vec{r},t\right)\right)$, pressure $p\left(\vec{r},t\right)$ and density $\rho\left(\vec{r},t\right)$

$$\frac{\mathrm{D}\vec{v}}{\mathrm{D}t} + 2\left[\vec{\Omega},\vec{v}\right] + \left[\vec{\Omega},\left[\vec{\Omega},\vec{r}\right]\right] = -\frac{1}{\rho}\nabla p + \vec{g}, \tag{3.1}$$

$$\frac{\mathrm{D}\rho}{\mathrm{D}t} = 0, \tag{3.2}$$

$$\nabla\cdot\vec{v} = 0, \tag{3.3}$$

where $\vec{g}$ is the acceleration due to gravity, $\vec{\Omega}$ is the planetary angular velocity and $\frac{\mathrm{D}}{\mathrm{D}t} = \frac{\partial}{\partial t} + \vec{v}\cdot\nabla$ is the material time derivative. Essentially, the fluid dynamics is governed by conservation of momentum (3.1), mass (3.2) and incompressibility condition (3.3).

On the left-hand side of Eq. (3.1) are present the Coriolis acceleration $2\left[\vec{\Omega},\vec{v}\right]$ and the centripetal acceleration $\left[\vec{\Omega},\left[\vec{\Omega},\vec{r}\right]\right]$. They are due to altered perception of particle's acceleration in the rotating reference frame attached to Earth. With help of the formula for triple vector product the formula for the centripetal acceleration simplifies to $\left[\vec{\Omega},\left[\vec{\Omega},\vec{r}\right]\right] = -\left|\vec{\Omega}\right|^2\vec{r}_\perp$ ($\vec{r}_\perp$ is the component of $\vec{r}$ perpendicular to the rotation axis). Moreover, it corresponds to a conservative force and can be combined with gravitational acceleration to produce so-called *effective* gravitational acceleration $\vec{g}_e = \vec{g} + \left|\vec{\Omega}\right|^2\vec{r}_\perp$. For most geophysical phenomena the local variation in $\vec{g}_e$ is unimportant (see Pedlosky [71], Holton [34]) as it only result is slight deviation of geopotential surfaces (the potential surfaces of the effective gravity) from perfect spheres. Then, we omit the index e and use the usual notation for gravity $\vec{g}$. In this work $\vec{g}$ is assumed to be constant and directed to the center of the earth.

Naturally, the Earth's atmosphere or ocean can be represented by a thin layer of stratified fluid on a rotating sphere of radius r_0. We introduce a spherical coordinate system as shown on Fig. 3.1. Then position of a fluid particle is given by the distance from the Earth's center r, latitude θ and longitude φ. Accordingly, w, u and v represent velocities in the vertical, eastward, and northward directions. In these coordinates Euler's

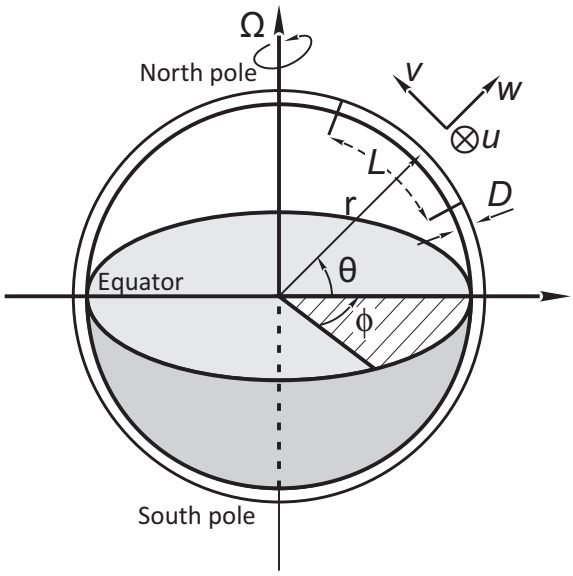

Figure 3.1: Spherical coordinates r, θ, φ on the Earth and characteristic horizontal and vertical length scales L, D.

equations (3.1) – (3.3) transform into (see Pedlosky [71])

$$\frac{\mathrm{d}u}{\mathrm{d}t} + \frac{uw}{r} - \frac{uv}{r}\tan\theta - (2\Omega\sin\theta)\,v + (2\Omega\cos\theta)\,w = -\frac{1}{\rho r\cos\theta}\frac{\partial p}{\partial\phi}, \tag{3.4}$$

$$\frac{\mathrm{d}v}{\mathrm{d}t} + \frac{wv}{r} + \frac{u^2}{r}\tan\theta + (2\Omega\sin\theta)\,u = -\frac{1}{\rho r}\frac{\partial p}{\partial\theta}, \tag{3.5}$$

$$\frac{\mathrm{d}w}{\mathrm{d}t} - \frac{u^2+v^2}{r} - (2\Omega\cos\theta)\,u = -\frac{1}{\rho}\frac{\partial p}{\partial r} - g, \tag{3.6}$$

$$\frac{d\rho}{dt} = 0, \tag{3.7}$$

$$\frac{\partial w}{\partial r} + \frac{2w}{r} + \frac{1}{r\cos\theta}\frac{\partial(v\cos\theta)}{\partial\theta} + \frac{1}{r\cos\theta}\frac{\partial u}{\partial\phi} = 0, \tag{3.8}$$

where

$$\frac{\mathrm{d}}{\mathrm{d}t} = \frac{\partial}{\partial t} + \frac{u}{r\cos\theta}\frac{\partial}{\partial\phi} + \frac{v}{r}\frac{\partial}{\partial\theta} + w\frac{\partial}{\partial r}. \tag{3.9}$$

Dealing with Eqs. (3.4) – (3.9) directly is an extremely difficult task. This system of nonlinear PDEs govern phenomena of all the spatial and time scales starting with tiny eddies and ending with planetary scale Rossby waves. It is sufficient for our present purposes to consider only large scale motions in mid-latitudes. The following scaling analysis will allow us to considerably simplify Eqs. (3.4) – (3.9).

3.2 Non-dimensionalization

We introduce characteristic horizontal and vertical scales of the motion L and D as shown in Fig. 3.1. We will refer to θ_0 as to the central latitude of the region (without loss of generality the central longitude $\phi_0 = 0$). In addition, we assume that a single well-defined horizontal velocity scale U exists so that magnitudes of time derivatives can also be estimated with its help.

For convenience we introduce new coordinates

$$x = r_0 \cos\theta_0 \, \phi, \tag{3.10}$$

$$y = r_0 \, (\theta - \theta_0), \tag{3.11}$$

$$z = r - r_0. \tag{3.12}$$

On one hand they are just rescaled longitude, latitude and height. But on the other hand, they measure eastward and northward distance from the central latitude θ_0 and height from a certain reference surface. They will play role of the Cartesian coordinates in the upcoming tangent plane approximation.

Now we shall scale Eqs. (3.4) – (3.9) in order to estimate the order of magnitude of the terms. The non-dimensional variables denoted by primes are introduced as below

$$\mathbf{x} = L\,\mathbf{x}', \tag{3.13a}$$

$$z = \delta L\, z', \tag{3.13b}$$

$$\mathbf{v} = U\,\mathbf{v}', \tag{3.13c}$$

$$t = \frac{L}{U}\, t', \tag{3.13d}$$

$$w = \delta U\, w', \tag{3.13e}$$

where $\mathbf{x} = (x,\, y)$ and $\mathbf{v} = (v,\, u)$ denotes horizontal coordinates and velocities; two parameters δ and Δ introduced in §1.1.3 represent the ratios of length scales

$$\delta = \frac{D}{L}, \qquad \Delta = \frac{L}{r_0}. \tag{3.14}$$

The aptness of the chosen vertical velocity scale $W = \delta U$ follows from incompressibility condition (3.1).

We separate the pressure and density fields into the basic motionless state representing

hydrostatic equilibrium given by $p_0(z)$ and $\rho_0(z)$ and fluctuations due to motion

$$p = p_0(z) + \tilde{p}(x,y,z,t), \tag{3.15}$$

$$\rho = \rho_0(z) + \tilde{\rho}(x,y,z,t), \tag{3.16}$$

$$\frac{\partial}{\partial z}(p_0(z)) = -\rho_0(z)\, g. \tag{3.17}$$

In order to proceed with non-dimensionalization we introduce the reference fluid's density at a certain point z_0, say, at the ocean's surface

$$\varrho_0 = \rho_0(z_0) \tag{3.18}$$

and we scale the equilibrium density and pressure functions as

$$\rho_0 = \varrho_0 \rho_0', \qquad p_0 = \varrho_0 g D\, p_0'. \tag{3.19}$$

The scaling of the pressure is based on the idea that horizontal pressure gradients are of the same order as the Coriolis force. Hence,

$$\tilde{p} = \varrho_0 f_0 U L\, \tilde{p}', \tag{3.20}$$

where as defined in (1.8) f_0 is the Coriolis parameter at the central latitude θ_0

$$f_0 = 2\Omega \sin\theta_0. \tag{3.21}$$

In addition, we expect the buoyancy force due to $\tilde{\rho}$ to be of the same order as vertical gradients of pressure fluctuations

$$\tilde{\rho} g = \mathrm{O}(\tilde{p}_z) = \mathrm{O}\left(\frac{\varrho_0 f_0 U L}{D}\right). \tag{3.22}$$

So the density and pressure fluctuations are non-dimensionalized as

$$\tilde{\rho} = \varrho_0\, Ro\, F\, \tilde{\rho}', \qquad \tilde{p} = \varrho_0 g D\, Ro\, F\, \tilde{p}', \tag{3.23}$$

where we ushered parameter F and the Rossby number Ro was introduced in §1.1.3

$$Ro = \frac{U}{f_0 L}, \qquad F = \left(\frac{L}{R_d}\right)^2. \tag{3.24}$$

The latter measures the ratio of the horizontal length L to the Rossby radius R_d and hence, estimates the influence of gravity wave effects (similarly to how the Burger number does it for IGWs, compare with (1.14) in §1.1.3). Substituting (3.17) – (3.24) into Eqs. (3.4) – (3.9) we obtain the rescaled system (primes are omitted)

$$(\rho_0 + Ro\,F\,\tilde{\rho})\left(Ro\left(\frac{\mathrm{d}u}{\mathrm{d}t} + \frac{L}{r^*}\left(\delta uw - uv\tan\theta^*\right)\right) - v\frac{\sin\theta^*}{\sin\theta_0} + \delta w\frac{\cos\theta^*}{\sin\theta_0}\right) = \\ = -\frac{r_0}{r^*}\frac{\cos\theta_0}{\cos\theta^*}\frac{\partial\tilde{p}}{\partial x}, \quad (3.25)$$

$$(\rho_0 + Ro\,F\,\tilde{\rho})\left(Ro\left(\frac{\mathrm{d}v}{\mathrm{d}t} + \frac{L}{r^*}\left(\delta wv - u^2\tan\theta^*\right)\right) + u\frac{\sin\theta^*}{\sin\theta_0}\right) = -\frac{r_0}{r^*}\frac{\partial\tilde{p}}{\partial y}, \quad (3.26)$$

$$(\rho_0 + Ro\,F\,\tilde{\rho})\left(Ro\left(\delta^2\frac{\mathrm{d}w}{\mathrm{d}t} - \frac{\delta L}{r^*}\left(u^2 + v^2\right)\right) - \delta u\frac{\cos\theta^*}{\sin\theta_0}\right) = -\frac{\partial\tilde{p}}{\partial z} - \tilde{\rho}, \quad (3.27)$$

$$Ro\,F\,\frac{\mathrm{d}\tilde{\rho}}{\mathrm{d}t} + w\frac{\partial\rho_0}{\partial z} = 0, \quad (3.28)$$

$$\frac{\partial w}{\partial z} + \frac{D}{r^*}2w + \frac{r_0}{r^*}\frac{\partial v}{\partial y} - \frac{L}{r^*}v\tan\theta^* + \frac{r_0}{r^*}\frac{\cos\theta_0}{\cos\theta^*}\frac{\partial u}{\partial x} = 0, \quad (3.29)$$

where

$$\frac{\mathrm{d}}{\mathrm{d}t} = \frac{\partial}{\partial t} + \frac{r_0}{r^*}\frac{\cos\theta_0}{\cos\theta^*}u\frac{\partial}{\partial x} + \frac{r_0}{r^*}v\frac{\partial}{\partial y} + w\frac{\partial}{\partial z}. \quad (3.30)$$

To keep the equations succinct some original dimensional variables (denoted with asterisks) are also present in Eqs. (3.25) – (3.29). But they always appear in combinations that can be written in terms of non-dimensional variables. For instance,

$$\frac{r_0}{r^*} = \frac{1}{1 + \delta\,\Delta\,z}. \quad (3.31)$$

Up to this point no approximations have been made as we have only rewritten the equations with help of scaled variables. Depending on which of parameters δ, Δ, Ro and F are small and their relative order different approximations can be obtained.

3.3 Tangent plane and hydrostatic approximations

We focus our attention on the dynamics of mesoscale systems (see 1.1.3) in a mid-latitude region of the ocean or atmosphere distant from the equator and North Pole. This assures

that the scales of the motion L and D satisfy condition (1.9) and, consequently,

$$\delta \ll 1 \qquad \text{and} \qquad \Delta \ll 1, \tag{3.32}$$

$$\sin\theta \in [\varepsilon;\, 1-\varepsilon]\,, \tag{3.33}$$

where ε is a positive number less than 1.

Next we write down the leading order approximation to Eqs. (3.25) – (3.29) with respect to small parameters δ and Δ. From condition $\delta \ll 1$ follows that only the normal component of the Earth's angular velocity $\Omega_n = \Omega \sin\theta$ is important. The component of $\vec{\Omega}$ proportional to $\cos\theta$ create Coriolis forces in Eqs. (3.25) – (3.27) which are $\mathrm{O}(\delta)$, *i.e.* the horizontal Coriolis acceleration due to the vertical motion and the vertical Coriolis acceleration due to the horizontal motion are insignificant compared to the pressure gradients.

In addition, condition $\delta \ll 1$ allows us to make use of the approximation of hydrostatic equilibrium in Eq. (3.27) even though the fluid is in motion. Physically it means that the pressure at any internal point is just due to the weight of overlying fluid. Note that fluctuations in pressure due to vertical acceleration $\frac{dw}{dt}$ in Eq. (3.27) are of order $\mathrm{O}\left(\delta^2\right)$.

With help of the second small parameter Δ we can neglect all the terms in (3.25)–(3.29) which are due to working in spherical geometry. In other words, in the limit $\Delta \to 0$ we can replace the de facto spherical-shell region with its flattened analogue using (3.10) – (3.12) as new Cartesian coordinates. This simplified domain can be visualised as the tangent plane touching the sphere at the central latitude and longitude θ_0, ϕ_0 supplemented with the z-axis perpendicular to this plane (Fig. 3.2).

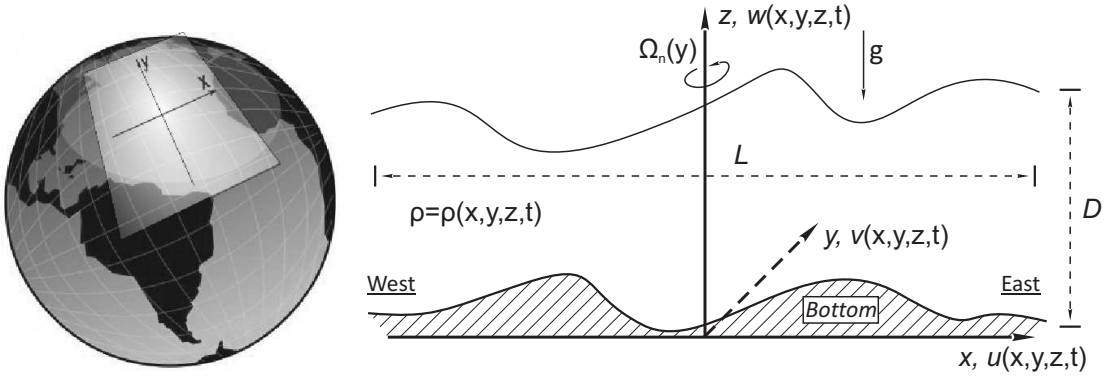

Figure 3.2: Tangent plane approximation in mid-latitudes.

Making use of (3.11) , (3.13a) functions of latitude θ appearing in Eqs. (3.25) – (3.27)

are expanded in Taylor series around the central latitude θ_0. For example, for the non-dimensional Coriolis parameter $f = \frac{\sin\theta^*}{\sin\theta_0}$ we have

$$f = 1 + \Delta \cot\theta_0 \, y - \frac{\Delta^2}{2} y^2 + \cdots .$$

We denote the linear coefficient of variation in $f(y)$ as β

$$\beta = \cot\theta_0 \, \Delta. \tag{3.34}$$

It is the dimensionless analogue of β^*, the northward gradient of Coriolis parameter at the latitude θ_0, was introduced in (1.8)

$$\beta^* = \frac{f_0}{L}\beta = \frac{2\Omega}{r_0} \cot\theta_0. \tag{3.35}$$

The $\mathrm{O}(\Delta)$ variation of the Coriolis parameter with y may or may not be important. The magnitude of this term should be compared with that of relative vorticity (acceleration terms on the left-hand side of Eqs. $(3.25) - (3.26)$). The relative significance is measured with the ratio β/Ro which is $\mathrm{O}(\Delta/Ro)$. Therefore, even though Δ is small the effect of change of the Coriolis parameter f can be important in approximations on scales where Ro is small too. The latter leads to so-called *β-plane approximation* in which the linear approximation for the Coriolis parameter is accepted

$$f(y) = 1 + \beta \, y. \tag{3.36}$$

On the other hand, when Ro is of order 1 then the variation in f can be ignored

$$f(y) \equiv 1, \tag{3.37}$$

and so-called *f-plane approximation* is obtained.

Therefore, under assumptions $(3.32) - (3.33)$ the tangent plane setting shown on Fig. 3.2 can be taken as the simplified setting for the problem. Eqs. $(3.25) - (3.29)$ are

transformed into

$$
\begin{aligned}
Ro\left(\frac{\partial u}{\partial t}+u\frac{\partial u}{\partial x}+v\frac{\partial u}{\partial y}+w\frac{\partial u}{\partial z}\right)+\frac{1}{\rho_0+Ro\,F\,\tilde{\rho}}\frac{\partial \tilde{p}}{\partial x} &= fv, && (3.38)\\
Ro\left(\frac{\partial v}{\partial t}+u\frac{\partial v}{\partial x}+v\frac{\partial v}{\partial y}+w\frac{\partial v}{\partial z}\right)+\frac{1}{\rho_0+Ro\,F\,\tilde{\rho}}\frac{\partial \tilde{p}}{\partial y} &= -fu, && (3.39)\\
\frac{\partial \tilde{p}}{\partial z} &= -\tilde{\rho}, && (3.40)\\
Ro\,F\left(\frac{\partial \tilde{\rho}}{\partial t}+u\frac{\partial \tilde{\rho}}{\partial x}+v\frac{\partial \tilde{\rho}}{\partial y}+w\frac{\partial \tilde{\rho}}{\partial z}\right)+w\frac{\partial \rho_0}{\partial z} &= 0, && (3.41)\\
\frac{\partial u}{\partial x}+\frac{\partial v}{\partial y}+\frac{\partial w}{\partial z} &= 0. && (3.42)
\end{aligned}
$$

Now that we have performed non-dimensionalization and provided the physical reasoning for it, proved the asymptotic validity of plane and hydrostatic approximations, with help of (3.19) and (3.23) we can recombine ρ_0 and $\tilde{\rho}$, p_0 and $\tilde{p}$ as

$$
Ro\,F\frac{\partial p}{\partial z}=\frac{\partial}{\partial z}\left(p_0'+Ro\,F\,\tilde{p}\right)=-\left(\rho_0+Ro\,F\,\tilde{\rho}\right)=-\rho \tag{3.43}
$$

in order to rewrite Eqs. $(3.38)-(3.43)$ in a more convenient form

$$
\begin{aligned}
Ro\left(\frac{\partial u}{\partial t}+u\frac{\partial u}{\partial x}+v\frac{\partial u}{\partial y}+w\frac{\partial u}{\partial z}\right)+\frac{1}{\rho}\frac{\partial p}{\partial x} &= fv, && (3.44)\\
Ro\left(\frac{\partial v}{\partial t}+u\frac{\partial v}{\partial x}+v\frac{\partial v}{\partial y}+w\frac{\partial v}{\partial z}\right)+\frac{1}{\rho}\frac{\partial p}{\partial y} &= -fu, && (3.45)\\
Ro\,F\frac{\partial p}{\partial z} &= -\rho, && (3.46)\\
\frac{\partial \rho}{\partial t}+u\frac{\partial \rho}{\partial x}+v\frac{\partial \rho}{\partial y}+w\frac{\partial \rho}{\partial z} &= 0, && (3.47)\\
\frac{\partial u}{\partial x}+\frac{\partial v}{\partial y}+\frac{\partial w}{\partial z} &= 0, && (3.48)
\end{aligned}
$$

where the Coriolis parameter f is given either by (3.37) or (3.36).

From here, the derivation of the *reduced gravity rotating shallow water (RGRSW) f-plane model* (relevant when $Ro\sim 1$, β effect is negligible) and *quasi-geostrophic (QG) β-plane model* (relevant when Ro is $\mathrm{O}(\Delta)$, β effect is important) will proceed differently. The two following sections are devoted to this.

3.4 RGRSW model on an f-plane

In the following three subsections RGRSW equations will be introduced. In order to obtain them we will replace the continuously stratified layer of fluid with two homogeneous layers

via vertical averaging and supplement the result with shallow water theory and rigid lid approximation.

RGRSW model will be used to simulate interaction of surface ocean currents with IGWs which is one of the main objectives of this work. As discussed in §1.1.2, the ocean is usually stably stratified. A realistic continuous function $\rho_0(z)$ would be difficult to handle mathematically but nontrivial stratification ($\rho_0(z) \neq \mathsf{const}$) is necessary for IGWs to be supported by the equations. So, we will content ourselves with a two-layer model that treats the main pycnocline $\rho_0(z)$ as a step function taking value ρ_2 in the upper layer and ρ_1 in the lower one ($\rho_2 < \rho_1$). We also assume the layers be immiscible. Then the sharp interface $z_1(x, y, t)$ separating the bulk of the fluid into 2 homogeneous layers at all times is introduced. The validity of this approximation is justified in the following subsection. Note also that one can obtain more complex $\mathtt{n}$-layer models when the stratification is approximated with $\mathtt{n} > 2$ homogeneous layers, however, they are not discussed in this thesis.

Observations suggest that fluid below the main thermocline moves much slower than that above it. Also, if the lower layer is sufficiently deep we can postulate that fluid is stagnant closer to the bottom. Hence, we will associate the thin upper layer with the surface current and the underlying one with heavier fluid at rest. We will refer to such a model which has one active layer only as *reduced gravity model* (or $\mathtt{1}^{1}\!/_{2}$-layer model). Generally, the assumption of motionless bottom layer transforms an $(\mathtt{n+1})$-layer model into $\mathtt{n}^{1}\!/_{2}$-layer (Fig. 3.3).

The setting as it is simplified so far includes two free surfaces $z_1(x, y, t)$ and $z_2(x, y, t)$. Hence, in addition to slowly oscillating IGWs the model inevitability supports the usual surface waves on $z_2(x, y, t)$ (Fig. 3.4). An effective way to get rid of these unnecessary waves is an assumption known as the *"rigid lid" approximation*. Within it the free surface $z_2(x, y, t)$ is replaced with a flat lid-like surface $z_2 = \mathsf{const}$ and its validity is justified in the third of the following subsections. There we show that rigid lid approximation does not change horizontal pressure gradients in all the layers. Moreover, we prove that both the free surface and the rigid lid are dynamically similar for IGWs. The latter is true due to the fact that surface and internal gravity waves virtually do not "feel" nor "affect" each other. Therefore, the original problem will be reduced to one with a flat upper boundary and a free internal boundary $z = z_1(x, y, t)$.

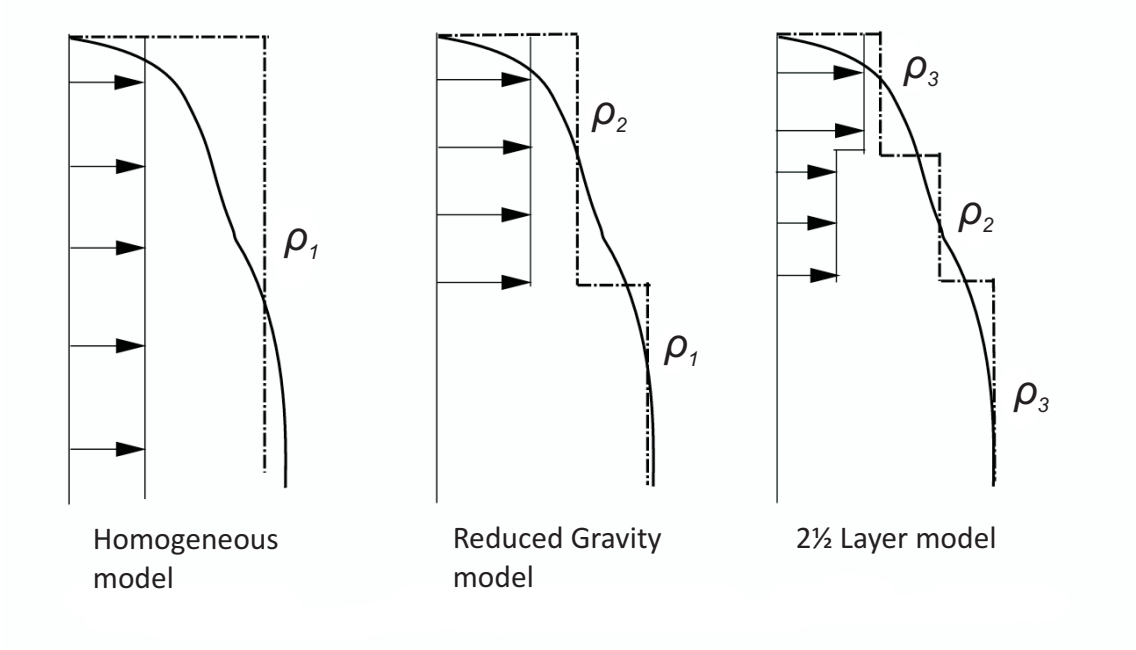

Figure 3.3: Comparison of basic layered models.

3.4.1 Vertical averaging and layered models

We expect motion in the thin layer of fluid $\delta = \frac{D}{L} \ll 1$ to be nearly horizontal with small variations of kinematic and dynamic characteristics in z-direction. Hence, a useful approximation can be obtained by smearing Eqs. $(3.44) - (3.48)$ along the z-direction over the regions separated by appropriate interfaces $z = z_i(x, y, t)$, $i = 0, 1, 2$ (see Fig. 3.5). The general approach of vertical averaging can be used to obtain the $\mathtt{n}$-layer approximation but for our purposes $\mathtt{n} = 2$ is sufficient.

It is not obvious at once whether the models that convert continuous function $\rho_0(z)$ into a piecewise constant one preserve important dynamical features. We take Eqs. $(3.44) - (3.45)$, $(3.47) - (3.48)$ as a starting point but rewrite them in a modified form

$$Ro\left(\frac{\partial(\rho u)}{\partial t} + \frac{\partial\left(\rho u^2\right)}{\partial x} + \frac{\partial(\rho uv)}{\partial y} + \frac{\partial(\rho uw)}{\partial z}\right) + \frac{\partial p}{\partial x} = \rho v, \tag{3.49a}$$

$$Ro\left(\frac{\partial(\rho v)}{\partial t} + \frac{\partial(\rho uv)}{\partial x} + \frac{\partial\left(\rho v^2\right)}{\partial y} + \frac{\partial(\rho vw)}{\partial z}\right) + \frac{\partial p}{\partial y} = -\rho u, \tag{3.49b}$$

$$\frac{\partial \rho}{\partial t} + \frac{\partial(\rho u)}{\partial x} + \frac{\partial(\rho v)}{\partial y} + \frac{\partial(\rho w)}{\partial z} = 0. \tag{3.49c}$$

The hydrostatics equation (3.46) allows to calculate pressure in an arbitrary internal point

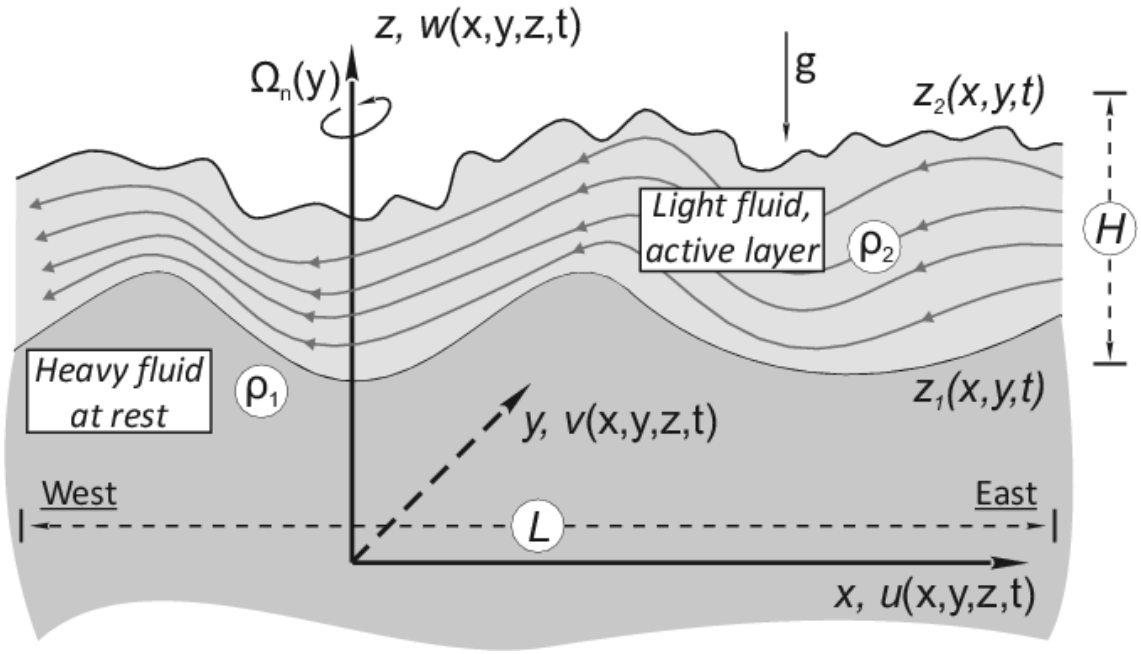

Figure 3.4: Surface current as a thin homogeneous active layer and a deep lower layer of heavier fluid at rest.

of a layer in terms of its position and pressure at the middle interface

$$p\left(x,y,z,t\right)=-\frac{1}{Ro\,F}\int_{z_1}^{z}\rho\left(x,y,z',t\right)\mathrm{d}z'+p|_{z_1}\,. \tag{3.50}$$

Here Eqs. (3.49a) – (3.49c) integrated between two material surfaces, say $z_1\left(x,y,t\right)$ and $z_2\left(x,y,t\right)$, yield

$$Ro\left(\frac{\partial}{\partial t}\int_{z_1}^{z_2}\rho u\mathrm{d}z+\frac{\partial}{\partial x}\int_{z_1}^{z_2}\rho u^2\mathrm{d}z+\frac{\partial}{\partial y}\int_{z_1}^{z_2}\rho uv\mathrm{d}z\right)-\int_{z_1}^{z_2}\rho v\mathrm{d}z= \\ =-\frac{\partial}{\partial x}\int_{z_1}^{z_2}p\mathrm{d}z-p|_{z_1}\frac{\partial z_1}{\partial x}+p|_{z_2}\frac{\partial z_2}{\partial x}, \tag{3.51}$$

$$Ro\left(\frac{\partial}{\partial t}\int_{z_1}^{z_2}\rho v\mathrm{d}z+\frac{\partial}{\partial x}\int_{z_1}^{z_2}\rho uv\mathrm{d}z+\frac{\partial}{\partial y}\int_{z_1}^{z_2}\rho v^2\mathrm{d}z\right)+\int_{z_1}^{z_2}\rho u\mathrm{d}z= \\ =-\frac{\partial}{\partial y}\int_{z_1}^{z_2}p\mathrm{d}z-p|_{z_1}\frac{\partial z_1}{\partial y}+p|_{z_2}\frac{\partial z_2}{\partial y}, \tag{3.52}$$

$$\frac{\partial}{\partial t}\int_{z_1}^{z_2}\rho\mathrm{d}z+\frac{\partial}{\partial x}\int_{z_1}^{z_2}\rho u\mathrm{d}z+\frac{\partial}{\partial y}\int_{z_1}^{z_2}\rho v\mathrm{d}z=0. \tag{3.53}$$

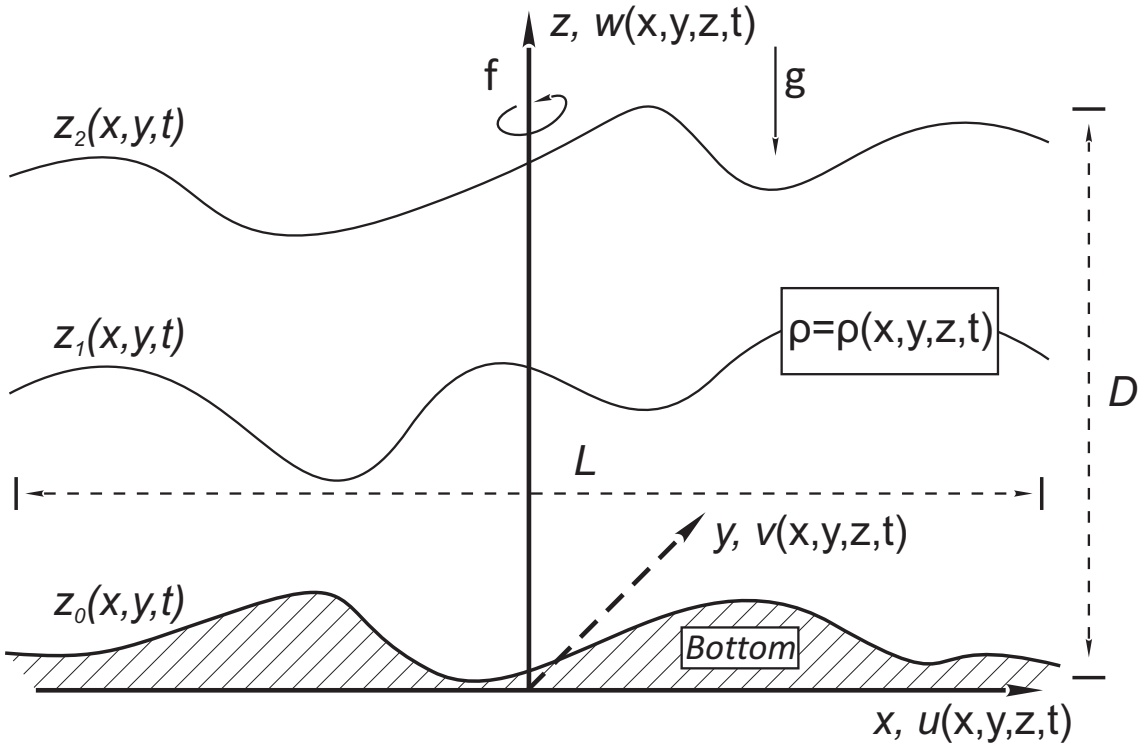

Figure 3.5: Averaging governing equations over two layers separated by arbitrary interface $z = z_1(x, y, t)$ with bottom topography $z = z_0(x, y, t)$ and free surface $z = z_2(x, y, t)$.

Eqs. (3.51) – (3.53) were obtain with use of Leibnitz formula for a function $\xi(z)$:

$$\int_{z_1}^{z_2} \frac{\partial \xi}{\partial x} \mathrm{d}z = \frac{\partial}{\partial x} \int_{z_1}^{z_2} \xi \mathrm{d}z - \xi|_{z_2} \frac{\partial z_2}{\partial x} + \xi|_{z_1} \frac{\partial z_1}{\partial x}, \tag{3.54}$$

and kinematic boundary conditions on the interfaces:

$$w|_{z_i} = \frac{\partial z_i}{\partial t} + u\frac{\partial z_i}{\partial x} + v\frac{\partial z_i}{\partial y}, \qquad i = 1, 2. \tag{3.55}$$

Averaging in the layer bounded by $z_0(x, y, t)$ and $z_1(x, y, t)$ can be performed similarly.

For convenience we introduce additional notation for the layer thickness, integrated and mean density:

$$h_i = z_i - z_{i-1}, \qquad \mu_i = \int_{z_{i-1}}^{z_i} \rho \mathrm{d}z, \qquad \bar{\rho}_i = \frac{\mu_i}{h_2}. \tag{3.56}$$

We define the vertical average of a quantity as

$$\langle\cdot\rangle_i = \frac{1}{\mu_i}\int_{z_{i-1}}^{z_i} (\rho\,\cdot)\,\mathrm{d}z. \tag{3.57}$$

With help of (3.56) – (3.57) Eqs. (3.51) – (3.53) transform into following equations for averages

$$Ro\left(\frac{\partial\left(\mu_2\langle u\rangle_2\right)}{\partial t} + \frac{\partial\left(\mu_2\left\langle u^2\right\rangle_2\right)}{\partial x} + \frac{\partial\left(\mu_2\langle uv\rangle_2\right)}{\partial y}\right) - \mu_2\langle v\rangle_2 = \\ = -\frac{\partial}{\partial x}\int_{z_1}^{z_2} p dz - p|_{z_1}\frac{\partial z_1}{\partial x} + p|_{z_2}\frac{\partial z_2}{\partial x}, \tag{3.58}$$

$$Ro\left(\frac{\partial\left(\mu_2\langle v\rangle_2\right)}{\partial t} + \frac{\partial\left(\mu_2\langle uv\rangle_2\right)}{\partial x} + \frac{\partial\left(\mu_2\left\langle v^2\right\rangle_2\right)}{\partial y}\right) + \mu_2\langle u\rangle_2 = \\ = -\frac{\partial}{\partial y}\int_{z_1}^{z_2} p dz - p|_{z_1}\frac{\partial z_1}{\partial y} + p|_{z_2}\frac{\partial z_2}{\partial y}, \tag{3.59}$$

$$\frac{\partial\mu_2}{\partial t} + \frac{\partial\left(\mu_2\langle u\rangle_2\right)}{\partial x} + \frac{\partial\left(\mu_2\langle v\rangle_2\right)}{\partial y} = 0. \tag{3.60}$$

To obtain a closed system of equations for the averages we introduce additional hypotheses. The first one is the widely used in the mean-field hydrodynamics hypothesis about decoupling of the averages

$$\left\langle u^2\right\rangle_i \approx \langle u\rangle_i\langle u\rangle_i, \qquad \langle uv\rangle_i \approx \langle u\rangle_i\langle v\rangle_i, \qquad \left\langle v^2\right\rangle_i \approx \langle v\rangle_i\langle v\rangle_i. \tag{3.61}$$

The second assumption proposes that mean density $\bar{\rho}_i(x,y,t)$ is nearly constant in each layer

$$\bar{\rho}_i(x,y,t) \approx \mathsf{const}. \tag{3.62}$$

The latter allows to rewrite the hydrostatics approximation (3.50) as (valid in layer 2)

$$p(x,y,z,t) \approx -\frac{\bar{\rho}_2}{Ro\,F}(z-z_1) + p|_{z_1}. \tag{3.63}$$

Substituting (3.61) and (3.63) into Eqs. (3.58)–(3.60) we obtain (the brackets of averaging

are omitted)

$$\bar{\rho}_2 h_2 \left(Ro \left(\frac{\partial u_2}{\partial t} + u_2 \frac{\partial u_2}{\partial x} + v_2 \frac{\partial u_2}{\partial y} \right) - v_2 \right) = \\ = -\frac{\partial}{\partial x} \left(-\frac{\bar{\rho}_2}{Ro\, F} \frac{h_2^2}{2} + p|_{z_1} h_2 \right) - p|_{z_1} \frac{\partial z_1}{\partial x} + p|_{z_2} \frac{\partial z_2}{\partial x}, \quad (3.64)$$

$$\bar{\rho}_2 h_2 \left(Ro \left(\frac{\partial v_2}{\partial t} + u_2 \frac{\partial v_2}{\partial x} + v_2 \frac{\partial v_2}{\partial y} \right) + u_2 \right) = \\ = -\frac{\partial}{\partial y} \left(-\frac{\bar{\rho}_2}{Ro\, F} \frac{h_2^2}{2} + p|_{z_1} h_2 \right) - p|_{z_1} \frac{\partial z_1}{\partial y} + p|_{z_2} \frac{\partial z_2}{\partial y}, \quad (3.65)$$

$$\frac{\partial h_2}{\partial t} + \frac{\partial \left(h_2 u_2 \right)}{\partial x} + \frac{\partial \left(h_2 v_2 \right)}{\partial y} = 0. \quad (3.66)$$

The latter then simplifies to

$$Ro \left(\frac{\partial u_2}{\partial t} + u_2 \frac{\partial u_2}{\partial x} + v \frac{\partial u_2}{\partial y} \right) - v_2 = -\frac{1}{\bar{\rho}_2} \frac{\partial \pi_2}{\partial x}, \quad (3.67)$$

$$Ro \left(\frac{\partial v_2}{\partial t} + u_2 \frac{\partial v_2}{\partial x} + v_2 \frac{\partial v_2}{\partial y} \right) + u_2 = -\frac{1}{\bar{\rho}_2} \frac{\partial \pi_2}{\partial y}, \quad (3.68)$$

$$\frac{\partial h_2}{\partial t} + \frac{\partial \left(h_2 u_2 \right)}{\partial x} + \frac{\partial \left(h_2 v_2 \right)}{\partial y} = 0, \quad (3.69)$$

where

$$\pi_2 = p|_{z_1} + \frac{\bar{\rho}_2}{Ro\, F} z_1. \quad (3.70)$$

Note that if pressure on upper(lower) interface is known from boundary conditions the hydrostatics allows to calculate pressure on lower(upper) surface

$$p|_{z_1} = p|_{z_2} + \frac{\bar{\rho}_2}{Ro\, F} \left(z_2 - z_1 \right), \quad (3.71)$$

and hence,

$$\pi_2 = p|_{z_1} + \frac{\bar{\rho}_2}{Ro\, F} z_1 = p|_{z_2} + \frac{\bar{\rho}_2}{Ro\, F} z_2. \quad (3.72)$$

Similar equations can be derived for the lower layer bounded by $z_0 \left(x, y, t \right)$ and $z_1 \left(x, y, t \right)$. In the next section the systems of equations (3.67) – (3.69) for both layers will be combined together to form the two-layer RSW equations. Classical rotating shallow water (RSW) equations for homogeneous fluid are obtained as its special case.

3.4.2 One- and two-layer RSW approximations

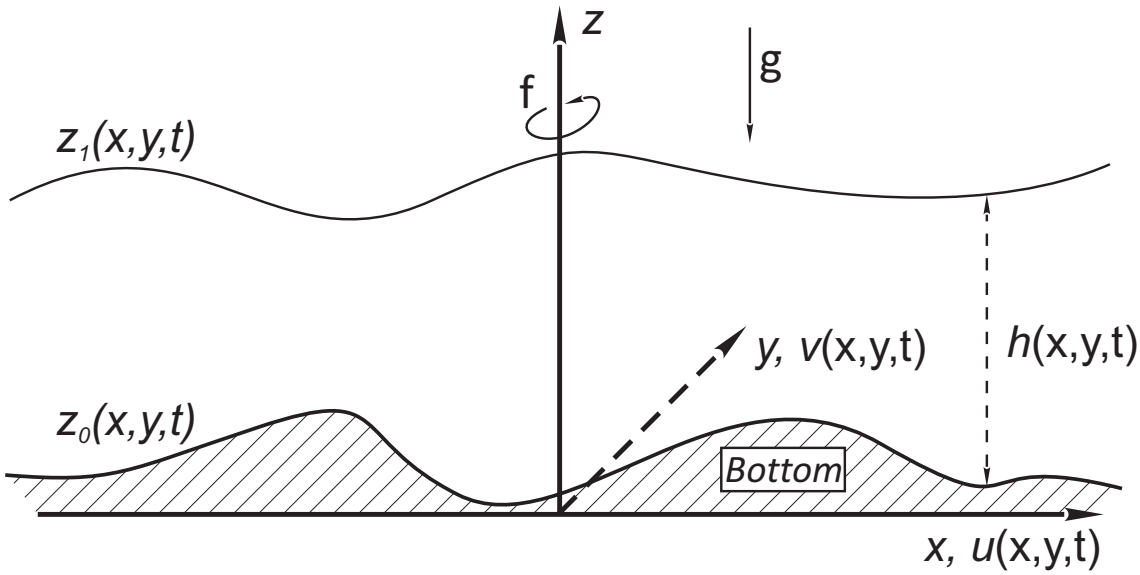

Figure 3.6: Single layer rotating shallow water model.

First, we write down RSW equations for 1 homogeneous layer with bottom topography presented on Fig. 3.6. The equations are obtained from Eqs. (3.67) – (3.69) using the condition at the free surface $p|_{z_1} = p_a$ (p_a stands for atmospheric pressure) and $h(x,y,t) = z_1(x,y,t) - z_0(x,y)$ as layer's thickness (unnecessary layer numbering is omitted)

$$Ro\left(\frac{\partial u}{\partial t} + u\frac{\partial u}{\partial x} + v\frac{\partial u}{\partial y}\right) - v + \frac{1}{Ro\,F}\frac{\partial(h+z_0)}{\partial x} = 0, \tag{3.73}$$

$$Ro\left(\frac{\partial v}{\partial t} + u\frac{\partial v}{\partial x} + v\frac{\partial v}{\partial y}\right) + u + \frac{1}{Ro\,F}\frac{\partial(h+z_0)}{\partial y} = 0, \tag{3.74}$$

$$\frac{\partial h}{\partial t} + \frac{\partial(hu)}{\partial x} + \frac{\partial(hv)}{\partial y} = 0, \tag{3.75}$$

where the scale for density in (3.18) is now chosen so that $\bar{\rho} = 1$. The system of 3 equations (3.73) – (3.75) must be resolved with respect to 3 unknowns $u(x,y,t)$, $v(x,y,t)$ and $h(x,y,t)$.

Two-layer RSW model (with flat bottom $z_0(x,y) = 0$) governs dynamics of the setting shown on Fig. 3.7. The equations are obtained when Eqs. (3.67) – (3.69) for both layers

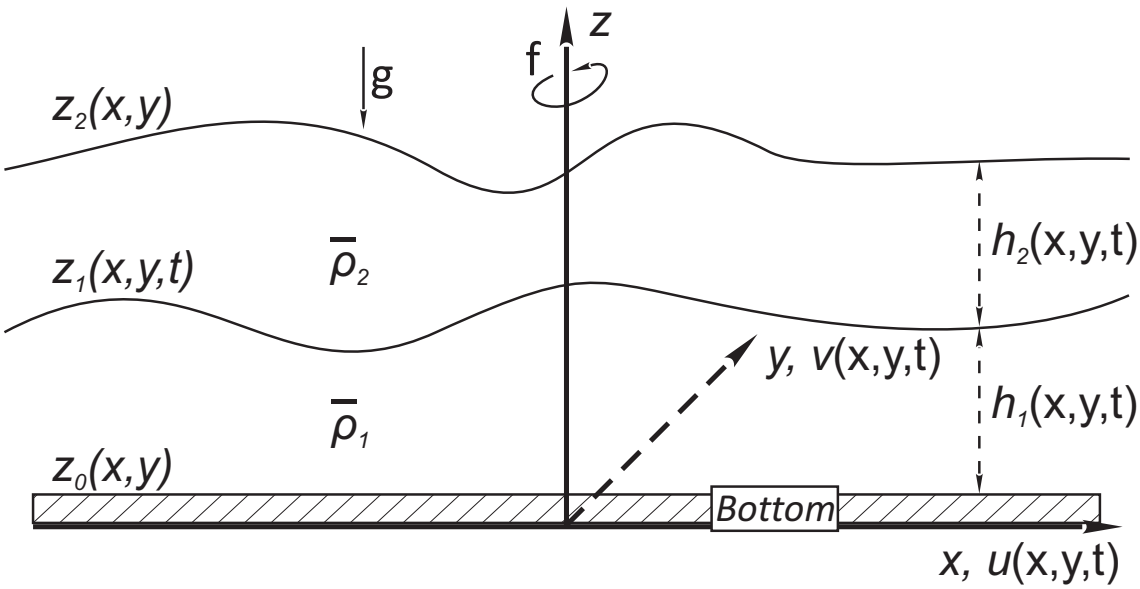

Figure 3.7: Two-layer rotating shallow water.

are written down simultaneously

$$Ro\left(\frac{\partial u_i}{\partial t}+u_i\frac{\partial u_i}{\partial x}+v_i\frac{\partial u_i}{\partial y}\right)-v_i+\frac{1}{\bar{\rho}_i}\frac{\partial \pi_i}{\partial x} = 0, \tag{3.76}$$

$$Ro\left(\frac{\partial v_i}{\partial t}+u_i\frac{\partial v_i}{\partial x}+v_i\frac{\partial v_i}{\partial y}\right)+u_i+\frac{1}{\bar{\rho}_i}\frac{\partial \pi_i}{\partial y} = 0, \tag{3.77}$$

$$\frac{\partial h_i}{\partial t}+\frac{\partial\left(h_i u_i\right)}{\partial x}+\frac{\partial\left(h_i v_i\right)}{\partial y} = 0, \tag{3.78}$$

where index $i=1,2$ tags the layer (the lower and upper respectively) to which quantities correspond to. To close the system of Eqs. (3.76) – (3.78) we will utilize dynamical conditions at the free surfaces $z_1(x,y,t)$ and $z_2(x,y,t)$.

Making use of comment (3.72) we write down expressions for π_i as

$$\pi_i = p|_{z_1}+\frac{\bar{\rho}_i}{Ro\,F}h_1. \tag{3.79}$$

Then the condition of continuity of pressure on the interface $z_1(x,y,t)$ yields

$$\pi_2 = \pi_1+\frac{\bar{\rho}_2-\bar{\rho}_1}{Ro\,F}h_1. \tag{3.80}$$

With help of Eq. (3.72) the free boundary condition at $z_2(x, y, t)$ can be written down as

$$\pi_2 = p_a + \frac{\bar{\rho}_2}{Ro\,F}(h_1 + h_2)\,. \tag{3.81}$$

Combining Eqs. (3.76) – (3.78) with (3.80) – (3.81) we obtain two-layer RSW equations. In the next subsection we will discuss how the free surface condition (3.81) can be replaced with so-called rigid lid condition. As the result, the two-layer RSW model simplifies to the RGRSW model (sometimes also referred to as 1½-layer model). We will see that the latter is mathematically identical to single-layer RSW model (3.73) – (3.75).

3.4.3 Rigid lid approximation

In this appendix we give grounds for the widely applied rigid lid approximation which replace the actual free ocean surface $z = \mu(x, y, t)$ with a flat surface $z = \text{const}$. We show that it is valid when the bottom layer is sufficiently thick to absorb small fluctuations propagating from the upper layers. This result can be obtained for an arbitrary number of layers but as we restrict ourselves to the simple case of the two-layer model.

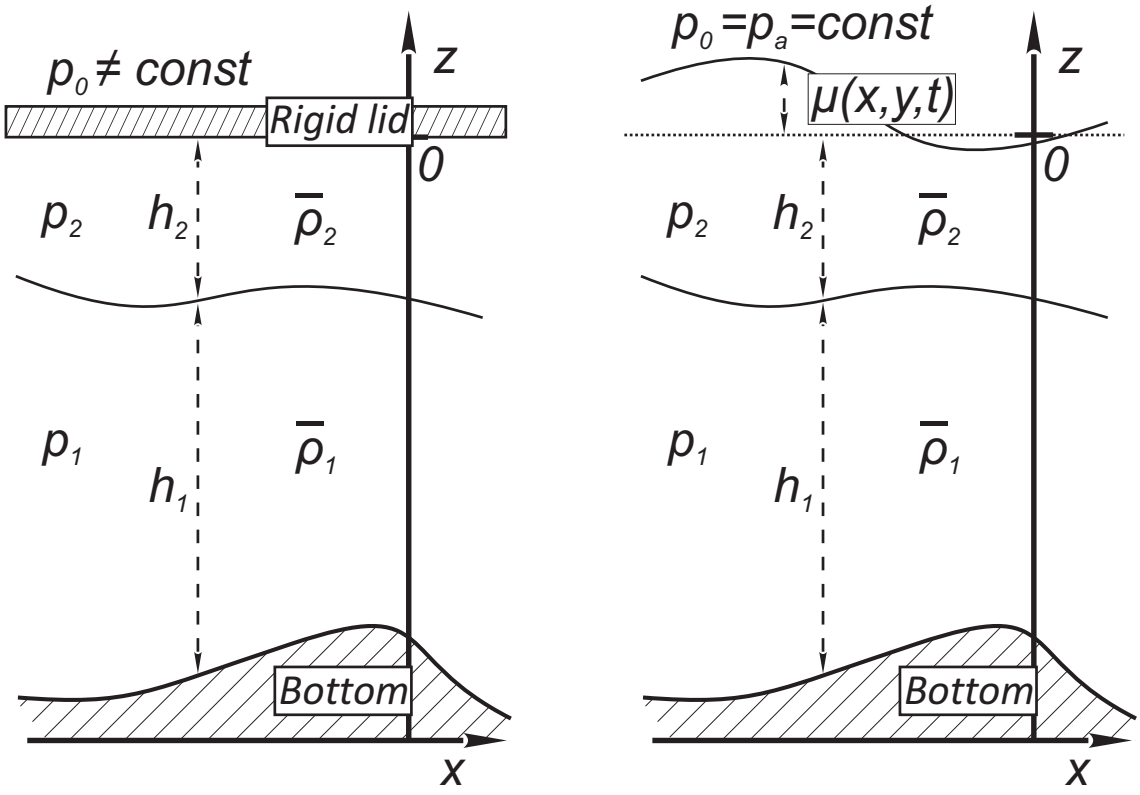

Figure 3.8: Multi-layer model with rigid lid and free surface.

Horizontal pressure gradients. Here we discuss how horizontal pressure gradients in layers differ between the two above-mentioned settings presented on Fig. 3.8. First of all, we consider the case of rigid lid approximation. Using assumption of hydrostatics (3.46) we obtain formulae for pressure in the layers:

$$p_2 = p_0 - \bar{\rho}_2 g z, \tag{3.82}$$

$$p_1 = p_0 + \bar{\rho}_2 g h_2 - \bar{\rho}_1 g \left(z + h_2\right). \tag{3.83}$$

Note that to make physics more clear we have temporary returned to dimensional variables. Expressions (3.82) – (3.83) include pressure at the lid p_0 which is unknown. But with assumption of the bottom layer being very thick and motionless ($\bar{\nabla} p_1 = 0$) this unknown can be eliminated

$$\bar{\nabla} p_0 = \left(\bar{\rho}_1 - \bar{\rho}_2\right) g \, \bar{\nabla} h_2, \tag{3.84}$$

where $\bar{\nabla}$ denotes the horizontal gradient operator. The latter formula is the same for the horizontal pressure gradients in the active layer $\bar{\nabla} p_2$. With help of the *reduced gravity coefficient* $g_r^* = \frac{\bar{\rho}_1 - \bar{\rho}_2}{\bar{\rho}_2} g$ introduced in (1.1) we rewrite the latter formulae as

$$\frac{1}{\bar{\rho}_2} \bar{\nabla} p_2 = g_r^* \, \bar{\nabla} h_2. \tag{3.85}$$

Next, we carry out the same calculations for a model with free upper material surface. As we integrate the hydrostatic equation downwards starting from the surface $z = \mu\left(x, y, t\right)$ we obtain

$$p_2 = p_a - \bar{\rho}_2 g \left(z - \mu\right), \tag{3.86}$$

$$p_1 = p_a + \bar{\rho}_2 g \left(h_2 + \mu\right) - \bar{\rho}_1 g \left(z + h_2\right), \tag{3.87}$$

where p_a is the atmospheric pressure (hence, $\bar{\nabla} p_a = 0$). As above, the unknown free surface elevation $\mu\left(x, y, t\right)$ can be eliminated if the bottom layer is stagnant. As the result we find

$$\bar{\nabla} p_2 = \left(\bar{\rho}_1 - \bar{\rho}_2\right) g \, \bar{\nabla} h_2, \tag{3.88}$$

which is exactly the same expression as in (3.84). Therefore, within rigid-lid approximation, dynamically important horizontal pressure gradients are identical to those in free surface model when lower layer is motionless.

Separation of surface and internal gravity waves. For a deep and motionless bottom layer Eqs. (3.76) – (3.77) become

$$\frac{\partial \pi_1}{\partial x} = 0, \qquad \frac{\partial \pi_1}{\partial y} = 0. \tag{3.89}$$

Hence, with help of condition (3.80) RSW Eqs. (3.76) – (3.78) for the top layer transform into

$$Ro\left(\frac{\partial u_2}{\partial t} + u_2\frac{\partial u_2}{\partial x} + v_2\frac{\partial u_2}{\partial y}\right) - v_2 - \frac{g'_r}{Ro\,F}\frac{\partial z_1}{\partial x} = 0, \tag{3.90}$$

$$Ro\left(\frac{\partial v_2}{\partial t} + u_2\frac{\partial v_2}{\partial x} + v_2\frac{\partial v_2}{\partial y}\right) + u_2 - \frac{g'_r}{Ro\,F}\frac{\partial z_1}{\partial y} = 0, \tag{3.91}$$

$$\frac{\partial\left(z_2 - z_1\right)}{\partial t} + \frac{\partial\left(\left(z_2 - z_1\right)u_2\right)}{\partial x} + \frac{\partial\left(\left(z_2 - z_1\right)v_2\right)}{\partial y} = 0, \tag{3.92}$$

where $g'_r = \frac{\bar{\rho}_1 - \bar{\rho}_2}{\bar{\rho}_2}$ is the non-dimensional reduced gravity.

Note that we could choose the following scales for L, U and D

$$L = R_d^i = \frac{\sqrt{g_r^* H_0^*}}{f_0^*}, \qquad U = \sqrt{g_r^* H_0^*}, \qquad D = H_0^*. \tag{3.93}$$

where R_d^i is the internal Rossby deformation radius introduced in (1.16) and H_0^* is the mean depth of the surface layer (asterisks indicate dimensional parameters). This choice entails that

$$Ro = 1, \qquad \frac{g'_r}{F} = 1, \tag{3.94}$$

as defined in §3.2 and, hence, Eqs. (3.90) – (3.92) become (index $'2'$ in u_2 and v_2 is omitted)

$$\frac{\partial u}{\partial t} + u\frac{\partial u}{\partial x} + v\frac{\partial u}{\partial y} - v = \frac{\partial z_1}{\partial x}, \tag{3.95}$$

$$\frac{\partial v}{\partial t} + u\frac{\partial v}{\partial x} + v\frac{\partial v}{\partial y} + u = \frac{\partial z_1}{\partial y}, \tag{3.96}$$

$$\frac{\partial\left(z_2 - z_1\right)}{\partial t} + \frac{\partial\left(\left(z_2 - z_1\right)u\right)}{\partial x} + \frac{\partial\left(\left(z_2 - z_1\right)v\right)}{\partial y} = 0, \tag{3.97}$$

The two free surfaces can support both surface and internal gravity waves. With use of Eqs. (3.95) – (3.97) we will investigate whether usual surface waves (which are ruled out by rigid-lid approximation) can influence internal gravity waves. We consider small

perturbations superposed on the motionless basic state

$$z_1(x,y,t) = -1 + \mu(x,y,t), \tag{3.98}$$

$$z_2(x,y,t) = \eta(x,y,t), \tag{3.99}$$

where $\eta(x,y,t)$ and $\mu(x,y,t)$ are small free surface elevations of the upper and lower interfaces. Eqs. (3.90) – (3.92) are linearized around the equilibrium

$$\frac{\partial u}{\partial t} - \frac{\partial \mu}{\partial x} = v, \tag{3.100a}$$

$$\frac{\partial v}{\partial t} - \frac{\partial \mu}{\partial y} = -u, \tag{3.100b}$$

$$\frac{\partial \eta}{\partial t} - \frac{\partial \mu}{\partial t} + \left(\frac{\partial u}{\partial x} + \frac{\partial v}{\partial y}\right) = 0. \tag{3.100c}$$

Cross-differentiation of first two yields

$$\left(\frac{\partial u}{\partial y} - \frac{\partial v}{\partial x}\right)_t = \left(\frac{\partial u}{\partial x} + \frac{\partial v}{\partial y}\right), \tag{3.101}$$

and divergence of these equations gives

$$\frac{\partial}{\partial t}\left(\frac{\partial u}{\partial x} + \frac{\partial v}{\partial y}\right) - \left(\frac{\partial^2 \mu}{\partial x^2} + \frac{\partial^2 \mu}{\partial y^2}\right) = -(u_y - v_x). \tag{3.102}$$

Combining equations (3.100c) – (3.102) we derive

$$\frac{\partial}{\partial t}\left(\frac{\partial^2}{\partial t^2} + 1\right)(\mu - \eta) - \frac{\partial}{\partial t}\left(\nabla^2 \mu\right) = 0. \tag{3.103}$$

We need to supplement (3.103) with another equation for μ and η. Eqs. (3.90) – (3.92) were obtained with help of pressure continuity (3.80) and assumption of a deep motionless bottom layer. Obviously, similar equations can be written for the air-water interface with help of condition (3.80) and the air above $z_2(x,y,t)$ playing the same role as the bottom motionless layer. Hence, we obtain

$$g_r' \frac{\partial}{\partial t}\left(\frac{\partial^2}{\partial t^2} + 1\right)(\mu - \eta) + \frac{\partial}{\partial t}\left(\nabla^2 \eta\right) = 0. \tag{3.104}$$

Density differences in the ocean rarely exceed 0.1%. Thus, the equality $g_r' = \frac{\rho_1 - \rho_2}{\rho_2} \ll 1$

allow us to simplify (3.103) – (3.104) to

$$\frac{\partial}{\partial t}\left(\frac{\partial^2}{\partial t^2}+1\right)h-\frac{\partial}{\partial t}\left(\nabla^2 h\right)=0, \tag{3.105}$$

where $h\left(x,y,t\right)=1+\eta\left(x,y,t\right)-\mu\left(x,y,t\right)$ is the total depth of the active layer. Latter we will see that Eq. (3.105) is identical to Eq. (4.8) governing free IGWs in RGRSW model derived under rigid lid approximation.

Physically this fact can be interpreted as separation of two types of waves. For instance, if we look for small amplitude plane wave solutions

$$\eta,\mu=\exp\left(i\left(\omega_{\eta,\mu}t-k_{\eta,\mu}x-l_{\eta,\mu}y\right)\right), \tag{3.106}$$

of Eqs. (3.103) – (3.104) we can find that dispersion relations for surface waves $\omega_\eta^2\left(k_\eta,l_\eta\right)$ and for IGWs $\omega_\mu^2\left(k_\mu,l_\mu\right)$ satisfy

$$\frac{\omega_\mu^2}{\omega_\eta^2}\approx\frac{\rho_1-\rho_2}{\rho_2}\ll 1. \tag{3.107}$$

So, frequencies and phase speeds of surface waves are much higher than those of IGWs. The two types of waves do not "feel" each other and can be separated.

3.4.4 RGRSW and one-layer RSW equations

Now we can finally derive the reduced gravity rotating shallow water (RGRSW) equations governing dynamics of the ocean consisting of a thin active upper layer and a deep lower layer on an f-plane. Since validity of the rigid lid approximation is established we can replace the two-layer setting shown on Fig. 3.5 with the one on Fig. 3.9.

As in (3.93) we use the following horizontal, vertical and velocity scales:

$$L=R_d^i=\frac{\sqrt{g_r^*H_0^*}}{f_0^*},\qquad D=H_0^*,\qquad U=C_0=\sqrt{g_r^*H_0^*}. \tag{3.108}$$

Here H_0^* is the mean depth of the upper layer. Internal Rossby deformation radius R_d^i represents the scale at which rotational and buoyancy effects are of equal importance. As we will observe later, constant C_0 is typical phase speed of IGWs in absence of rotation.

As discussed in §1.1.1 – 1.1.3 typical values of R_d and C_0 calculated according to (3.108) with $H_0^*\sim 500\,\mathrm{m}$, $g_r^*\sim 0.01\,\mathrm{m/s^2}$ and $f_0^*\sim 10^{-4}\,\mathrm{1/s}$ (corresponding central latitude

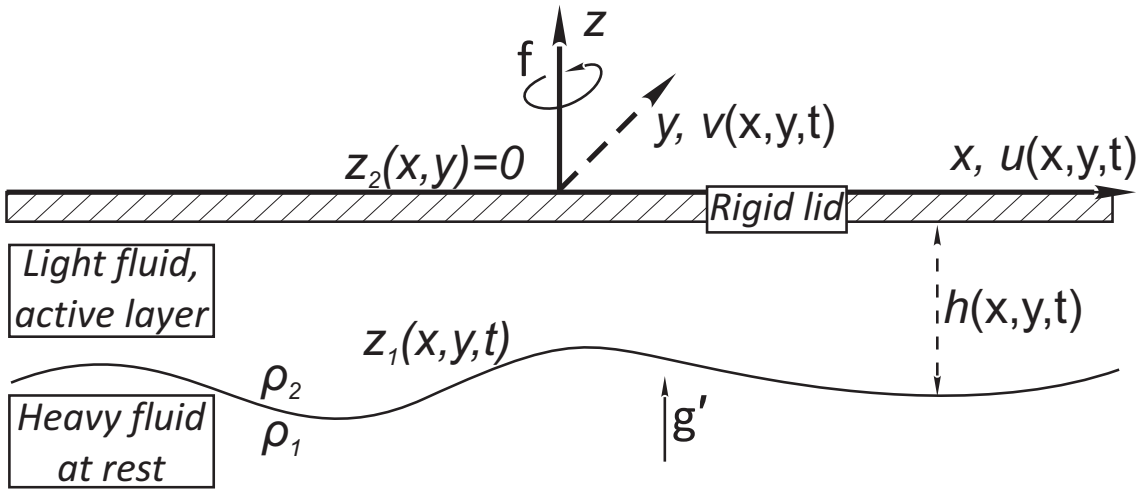

Figure 3.9: 1½-layer (reduced gravity) model with rigid lid approximation.

$\theta_0 \sim 45^\circ$) are

$$R_d^i \sim 20\,\mathrm{km}, \qquad U \sim 2\,\mathrm{m/s}. \tag{3.109}$$

These are in agreement with the observed widths, depths and speeds of the surface currents, such as the Gulf Stream and Kuroshio. Hence, characteristic scales (3.108) and resulting Eqs. (3.110) – (3.112) are suitable to study interaction of IGWs and large-scale surface ocean currents.

With use of the condition $z_2(x,y,t) = 0$, Eqs. (3.95) – (3.97) yield the RGRSW equations

$$\frac{\partial u}{\partial t} + u\frac{\partial u}{\partial x} + v\frac{\partial u}{\partial y} + \frac{\partial h}{\partial x} = v, \tag{3.110}$$

$$\frac{\partial v}{\partial t} + u\frac{\partial v}{\partial x} + v\frac{\partial v}{\partial y} + \frac{\partial h}{\partial y} = -u, \tag{3.111}$$

$$\frac{\partial h}{\partial t} + \frac{\partial (hu)}{\partial x} + \frac{\partial (hv)}{\partial y} = 0, \tag{3.112}$$

where $h(x,y,t)$ is the thickness of the upper layer. Equations for the bottom layer are trivial due to its motionless.

Note that the setting Fig. 3.9 is identical to the one representing 1 homogeneous layer with flat bottom. The analogy is visualized when we mentally turn Fig. 3.9 upside down. Moreover, classical RSW equations (3.73) – (3.75) for 1 homogeneous layer with the flat bottom $z_0(x,y) = \mathrm{const}$ are identical to the RGRSW equations (3.110) – (3.112). The only difference is in the scaling. Eqs. (3.73) – (3.75) simplify to Eqs. (3.110) – (3.112)

when usual gravity g replaces the reduced gravity g_r in (3.108)

$$L = R_d = \frac{\sqrt{g^* H_0^*}}{f_0^*}, \qquad D = H_0^*, \qquad U = c_0 = \sqrt{g^* H_0^*}, \tag{3.113a}$$

where Rossby deformation radius R_d represents the scale at which rotational effects are strong enough to compete with the full gravity g^* and constant c_0 is characteristic phase speed of gravity waves in absence of rotation. Hence, within this scaling Eqs. (3.110) – (3.112) can be used to model usual surface waves.

Tabs. 1.1 and 1.2 show that R_d is too large to be a suitable length scale for problems including modeling of the narrow surface currents, such as the Gulf Stream and Kuroshio. However, it might be useful for problems involving slow and wide surface currents, such as the Antarctic Circumpolar Current. Moreover, scaling (3.113a) might be appropriate in hydrodynamic problems coming from industry. One can imagine a setting where a thin layer of fluid with a free upper boundary exist on a rotating plane. Our results can be directly extended to such problems as the governing equations (3.110) – (3.112) remain exactly the same.

3.5 QG Approximation on a β-plane

In this section the quasi-geostrophic (QG) approximation will be introduced as an asymptotic simplification of the tangent β-plane model obtained in §3.3 when $Ro \ll 1$. Later it will be used to study interaction of ocean currents with large-scale Rossby waves.

As has been noted variations of the Coriolis parameter f with latitude can be important in approximations on scales when $Ro = \mathrm{O}(\Delta) \ll 1$. The definition of Rossby number (3.24) implies that we focus on motions whose time scales L/U are long compared to the time of Earth's revolution $1/f_0$. While non-constant density was necessary for IGWs to exist, Rossby waves are supported by the variability of the Coriolis parameter $f = 1 + \beta\, y$. For simplicity stratification effects are neglected, so the non-dimensional density is constant: $\rho \equiv 1$. Such assumption rules out any influence of baroclinicity and only allows for *barotropic* Rossby wave in the model.

We continue the derivations from where we left them as Eqs. (3.44) – (3.48). We assume that the free surface of the ocean in motion $\eta(x, y, t)$ is a perturbation the static surface is $\eta \equiv 0$. The bottom is assumed to be flat: $z_0(x, y, t) = -1$. Then the hydrostatics equation (3.46) yields

$$p = \frac{1}{Ro\, F}(\eta - z) + p_a. \tag{3.114}$$

Consequently, Eqs. (3.44) – (3.45), (3.47) – (3.48) can be written as

$$Ro\left(\frac{\partial u}{\partial t}+u\frac{\partial u}{\partial x}+v\frac{\partial u}{\partial y}+w\frac{\partial u}{\partial z}\right)+\frac{1}{Ro\,F}\frac{\partial \eta}{\partial x} = (1+\beta y)\,v, \tag{3.115}$$

$$Ro\left(\frac{\partial v}{\partial t}+u\frac{\partial v}{\partial x}+v\frac{\partial v}{\partial y}+w\frac{\partial v}{\partial z}\right)+\frac{1}{Ro\,F}\frac{\partial \eta}{\partial y} = -(1+\beta y)\,u, \tag{3.116}$$

$$\frac{\partial u}{\partial x}+\frac{\partial v}{\partial y}+\frac{\partial w}{\partial z} = 0. \tag{3.117}$$

where we used the beta approximation (3.36) for the Coriolis parameter f.

Forcing terms in (3.115) – (3.116) do not depend on z coordinate. This allows us to look for solution in the form

$$u=u\,(x,y,t)\,,\qquad v=v\,(x,y,t)\,. \tag{3.118}$$

Kinematic conditions at the free boundary and bottom are

$$w = \frac{\partial \eta}{\partial t}+u\frac{\partial \eta}{\partial x}+v\frac{\partial \eta}{\partial y}\qquad \text{at}\qquad z=\eta\,(x,y,t)\,, \tag{3.119a}$$

$$w = 0\qquad \text{at}\qquad z=-1. \tag{3.119b}$$

Hence, Eq. (3.117) can be replaced with its integrated with respect to z version

$$\frac{\partial \eta}{\partial t}+\frac{\partial\,(u\eta)}{\partial x}+\frac{\partial\,(v\eta)}{\partial y}+\left(\frac{\partial u}{\partial x}+\frac{\partial v}{\partial y}\right)=0. \tag{3.120a}$$

Observe that essentially Eqs. (3.115) – (3.116), (3.120a) are RSW equations (3.73) – (3.75) for a layer of thickness $h\,(x,y,t)=1+\eta\,(x,y,t)$ with flat bottom and $f=1+\beta\,y$ as the Coriolis parameter.

3.5.1 Geostrophic Approximation

We look for solutions of Eqs. (3.115) – (3.116), (3.120a) in asymptotic series in Ro and expand the unknowns u, v in the form

$$\xi=\xi_0+Ro\,\xi_1+Ro^2\,\xi_2\,\ldots, \tag{3.121}$$

and η as

$$\eta=Ro\left(\eta_0+Ro\,\eta_1+Ro^2\,\eta_2\,\ldots\right). \tag{3.122}$$

Note that $\eta\sim Ro$ is necessary for Eq. (3.115)–(3.116) to be consistent. This assumption of

the small elevation of the free surface is essential for the quasi-geostrophic approximation. Note that the more general RSW model does not require the variation of active-layer depth to be small unlike the QG model (remark that actually the current derivations take RSW equations as a starting point).

The leading order approximation to Eq. (3.115) – (3.116) is

$$\frac{1}{F}\frac{\partial \eta_0}{\partial x} = v_0, \tag{3.123}$$

$$\frac{1}{F}\frac{\partial \eta_0}{\partial y} = -u_0. \tag{3.124}$$

Recalling relationship (3.114) between surface elevation η and pressure p, Eqs. (3.123) – (3.124) should be recognized as the *geostrophic relation* in which the Coriolis force and pressure gradient balance each other. Hence, in this 0-order approximation fluid runs parallel to surface elevation contours (see Fig. 1.8).

Eqs. (3.123) – (3.124) imply that the geostrophic velocities u_0, v_0 are non-divergent and Eq. (3.120a) is automatically satisfied at this order

$$\frac{\partial u_0}{\partial x} + \frac{\partial v_0}{\partial y} = 0. \tag{3.125}$$

Therefore, the $\mathrm{O}(1)$ motion can be characterised by the stream function $\psi(x, y, t)$

$$\psi = \frac{\eta_0}{F}, \qquad u_0 = -\frac{\partial \psi}{\partial y}, \qquad v_0 = \frac{\partial \psi}{\partial x}. \tag{3.126}$$

Note that Eqs. (3.123) – (3.124) are not sufficient to determine the solution u_0, v_0, η_0 but rather give the necessary condition that the leading order motion is in geostrophic balance. To close the system we need to consider the next order approximation.

3.5.2 QG vorticity Equation

The $\mathrm{O}(Ro)$ terms in Eqs. (3.115) – (3.117) yield

$$\frac{\partial u_0}{\partial t} + u_0\frac{\partial u_0}{\partial x} + v_0\frac{\partial u_0}{\partial y} + \frac{1}{F}\frac{\partial \eta_1}{\partial x} = v_1 + \beta' y\, v_0, \tag{3.127}$$

$$\frac{\partial v_0}{\partial t} + u_0\frac{\partial v_0}{\partial x} + v_0\frac{\partial v_0}{\partial y} + \frac{1}{F}\frac{\partial \eta_1}{\partial y} = -u_1 - \beta' y\, u_0, \tag{3.128}$$

$$\frac{\partial \eta_0}{\partial t} + u_0\frac{\partial \eta_0}{\partial x} + v_0\frac{\partial \eta_0}{\partial y} + \left(\frac{\partial u_1}{\partial x} + \frac{\partial v_1}{\partial y}\right) = 0. \tag{3.129}$$

where $\beta' = \beta/Ro = (\Delta/Ro)\cot\theta_0$ is an $\mathrm{O}(1)$ parameter. The velocities u_1 and v_1 are first order ageostrophic corrections to the geostrophic motion u_0, v_0 and their divergence differs from zero

$$\frac{\partial\left(\nabla^2\psi\right)}{\partial t} + \frac{\partial\psi}{\partial x}\frac{\partial\left(\nabla^2\psi\right)}{\partial y} - \frac{\partial\psi}{\partial y}\frac{\partial\left(\nabla^2\psi\right)}{\partial x} = -\left(\frac{\partial u_1}{\partial x} + \frac{\partial v_1}{\partial y}\right) - \beta'\frac{\partial\psi}{\partial x}, \tag{3.130}$$

where we used the stream function representation (3.126). With help of Eq. (3.129) we rewrite Eq. (3.130) in the closed form as

$$\frac{\partial\left(\nabla^2\psi - F\,\psi\right)}{\partial t} + \frac{\partial\psi}{\partial x}\frac{\partial\nabla^2\psi}{\partial y} - \frac{\partial\psi}{\partial y}\frac{\partial\nabla^2\psi}{\partial x} + \beta'\frac{\partial\psi}{\partial x} = 0, \tag{3.131}$$

which is traditionally referred to as *QG vorticity equation*. It governs geostrophically balanced motions on the β-plane.

One can show that Eq. (3.131) is a statement of conservation for the quantity known as *potential vorticity (PV)* (Pedlosky [71]). Within the QG β-plane model PV is given by the formula

$$Q_g = \nabla^2\psi - F\,\psi + f. \tag{3.132}$$

In this sum the first term is due to the relative vorticity of the flow. The second represents contribution of the free surface variation (proportional to ψ) and its importance is measured by the parameter F. And the last term is the the background PV due to planetary rotation.

Now lets look at the magnitudes of non-dimensional parameters appearing above when calculated for the major surface currents (note, that we take $\theta_0 \sim 45^\circ$, hence, $f_0^* \sim 10^{-4}\,1/\mathrm{s}$). The typical parameter values given in Tabs. 1.1 and 1.2 suggest two typical scenarios and the following conclusions:

- The QG β-plane model is inappropriate for modelling dynamics of fast and narrow surface currents, such as the Gulf Stream and Kuroshio, in mid-latitudes:
  - condition $Ro \sim \Delta$ is hardly satisfied and $\beta' = (\Delta/Ro)\cot\theta_0 \sim 0.03$, so β-effects and Rossby waves can be neglected,
  - parameter $F \sim 0.005$, *i.e.* L is small compared to R_d.
- Dynamics of slow and wide surface currents, such as the Antarctic Circumpolar Current, can be well captured by the discussed model:
  - condition $Ro \sim \Delta$ is satisfies and $\beta' = (\Delta/Ro)\cot\theta_0 \sim 10$,

– parameter $F \sim 0.5$, *i.e.* the horizontal length scale L is of the same order as the Rossby radius R_d.

A useful simplification of Eq. (3.131) emerge when $L \ll R_d$ (F is small).

$$\frac{\partial \nabla^2 \psi}{\partial t} + \frac{\partial \psi}{\partial x}\frac{\partial \nabla^2 \psi}{\partial y} - \frac{\partial \psi}{\partial y}\frac{\partial \nabla^2 \psi}{\partial x} + \beta' \frac{\partial \psi}{\partial x} = 0. \tag{3.133}$$

This QG model is then referred to as "non-divergent" (as opposed to the original equation being "divergent"). Note that $\eta \sim Ro\, F$ must hold for equations to be consistent and hence, the elevation of the free surface is exceptionally small and has negligible influence on the dynamics. Thus, if Rossby deformation radius is infinite then free surface is effectively flat (*i.e.* the rigid lid approximation) Fluid motion becomes two-dimensional and, hence, *barotropic*. Consequently, Rossby waves found within the framework of Eq. (3.131) are traditionally referred to as barotropic Rossby waves.

Chapter 4

Gravity Wave Scattering by Zonal Jets on the f-plane

Here we consider scattering of small amplitude internal gravity waves (IGWs) by surface currents within the framework of the reduced gravity rotating shallow water (RGRSW) model for the rotating ocean. The current is represented by a zonal jet in geostrophic balance which is an approximation for the zonal parts of the major world ocean current systems (the zonal Kuroshio extension, Gulf Stream extension, and Antarctic Circumpolar Current, see [23]).

The governing scattering equation (4.21) contains two types of singularities. One is so-called *apparent singularity* which does not give rise to actual singular behaviour of the solution. The other one, so-called *critical layer singularity*, plays crucial role in wave-flow interaction theory because at such points wave energy can be transferred to or extracted from the mean flow or vice-versa. The last case is sometimes referred to as "over-reflection" or "over-transmission" when the incident wave gives rise to, respectively, a reflected or transmitted wave with amplitudes greater than that of the incident wave. We solve the problem numerically and obtain the coefficients of reflection and transmission as functions of wavenumber.

We find that in some cases over-reflection and over-transmission can be infinitely strong, *i.e.* jets can spontaneously emit IGWs. This is so-called *resonant over-reflection* where within linear theory reflected and transmitted waves exist without the incoming incident one. For the first time, resonant over-reflection was found within the framework of the RGRSW model. The generation mechanism is proposed based on the analogy with the Schrödinger equation governing scattering of quantum particles by a potential and,

hence, the phenomena is given a physical explanation. In the last section we summarize and discuss the results.

4.1 Introduction

4.1.1 Surface currents in geostrophic balance

In section 1.1 we discussed the data of oceanographic observations and in §3.5.2 we presented the mathematical reasonings (leading order asymptotics for $Ro \ll 1$) all of which support the fact that major surface currents in the ocean are largely in geostrophic balance. Eqs. $(3.110) - (3.112)$ which govern the dynamics of fluid within the RGRSW model also admit a steady zonal geostrophic current as a solution

$$u\left(x,y,t\right) = U\left(y\right), \qquad v\left(x,y,t\right) = 0, \qquad h\left(x,y,t\right) = H\left(y\right), \tag{4.1}$$

regardless of the fact that $Ro = 1$ (unlike QG assumption $Ro \ll 1$). For the flow of the form (4.1) RSW equations impose the geostrophy condition

$$\frac{\mathrm{d}H}{\mathrm{d}y} = -U. \tag{4.2}$$

The zonal current, by definition, is homogeneous in x-direction. We will consider jet-like currents with natural condition at infinity

$$H\left(y\right) \to H_{\pm}, \qquad U\left(y\right) \to 0 \qquad \text{as } y \to \pm\infty, \tag{4.3}$$

where

$$H_{+} = H_{-} - \int_{-\infty}^{+\infty} U\left(y\right)\,\mathrm{d}y. \tag{4.4}$$

We restrict ourselves to the case of single-extremum but not necessarily symmetric jets. The unique extremum point is placed at the origin $y = 0$. Thus, function $U(y)$ is monotonous on $(-\infty; 0)$ and $(0; +\infty)$ and either positive or negative everywhere. The resulting thickness profile $H\left(y\right)$ is a smooth monotonous step function. Hence, a bell-shaped meridionally localised jet $U\left(y\right)$ like the one on Fig. 4.1 induces upwelling of the interface between the active and stagnant layers according to Eq. (4.2). For fast currents like the Gulf Stream these deviations of the interface can be of the same order as layer thickness.

Even though purely zonal geostrophic currents are rarely found in the ocean we take

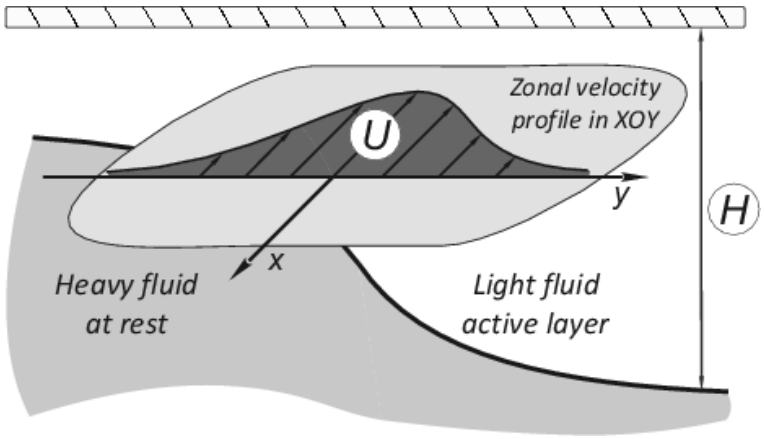

Figure 4.1: Interface elevation induced by the geostrophic current.

(4.1) as a reasonable approximation for the basic flow. The observed deviations such as nonzonality and ubiquitous turbulent eddies are not taken into account in this study.

4.1.2 Free inertia-gravity waves

Away from the jet core the fluid layer is motionless and of constant thickness H_0. Consider small amplitude perturbations of this state, *i.e.* look for a solution of the RGRSW equations (3.110) – (3.112) in the form

$$u = \varepsilon\,\tilde{u}, \qquad v = \varepsilon\,\tilde{v}, \qquad h = H_0 + \varepsilon\,\tilde{h}, \tag{4.5}$$

where ε is small. In these notations the linearized RSW equations are

$$\frac{\partial u}{\partial t} + \frac{\partial h}{\partial x} = v, \tag{4.6a}$$

$$\frac{\partial v}{\partial t} + \frac{\partial h}{\partial y} = -u, \tag{4.6b}$$

$$\frac{\partial h}{\partial t} + H_0\left(\frac{\partial u}{\partial x} + \frac{\partial v}{\partial y}\right) = 0. \tag{4.6c}$$

Cross-differentiating Eqs. (4.6a) – (4.6b) one can relate u and v to h

$$\frac{\partial^2 u}{\partial t^2} + u = -\frac{\partial^2 h}{\partial x\,\partial t} - \frac{\partial h}{\partial y}, \tag{4.7a}$$

$$\frac{\partial^2 u}{\partial t^2} + v = -\frac{\partial^2 h}{\partial y\,\partial t} + \frac{\partial h}{\partial x}, \tag{4.7b}$$

and reduce the system to a single equation for h

$$\left(\frac{\partial^2}{\partial t^2}+1\right)h - H_0\,\nabla^2 h = 0. \tag{4.8}$$

This equation has harmonic wave solutions in the form

$$h = h_0 \cos\left(kx + ly - \omega t\right) \tag{4.9}$$

which parameters satisfy

$$\omega^2 = 1 + H_0\left(k^2 + l^2\right), \tag{4.10}$$

where (k,l) is the horizontal wave vector and $\omega\,(k,l)$ is the wave frequency. Note that if there were no rotation, free IGWs in RGRSW model would be non-dispersive. However, this is not the case and the *dispersion relation* (4.10) indicates that the frequency has a minimum value of ± 1 (corresponds to $\pm f_0$ in the physical space). Substituting formula (4.9) into (4.7a) – (4.7b) we obtain the relations (after aligning the x-axis with the wave vector)

$$u = \frac{h_0}{H_0}\frac{\omega}{\hat{k}}\cos\left(\hat{k}\hat{x} - \omega t\right), \tag{4.11a}$$

$$v = \frac{h_0}{H_0}\frac{1}{\hat{k}}\sin\left(\hat{k}\hat{x} - \omega t\right), \tag{4.11b}$$

where $\hat{x}$ and $\hat{k}$ are the transformed x-coordinate and wavenumber. So, as the wave progresses the velocity vector traces an ellipse in the $x-y$-plane whose major axis is in the direction of the wave vector.

Typically, an arbitrary smooth disturbance $h\,(x,y,t)$ can be written in form of Fourier integral (note that we specified $\operatorname{sign}(\omega)$):

$$h\,(x,y,t) = \operatorname{Re}\left(\int\int C_{k,l}\,\exp\left(\mathrm{i}\mathbf{k}\cdot\mathbf{x} - \mathrm{i}\sqrt{1+H_0\,|\mathbf{k}|^2}\,t\right)\,\mathrm{d}k\,\mathrm{d}l\right), \tag{4.12}$$

where $\mathbf{k} = (k,l)$ and $\mathbf{x} = (x,y)$. This approach to separate the perturbation into an ensemble of plane waves with help of Fourier integral (4.12) is convenient. However, in reality an initially localized disturbance gets spread out with time due to the dispersive nature of the medium. This process is described with help of the concept of a *wave packet*. The original disturbance is represented as a superposition of an infinite number of packets of constant wavenumber, each propagating with its group velocity (LeBlond and Mysak [50]).

Within the RGRSW model the dispersion relation (4.10) entails the following formulae

for IGW group velocity in calm water $\vec{c}_{gr}$:

$$c_{gr}^{(x)} = \frac{\partial \omega}{\partial k} = \frac{H_0 k}{\sqrt{1 + H_0 \left(k^2 + l^2\right)}}, \qquad c_{gr}^{(y)} = \frac{\partial \omega}{\partial l} = \frac{H_0 l}{\sqrt{1 + H_0 \left(k^2 + l^2\right)}}. \tag{4.13}$$

Hence, the group velocity which defines the direction of energy propagation is aligned with the wave vector and

$$\operatorname{sign}\left(c_{gr}^{(x)}\right) = \operatorname{sign}\left(k\right), \qquad \operatorname{sign}\left(c_{gr}^{(y)}\right) = \operatorname{sign}\left(l\right).$$

Note that the velocity reaches its maximum group $|\vec{c}_{gr}| = \sqrt{H_0}$ for short waves and tends to 0 for long waves. Finally, the group velocity of a wave packet should not be confused with the phase velocity of a monochromatic wave $\vec{c}_{ph}$ which in this case is

$$c_{ph}^{(x)} = \frac{\omega}{k} = \frac{\sqrt{1 + H_0 \left(k^2 + l^2\right)}}{k}, \qquad c_{ph}^{(y)} = \frac{\omega}{l} = \frac{\sqrt{1 + H_0 \left(k^2 + l^2\right)}}{l}. \tag{4.14}$$

Now we can consider a situation when IGWs originate in the calm regions far from the mean flow (regions $y \to \pm\infty$). They will propagate either towards to or away from the the jet. However, only incident waves whose group velocities are directed towards the mean flow are of interest to us. In particular, waves originating at $y = -\infty\,(+\infty)$ propagate towards the jet when $l > 0$ ($l < 0$).

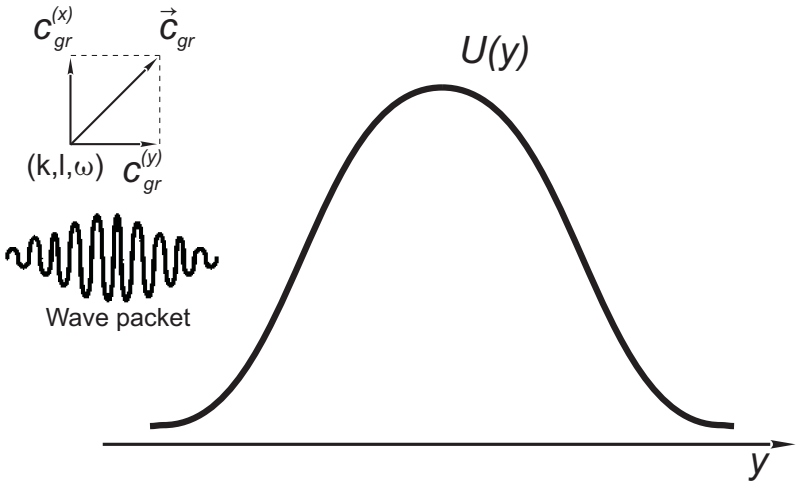

Figure 4.2: Velocity profile $U\left(y\right)$ of the jet and an IGW packet propagating with group speed $\vec{c}_{gr}$ towards the former.

The waves do not encounter any boundaries or obstacles except the zonal jet and after

penetrating through can propagate freely away. A sketch of the wave-mean flow interaction problem and a typical velocity profile $U(y)$ of a zonal current is outlined on Fig. 4.2.

4.2 Scattering equation

We consider the problem of propagation of internal gravity waves through a zonal jet. Hence, small disturbances are imposed upon the basic state specified by Eq. (4.1)

$$u(x,y,t) = U(y) + \varepsilon\,\tilde{u}(x,y,t), \tag{4.15a}$$

$$v(x,y,t) = \varepsilon\,\tilde{v}(x,y,t), \tag{4.15b}$$

$$h(x,y,t) = H(y) + \varepsilon\,\tilde{h}(x,y,t). \tag{4.15c}$$

Assuming the fluctuations are of small amplitudes ε one can substitute Eqs. (4.15a) – (4.15c) into Eqs. (3.110) – (3.112) and subsequently linearize them by discarding terms proportional to ε^2. The resulting system is

$$\frac{\partial\tilde{u}}{\partial t} + U\frac{\partial\tilde{u}}{\partial x} + U'\tilde{v} + \frac{\partial\tilde{h}}{\partial x} = \tilde{v}, \tag{4.16a}$$

$$\frac{\partial\tilde{v}}{\partial t} + U\frac{\partial\tilde{v}}{\partial x} + \frac{\partial\tilde{h}}{\partial y} = -\tilde{u}, \tag{4.16b}$$

$$\frac{\partial\tilde{h}}{\partial t} + \frac{\partial\left(U\tilde{h} + \tilde{u}H\right)}{\partial x} + \frac{\partial\left(\tilde{v}H\right)}{\partial y} = 0, \tag{4.16c}$$

where prime denotes differentiation with respect to y.

The coefficients of the system of linear PDEs (4.16a) – (4.16c) are independent of x and t, depending only on y. Hence, one can find solutions with dependence on the former two variables reduced to an exponential multiplier. Then, the solution of Eqs. (4.16a) – (4.16c) is represented in the form of Fourier integral

$$\zeta(x,y,t) = \mathrm{Re}\left(\int\int \hat{\zeta}_{k,\omega}(y)\,\mathrm{e}^{\mathrm{i}kx-\mathrm{i}\omega t}\,\mathrm{d}k\,\mathrm{d}\omega\right), \tag{4.17}$$

where $\zeta(x,y,t)$ denotes either of the functions $\tilde{u}$, $\tilde{v}$ and $\tilde{h}$. Function $\hat{\zeta}_{k,\omega}(y)$ describes the scattering of an incident unitary wave with parameters k and ω by the background flow.

Formula (4.17) contains a simple physical notion that during the interaction with a zonal flow free waves oncoming from infinities preserve their latitudinal wavenumbers k and frequencies ω. At the same time, the meridional wavenumber l of a wave disturbance can only be defined far from the shear and differs at $y \to \pm\infty$.

Substitution of a single mode (4.18)

$$\tilde{u} = \mathrm{Re}\left[\hat{u}(y)\ \mathrm{e}^{\mathrm{i}kx-\mathrm{i}\omega t}\right], \qquad \tilde{v} = \mathrm{Re}\left[\hat{v}(y)\ \mathrm{e}^{\mathrm{i}kx-\mathrm{i}\omega t}\right], \qquad \tilde{h} = \mathrm{Re}\left[\hat{h}(y)\ \mathrm{e}^{\mathrm{i}kx-\mathrm{i}\omega t}\right], \quad (4.18)$$

into Eqs. (4.16a) – (4.16c) yields (omitting the hats)

$$\mathrm{i}\,(kU-\omega)\,u + \left(U'-1\right)v + \mathrm{i}kh = 0, \quad (4.19a)$$

$$\mathrm{i}\,(kU-\omega)\,v + u + h' = 0, \quad (4.19b)$$

$$\mathrm{i}\,(kU-\omega)\,h + \mathrm{i}kHu + (Hv)' = 0. \quad (4.19c)$$

Resolving Eqs. (4.19a)–(4.19b) with respect to u and v and substituting resulting formulae

$$u = \frac{k\,(\omega-kU)\,h - (U'-1)\,h'}{(\omega-kU)^2 + (U'-1)}, \quad (4.20a)$$

$$v = -i\frac{kh + (\omega-kU)\,h'}{(\omega-kU)^2 + (U'-1)}, \quad (4.20b)$$

into Eq. (4.19c) we obtain a single 2^{nd} order ODE governing the surface height perturbation mode h

$$\left(Fh'\right)' + \left(\frac{kF'}{\omega-kU} - k^2F + 1\right)h = 0, \quad (4.21)$$

where

$$F = \frac{H}{(\omega-kU)^2 - 1 + U'}. \quad (4.22)$$

4.2.1 Boundary conditions

The scattering problem (4.21) under consideration should be supplemented with boundary conditions at $y \to \pm\infty$. In the limit $y \to \pm\infty$ the Eq. (4.21) simplifies to

$$h_{yy} + l_\pm^2\,h = 0, \quad (4.23)$$

where $l_\pm$, defined by

$$l_\pm^2 = \frac{\omega^2-1}{H_\pm} - k^2, \quad (4.24)$$

are the y-wavenumbers at the two sides of the jet. Hence, far from the jet's core the solutions turn into free propagating IGWs (if $l_{\pm\infty}^2 > 0$). Essentially, formula (4.24) is the dispersion relation (4.10) for free IGWs.

Formula (4.24) implies that knowing two characteristics k and ω of the harmonic allows

us to find the "secondary" parameters $l_\pm$. However, the boundary conditions are easier formulated using the wave vector $(k, l_\pm)$ of the incident wave as the primal parameter (for waves incoming from $\pm\infty$ respectively). The two meridional wavenumbers are related by the formula

$$l_+ = \sqrt{\frac{H_- l_-^2 - (H_+ - H_-)\, k^2}{H_+}}. \tag{4.25}$$

Note that the right hand side of (4.25) can give complex-valued numbers, say, if l_- is small and $H_+ > H_-$. It entails that not all the waves propagating from the infinity where the layer is shallower can penetrate the jet barrier and reach the opposite side. This can be better understood with help of the dispersion relation (4.10). As mentioned above, a cross-jet propagating wave retains its k and ω parameters while l is adjusted to satisfy the the dispersion relation. The latter can become complex $l_{\pm\infty}^2 < 0$ in which case the appropriate sign of $\operatorname{Im} l_+$ is chosen to ensure decays at $y \to +\infty$. Note that for l_+ to be real, the following condition must hold

$$|l_-| \geq |k| \sqrt{\frac{H_+}{H_-} - 1}. \tag{4.26}$$

Without loss of generality we consider an IGW of unit amplitude incident upon the zonal current from $y \to -\infty$. It gives rise to a reflected wave propagating towards $y \to -\infty$ and transmitted wave at $y \to +\infty$ as shown on Fig. 4.3. Then, the boundary conditions for the scattering problem are

$$\left.\begin{aligned} h &\to \mathrm{e}^{\mathrm{i}l_- y} + r_{k,l}\, \mathrm{e}^{-\mathrm{i}l_- y} && \text{as } y \to -\infty, \\ h &\to t_{k,l}\, \mathrm{e}^{\mathrm{i}l_+ y} && \text{as } y \to +\infty, \end{aligned}\right\} \tag{4.27}$$

where $r_{k,l}$ and $t_{k,l}$ are coefficients of reflection and transmission. Although, if inequality (4.26) is not satisfied and l_+ is imaginary we impose the decay condition at $y \to +\infty$

$$\left.\begin{aligned} h &\to \mathrm{e}^{\mathrm{i}l_- y} + r_{k,l}\, \mathrm{e}^{-\mathrm{i}l_- y} && \text{as } y \to -\infty, \\ h &\to t_{k,l}\, \mathrm{e}^{-|l_+| y} && \text{as } y \to +\infty. \end{aligned}\right\} \tag{4.28}$$

So, Eq. (4.21) together with (4.27) or (4.28) form a well-posed boundary-value problem which determines r and t together with the mode $h\,(y)$.

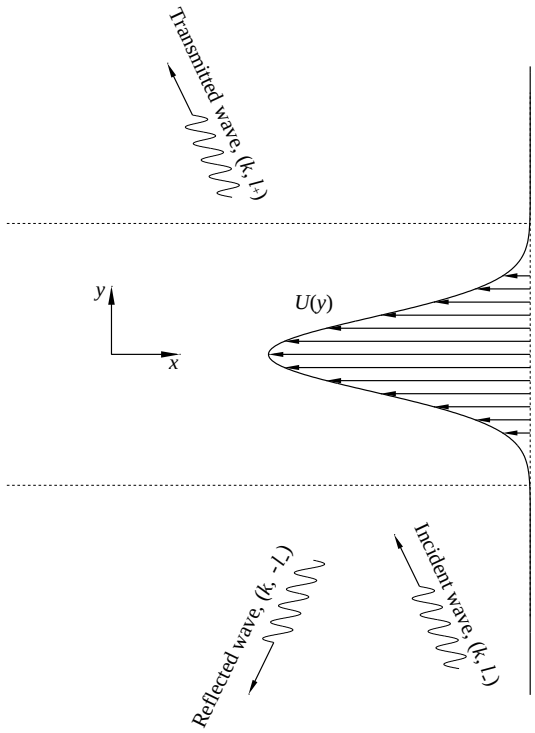

Figure 4.3: Scattering of waves by the jet.

4.2.2 Singular points of Eq. (4.21)

We rewrite Eq. (4.21) as

$$\left(\frac{H}{A}h'\right)' + \left(\frac{k}{\Omega}\left(\frac{H}{A}\right)' - k^2\frac{H}{A} + 1\right)h = 0, \tag{4.29}$$

where the following notation is ushered

$$\Omega = \omega - kU, \qquad A = \Omega^2 - \omega_i^2, \qquad \omega_i^2 = 1 - U'. \tag{4.30}$$

Function Ω represents the intrinsic wave frequency (relative to the jet). Function ω_i^2 is related to the sufficient condition for a zonal geostrophic flow on an f-plane to be inertially stable:

$$\omega_i^2 > 0 \qquad \text{or} \qquad f\left(f - U'\right) > 0 \tag{4.31}$$

in dimensional variables (see Holton [34], Gill [27]).

Easy to notice that Eq. (4.29) contain two types of singularities, which will be denoted by y_c and y_a. One is associated with so-called critical layers y_c where the intrinsic wave

frequency vanishes

$$\Omega\left(y_c\right) = \omega - kU\left(y_c\right) = 0 \tag{4.32}$$

or, equivalently, the phase velocity in x-direction $c_{ph}^{(x)} = \omega/k$ matches the mean flow velocity $U\left(y_c\right) = c_{ph}^{(x)}$. Singularities of another type, so-called apparent singularities y_a, occur when the denominator of (4.22) vanishes

$$A\left(y_a\right) = \left[\omega - kU(y_a)\right]^2 - 1 + U'(y_a) = 0. \tag{4.33}$$

The type of critical layer singularity in Eq. (4.21) is similar to that examined by Booker in [8]. These authors were first to acknowledge the crucial role that it plays in wave-flow interaction theory because waves and the zonal jet can exchange energy there. As the result propagating waves can be absorbed or amplified by the mean flow.

The inequality

$$\left|c_{ph}^{(x)}\right| = \sqrt{H_0}\sqrt{1 + l^2/k^2 + 1/\left(H_0 k^2\right)} > \sqrt{H_0} \tag{4.34}$$

entails that only fast jets ($\max_{y\in\mathbb{R}} |U\left(y\right)| > \sqrt{H_0}$) can produce critical layers for IGWs. Also note that a wave can encounter a critical layer y_c only when k and $U\left(y_c\right)$ are of the same sign ($kU\left(y_c\right) = \omega > 0$).

Later we will see that singularities y_a do not give rise to actual singular behavior in the solution and $h\left(y\right)$ remains smooth in their vicinity. Accordingly, points y_a are referred to as *apparent singularities*. Within the context of GFD apparent singularities were first described by Boyd [9] (in his notations, $\Delta = 0$ singularity) and later by Dunkerton [24].

Finally, we assume that singular points of different types do not coincide,

$$y_c \neq y_a,$$

and that the singularities are simple poles, *i.e.*

$$U'(y_c) \neq 0, \qquad 2\left[\omega - kU(y_a)\right]\left[-kU'(y_a)\right] + U''(y_a) \neq 0.$$

Apparent singularity

Here we show that two fundamental solutions of Eq. (4.21) are regular in the vicinity of an apparent singularity y_a. Frobenius method can be applied to find the general solution

in form of infinite series (similarly to how it is done in **Appendix A** for critical layers)

$$h = C_a^1 \left[1 - \frac{k}{\Omega^a}\xi + \mathrm{O}\left(\xi^2\right)\right] + C_a^2 \left[\xi^2 + \mathrm{O}\left(\xi^3\right)\right] \qquad \text{as } y \to y_a, \tag{4.35}$$

where $\xi = y - y_a$; C_a^1 and C_a^2 are constants of integration and superscript $'a'$ denotes that the function is evaluated at y_a. To derive (4.35) we will not apply Frobenius method directly but rather illustrate how the general solution happens to be regular.

The alternative method is to expand the coefficients in Eq. (4.29) as series in $\xi = y - y_a$. Retaining only terms containing negative powers ξ we obtain

$$\left(\frac{h'}{\xi}\right)' + \left(\frac{p}{\xi^2} + \frac{q}{\xi}\right) h' = 0, \tag{4.36}$$

where

$$p = -\frac{k}{\Omega^a}, \qquad q = \left(\frac{k}{\Omega^a}\right)^2 \left(\frac{(\Omega')^a}{k} - (\Omega^a)^2\right). \tag{4.37}$$

Taking into account the definition of points y_a

$$A^a = -(\Omega^a)^2 + \frac{(\Omega')^a}{k} + 1 = 0, \tag{4.38}$$

we find that

$$p^2 + q = \frac{k^2}{(\Omega^a)^2}\left(-(\Omega^a)^2 + \frac{(\Omega')^a}{k} + 1\right) = 0. \tag{4.39}$$

Condition (4.39) allows Eq. (4.36) to be transformed into

$$\left(\frac{\mathrm{d}}{\mathrm{d}\xi} + p - \frac{1}{\xi}\right)\left(\frac{\mathrm{d}}{\mathrm{d}\xi} - p\right) h = 0. \tag{4.40}$$

The latter has two regular fundamental solutions which can be calculated by hand

$$\varphi_1 = \exp(p\xi) \qquad \text{and} \qquad \varphi_2 = (2p\xi + 1)\exp(-p\xi). \tag{4.41}$$

The first terms of Taylor expansion of φ_1 match the first fundamental solution in (4.35) $\varphi_1 - \varphi_2$ match the second one. It is condition (4.39) which directly follows from the definition of apparent singularities (4.33) that cancels singular logarithmic terms in the general solution of Eq. (4.36) with arbitrary p and q.

Critical layer singularity

Here, we examine the behavior of the solution of Eq. (4.21) in the vicinity of critical layer singularities (4.32). The simplest equation to contain a singularity of this type is

$$\frac{d^2z}{dx^2} - \frac{z}{x} = 0. \tag{4.42}$$

It is well-known that one of the fundamental solutions of Eq. (4.42) have a logarithmic branch point at $x = 0$.

In **Appendix A** we found the solution of Eq. (4.21) in asymptotic series around critical layers y_c

$$h = C_c^1 \left[1 + \left(\frac{F'}{FU'}\right)^c \left[\eta \ln \eta + \tfrac{1}{2}\left(1 - \left(U'\right)^c\right)\eta\right] + \mathrm{O}\left(\eta^2 \ln \eta\right)\right] + C_c^2 \left[\eta + \mathrm{O}\left(\eta^2\right)\right] \qquad \text{as } y \to y_c, \tag{4.43}$$

where $\eta = y - y_c$ and C_c^1 and C_c^2 are constants of integration; superscript $'c'$ denotes that the function is evaluated at y_c. Hence, the question arises of how to choose the physically correct branch of the logarithm in (4.43) for $\eta < 0$.

Classical theory of hydrodynamic stability prompts to introduce infinitesimal dissipation into Eq. (4.21) in order to regularize the behaviour of $h\,(y)$ at critical layers (Rayleigh [74]). This determines the choice of logarithm branch and, hence, fixes the integration contour around the singularity in the complex plane.

Curiously, the results of regularization do not depend on the used dissipation model (*e.g.* Case [14], Maslowe [60]). So, instead of the introducing physical viscosity into RGRSW model we shall simply adjust the frequency ω to have a positive imaginary part (which is sometimes referred to as the "Rayleigh viscosity").

So, we introduce infinitesimal Rayleigh viscosity into Eq. (4.21) replacing ω with $\omega + \mathrm{i}0$

$$\left(Fh'\right)' + \left(\frac{kF'}{\omega + \mathrm{i}0 - kU} - k^2F + 1\right)h = 0, \tag{4.44}$$

$$F = \frac{H}{\left(\omega + \mathrm{i}0 - kU\right)^2 - 1 + U'}. \tag{4.45}$$

Then, multiplying Eq. (4.44) by the complex conjugate of h and taking the imaginary part we obtain

$$\left(W_h\right)' + kF' \operatorname{Im}\left(\frac{1}{\omega + \mathrm{i}0 - kU}\right)|h|^2 = 0, \tag{4.46}$$

where we introduced the Wronskian of the solution $h\,(y)$

$$W_h = F\,\mathrm{Im}\left(h'h^*\right). \tag{4.47}$$

Eq. (4.46) is derived under implicit assumption that F is real which implies that $A \neq 0$. However, calculations in **Appendix B** show the equation is valid everywhere and apparent singularities y_a are no exception.

Making use of the Sokhotsky–Weierstrass formula from the theory of generalized functions $\mathrm{Im}\,(\alpha + \mathrm{i}0)^{-1} = -\pi\delta\,(\alpha)$ (see Vladimirov [86],) we acquire

$$(W_h)' = \pi k F' \left|h\right|^2 \delta\,(\omega - kU)\,, \tag{4.48}$$

where we ushered the Dirac delta function $\delta\,(y)$. In what follows, with help of formula (4.48) conclusions about energy exchange during the interaction between waves and background flow will be derived.

Note that the Wronskian defined by (4.47) is closely related to the wave energy flux $\tau\,(k, l, y)$ conveyed by individual inertia-gravity waves. With help of Eqs. (4.20a) – (4.20b) we derive

$$\begin{gathered}\tau \equiv H\,\mathrm{Re}\,(uv^*) = H\,\mathrm{Re}\left(\tfrac{k(\omega-kU)h-(U'-1)h'}{(\omega-kU)^2+(U'-1)}\left(-i\tfrac{kh+(\omega-kU)h'}{(\omega-kU)^2+(U'-1)}\right)^*\right) = \\ = \tfrac{kH\,\mathrm{Im}(h'h^*)}{(\omega-kU)^2+(U'-1)} = k\,\mathrm{Im}\,(Fh'h^*) = kW_h\end{gathered} \tag{4.49}$$

Making use of the formula $\delta\,[f\,(q)] = \left|\mathrm{d}f/\mathrm{d}q\right|^{-1}\delta\,(q - q_0)$, where q_0 is a root of $f\,(q)$ ($f\,(q_0) = 0$) we can integrate Eq. (4.48) to find the value of the jump in W_h (and, hence, momentum flux τ) across a critical layer y_c

$$\begin{gathered}W_h|_{y_c-0}^{y_c+0} = \tfrac{1}{k}\,\tau|_{y_c-0}^{y_c+0} = \mathrm{sign}\,(U)\,\pi\left(\tfrac{F'}{|U'|}\left|h\right|^2\right)^c = \\ = \mathrm{sign}\,(U)\,\pi\left(\tfrac{Q'|h|^2}{Q^2|U'|}\right)^c,\end{gathered} \tag{4.50}$$

where the equality $\mathrm{sign}\,(k) = \mathrm{sign}\,(U)$ was used and

$$Q(y) = \frac{1 - U'}{H} = \frac{\omega_i^2}{H} \tag{4.51}$$

is the jet's *potential vorticity (PV)* (Pedlosky [71]).

Hence, critical layers play crucial role in wave-flow interaction process. The delta function in Eq. (4.48) indicates that within the framework of linear theory each wave

interacts with the mean flow in its critical layer. In the absence of critical layers Eqs. (4.48) and (4.50) imply that the momentum flux τ is constant. Vice versa, when intrinsic wave frequency $\Omega = \omega - kU$ vanishes for some value y_c the flux τ and the Wronskian W_h undergo a jump in their values there and exchange in energy occurs.

4.2.3 Over-reflection and absorption

Now when we have investigated the local influence of the singularities on the solution, the integral scattering properties of the mean flow will be discussed. While the exact values of the scattering coefficients $r_{k,l}$ and $t_{k,l}$ can be determined only together with the solution h of the boundary-value problem (4.44), (4.27) (or (4.28)), a useful *unitarity condition* can be obtained (see **Appendix B**)

$$l_+ H_+ T^2 + l_- H_- \left(R^2 - 1\right) = \operatorname{sign}(U)\, \pi \left(\omega^2 - 1\right) \sum_c \left[\frac{Q' |h|^2}{Q^2 |U'|}\right]_{y=y_c}, \tag{4.52}$$

where $R = |r_{k,l}|$ and $T = |t_{k,l}|$. Note that apparent singularities do not contribute to the unitarity condition – hence, wave energy is neither generated nor absorbed there. Formula (4.52) can be rewritten as a relation between the amplitudes of reflected and transmitted waves and total jump in the Wronskian (and momentum flux)

$$S^2(k, l_-) \equiv R^2 + \frac{l_+ H_+}{l_- H_-} T^2 = 1 + \frac{k^2 + l_-^2}{|l_-|}\, W_h|_{-\infty}^{+\infty}, \tag{4.53}$$

where we ushered *non-unitarity coefficient* S which is a convenient characteristic of scattering problem. The latter is similar to the unitarity condition (1.24) for the 1-D Schrödinger equation (see §1.1.4).

In the case when Eq. (4.21) has no critical layer singularities the right-hand side of (4.52) vanishes, and the unitarity condition reduces to a requirement that the energy fluxes of the reflected and transmitted waves add up to that of the incident wave. And Eq. (4.53) transforms into

$$R^2 + \frac{l_+ H_+}{l_- H_-} T^2 = 1. \tag{4.54}$$

It indicates that wave energy is conserved. The multiplier $l_{\pm\infty} H_{\pm\infty} / \left(l_{\mp\infty} H_{\mp\infty}\right)$ is attributed to the fact that energy of free shallow water gravity waves depends on the depth of the fluid layer and the wavenumber.

If, however, critical levels *are* present, the wave energy is *not* conserved. It is generated or dissipated depending on the sign of the jump in the Wronskian across the critical layers

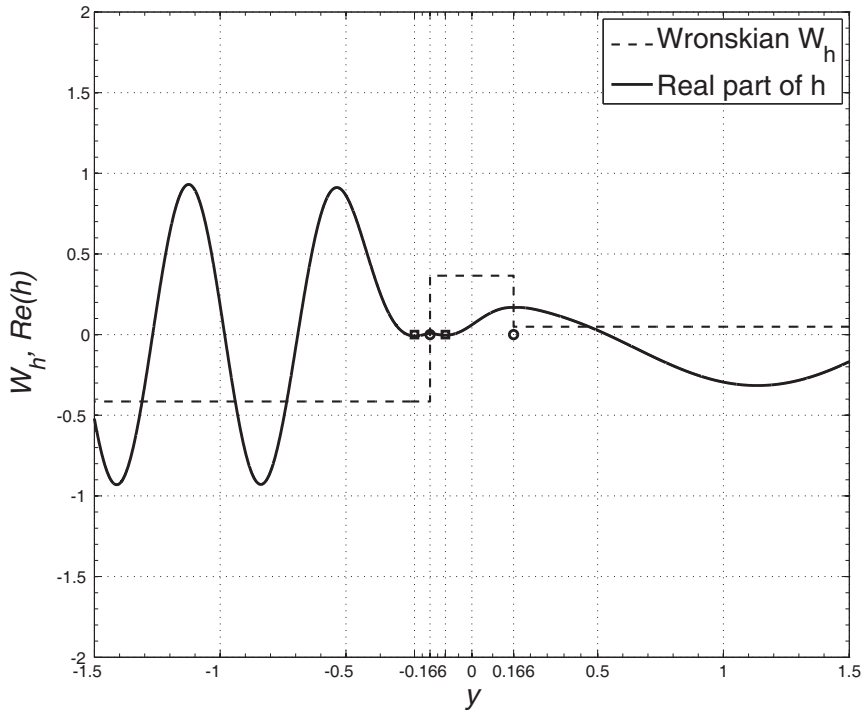

(a) Over-reflection with $T \approx 0.32$, $R \approx 1.28$ and $S \approx 1.31$ for $(k, l_-) = (-7, 11)$.

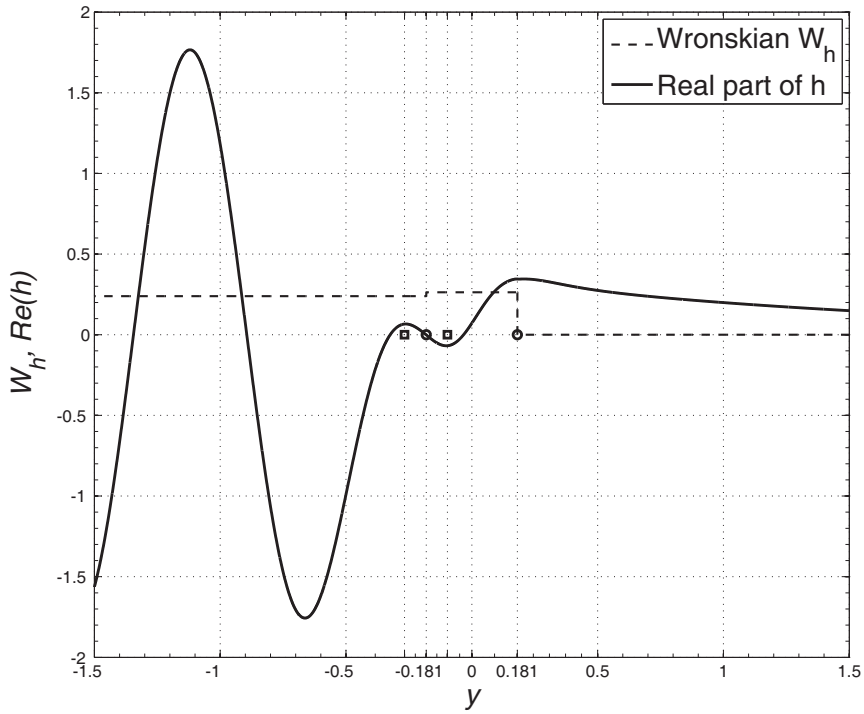

(b) Absorption with $T \approx 0.25$, $R \approx 0.87$ and $S \approx 0.89$ for $(k, l_-) = (-5, 7)$.

Figure 4.4: Examples of scattering of IGWs by a Bickley jet (4.55)–(4.57) (see next section). Apparent singularities and critical layers are denoted by boxes and circles.

as Eq. (4.53) shows. The latter is determined by the PV gradient at $y = y_c$ as described by Eq. (4.50):

- if $\operatorname{sign}(U)\, Q'(y_c) > 0$, then critical level y_c *amplifies* the wave (conductive to over-reflection),
- if $\operatorname{sign}(U)\, Q'(y_c) < 0$, the critical level *absorbs* the wave (conductive to absorption).

Typically, two critical levels arise for the bell-shaped jets given considered in this work. And it is a commonplace situation that one of the critical layers absorbs the wave while the other amplifies. This means that the total increase/decrease of wave energy is determined by the 2 critical layers collectively:

- if $W_h|_{-\infty}^{+\infty} > 0$, then $S > 1$ and the wave is *over-reflected*,
- if $W_h|_{-\infty}^{+\infty} < 0$, then $S < 1$ and the wave is *absorbed*.

Strictly speaking, over-reflection (over-transmission) happens when the amplitude of the reflected (transmitted) wave are greater that 1. Although, in this work we use these terms to describe the case when $S > 1$ even if $R < 1$ or $T < 1$.

4.3 Numerical results

Although being linear, Eq. (4.21) seems too complicated to be resolved analytically for any value of k except maybe for $k = 0$. Therefore, the scattering problem is integrated numerically in order to find reflection and transmission coefficients. The input parameters include the layer's depth $H(y)$ and wavenumbers k and $l_\pm$ of the incident wave (ω and $l_\mp$ are calculated with help of Eqs. (4.10) and (4.24)). We will present the results for the so-called *Bickley jet*,

$$H = 1 + \tfrac{1}{2}\Delta H \tanh \frac{y}{W}, \tag{4.55}$$

which determines $U(y)$ according to Eq. (4.2) as

$$U = -\tfrac{1}{2}\frac{\Delta H}{W} \operatorname{sech}^2 \frac{y}{W}, \tag{4.56}$$

where ΔH is the depth change across the jet and W is the jet's width. Note that, for positive ΔH and W, the jet flows westwards ($U < 0$).

The boundary-value problem (4.21), (4.27) / (4.28) was solved numerically using an algorithm described in **Appendix C** and implemented in Matlab. We calculate S for

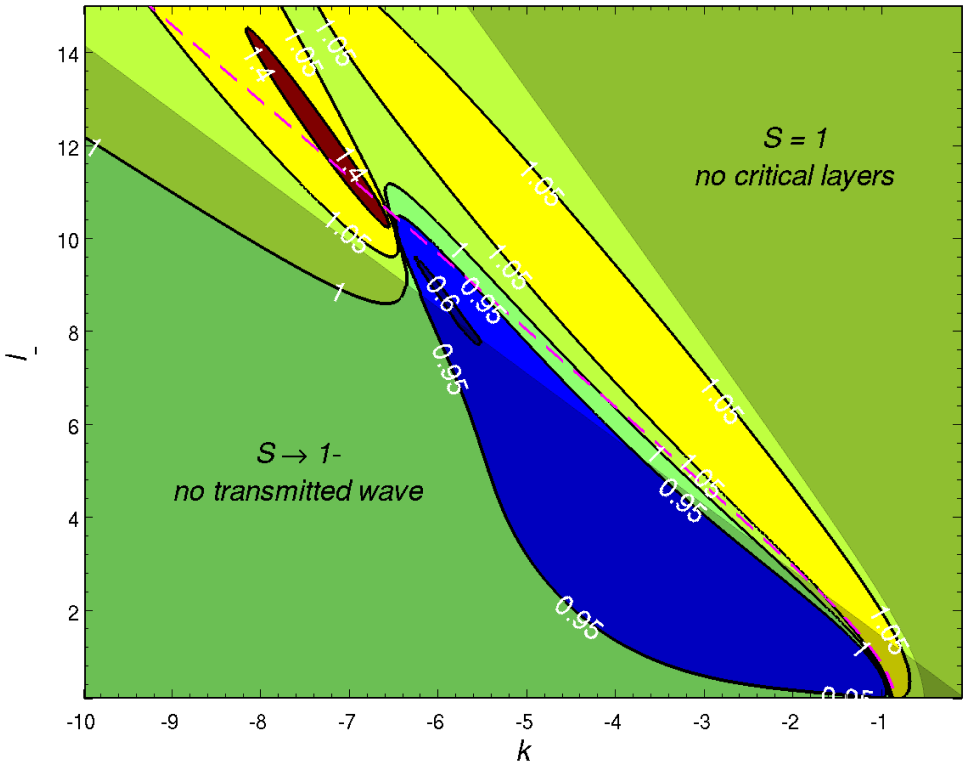

Figure 4.5: Filled contour plot displays isolines of non-unitarity coefficient S as function of wavenumbers $(k; l_-)$. Regions of absorption $(S < 1)$ and over-reflection $(S > 1)$ are shown in shades of blue and red respectively. A curve of fixed $c_{ph}^{(x)} = -1.34929$ for Fig. 4.6 is indicated by a magenta dashed line.

wavenumbers $\left\{\left(k^i,\, l_-^j\right)\right\}_{i,j}$ which can be visualised as points of a uniform grid for a rectangular $\left[k^{\min};\, k^{\max}\right] \times \left[l_-^{\min};\, l_-^{\max}\right]$ for jet (4.55) with

$$\Delta H = 1, \qquad W = 0.25. \tag{4.57}$$

2D contour plot displaying isolines of the non-unitarity function is shown on Fig. 4.5. The following observations should be made:

- For sufficiently large values of the incident wavenumber l_-, the waves no longer encounter any critical layers because $c_{ph}^{(x)} > \max\limits_{y} U$ and Eq. (4.32) has no solutions. Hence, according to (4.54) $S = 1$ there.

- For small l_-, the transmitted wave does not exist (becomes "non-propagating").

Indeed, as follows from (4.25), if l_- does not satisfy condition (4.26) then l_+ is imaginary. The reflected wave still exists, however, and R can still be computed if decay boundary conditions (4.28) are used. However, the shaded regions on Fig. 4.5 are not particularly interesting as $S \sim 1$ there.

4.3.1 Resonant over-reflection

Next we will specifically examine the region of intense over-reflection. It will be convenient to keep the zonal phase speed $c_{ph}^{(x)}$ constant (which fixes the location of the critical level) and plot the non-unitarity coefficient S as a function of l_- for various values of ω/k. An example of such a curve in the (k, l_-) space along which S is plotted is given on Fig. 4.5.

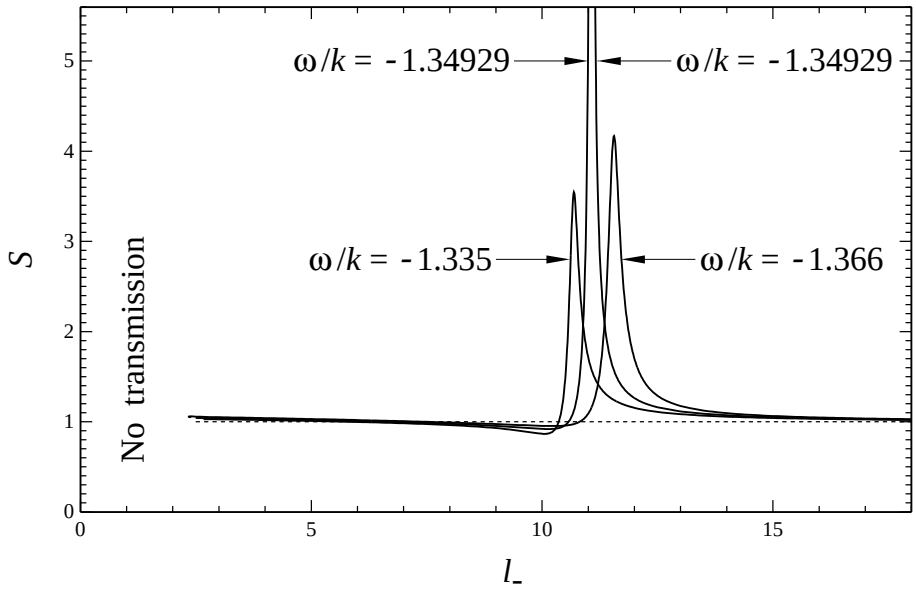

Figure 4.6: The dependence of the non-unitarity coefficient S on the meridional wavenumber l_- of the incident wave, for the Bickley jet (4.55)–(4.57). Each curve is computed for a fixed value of the phase velocity ω/k (indicated on the graph). The curves are terminated in the small$-l_-$ region of no-transmission.

Unexpectedly, anomalously high over-reflection is found for $\omega/k \approx -1.34$ and $l_- \approx 11$ as shown on Fig. 4.6. The corresponding value of the zonal wavenumber [which can be determined using (4.24)] is $k \approx -6.9$.

Additional computations specifically targeting the region of anomalously large S were performed. When the maximum of S at grid points $\left\{\left(k^i, l_-^j\right)\right\}_{i,j}$ is found the algorithm zooms into a small region around the maximum and continues the calculations on a finer grid in this region. The iterations are terminated when sufficiently large values of S are

found or no significant increase is observed. As Fig. 4.6 suggests, the peaks in S appear to be extremely narrow and, consequently, a fine initial grid $\left\{\left(k^i, l_-^j\right)\right\}_{i,j}$ and high precision of calculations are needed. We also emphasise that, even though Fig. 4.6 illustrates the results with moderate S, the full range of the computations performed reached $S \sim 1000$ and higher.

Hence, numerics suggest that for certain values $k = K$ and $l_- = L_-$, the non-unitarity coefficient S is truly infinite – *i.e.* over-reflection turns into *hyper*-reflection. In the literature ([54], [62]) this phenomena is referred to as *resonant over-reflection*. For the Bickley jet (4.55) – (4.57) the wave vector for which resonant over-reflection occurs is

$$K \approx -6.8665, \qquad L_- \approx 11.0693. \tag{4.58}$$

Some numerical characteristics of the solution are presented on Fig. 4.7. So far, this

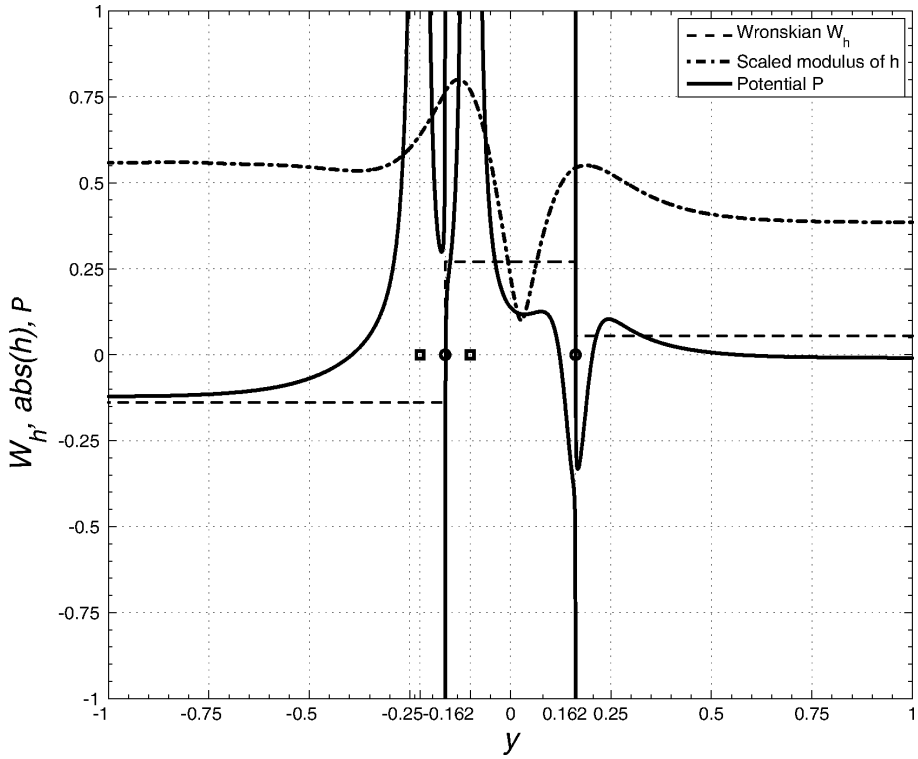

Figure 4.7: An example of resonant over-reflection of a wave (4.58) with $T \approx 447.5$, $R \approx 651.29$, $S \approx 768.55$ $|a| \approx 0.002$. The mean flow profile and other notations are the same as in Fig. (4.4).

conclusion is based on numerical evidence only – but later it will be supported by analytical and qualitative arguments.

But how can the non-unitarity coefficient S become infinite? When looking at formula (4.53) one is tempted to conclude that because infinite S require infinite discontinuity in Wronskian W_h, then Wronskian must also be infinite in a non-singular region. This apparent contradiction can be easily explained. As described in **Appendix C** the boundary-value problem (4.21), (4.27) is integrated starting from the transmitted wave (of unitary amplitude). Then, complex amplitudes a and b (see (C.3)) of the corresponding incident and reflected waves are found. Hence, according to (C.4) if the incident wave amplitude is small $a\,(K, L_-) \sim 0$ then the reflection and transmission coefficients R and T (which are $\sim |a|^{-1}$) approach infinity. Therefore, this phenomena can be interpreted as spontaneous emission of IGWs by zonal jets within the framework of the RGRSW model.

Easy to notice that for such radiating solution with boundary conditions

$$\left.\begin{aligned} h &\to b\,\mathrm{e}^{-\mathrm{i}l_- y} \quad \text{as } y \to -\infty, \\ h &\to \mathrm{e}^{\mathrm{i}l_+ y} \qquad \text{as } y \to +\infty, \end{aligned}\right\} \tag{4.59}$$

unitarity condition (4.53) transforms into

$$|b|^2 + \frac{l_+ H_+}{l_- H_-} = \frac{k^2 + l_-^2}{|l_-|}\, W_h|_{-\infty}^{+\infty}\,. \tag{4.60}$$

This condition implies $W_h|_{-\infty}^{+\infty} > 0$ which requires at least one critical layer of amplifying type as discussed in §4.2.3.

The asymptotics of S as $(k, l_-) \to (K, L_-)$ turned out to be difficult to compute. We can only state that $S \sim |a|^{-1}$ according to the definition (4.53). Additionally, we checked that the integral of S in the (k, l_-) plane over a region including the hyper-reflection point (K, L_-) diverges.

4.3.2 Dependence on flow parameters

Clearly, at most countable number of radiating wave solutions satisfying the boundary-value problem (4.21), (4.59) can exist. The numerical results obtained for the Bickley jets given by (4.55) indicate that this solution is unique for every jet. We have computed the hyper-reflection wave vector (K, L_-) as a function of the jet's parameters: the jet's width W and the depth change ΔH. The results are shown in Figs. 4.8, 4.9.

The given dependence on W demonstrates that as the jet's core becomes narrower, the hyper-reflected wave becomes shorter ($L_- \to \infty$). It would be interesting to investigate the limit of these velocity profiles as $W \to 0$. Then H becomes a step-function and its

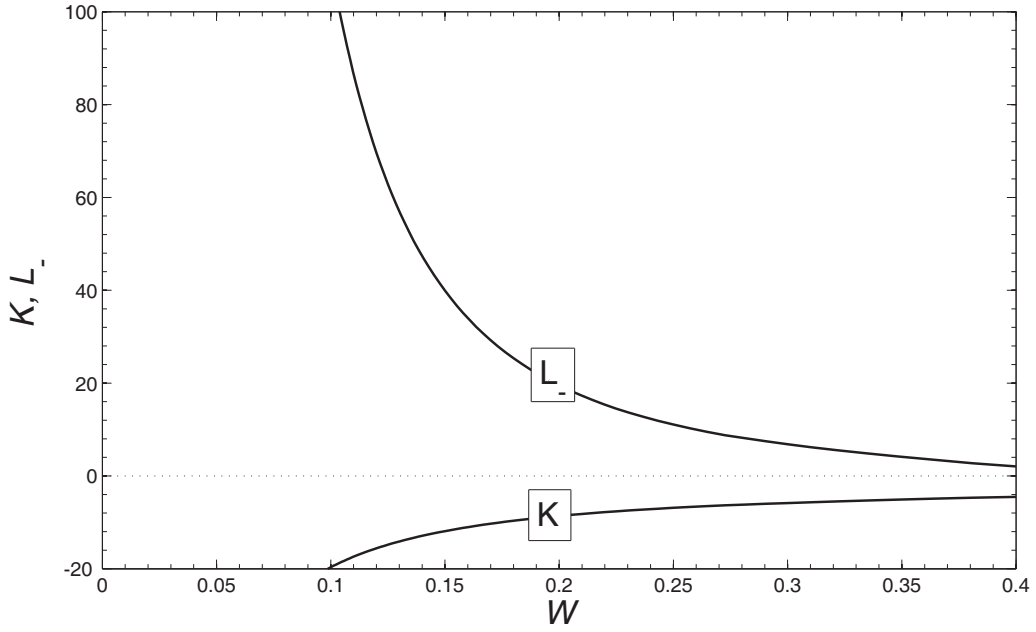

Figure 4.8: The wave vector (K, L_-) of the hyper-reflected wave vs. the width W of the Bickley jet (4.55) with $\Delta H = 1$.

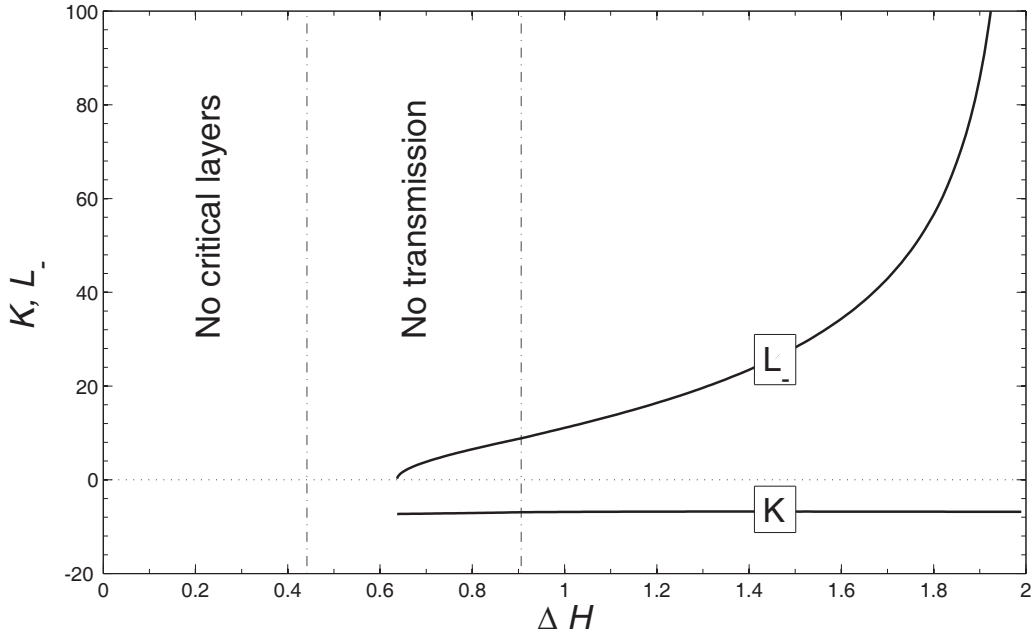

Figure 4.9: The wave vector (K, L_-) of the hyper-reflected wave vs. the depth change ΔH of the Bickley jet (4.55) with $W = 0.25$. The medium becomes non-transparent as $y \to +\infty$, *i.e.* l_+ becomes imaginary.

derivative U is proportional to Dirac's delta function $\delta(y)$ and our results would be possible to compare with a recent study of instabilities of such flow by Dritschel & Vanneste [22]. It has to be noted that a geostrophically balanced localised jet flow and the corresponding shelf in the free surface are perfectly valid solution of the RGRSW model as well as the full Euler equations. However, as the wavelength of IGWs tends to 0 they eventually violate the implicit long-wave approximation of the RGRSW model and the results become inapplicable.

The dependence of (K, L_-) on the depth change across the jet is shown in Fig. 4.9. Observe that, as $\Delta H \to 2$, the meridional wavenumber L_- of the incident wave tends to infinity. This is caused by the fact that, in this limit, the ocean's depth $H(y)$ vanishes at $y \to -\infty$. For $\Delta H \lesssim 0.906$, the meridional wavenumber L_+ becomes imaginary, *i.e.* no transmitted wave exists. Note, however, that hyper-reflection can still occur for this range of ΔH (as the reflection coefficient can still be infinite), and our computations show that $L \to 0$ as $\Delta H \to H_{\min}$, where $H_{\min}$ can be calculated from the requirement that critical layers must be present and condition (4.34)

$$|\max U| = \tfrac{1}{2}\frac{\Delta H}{W} > \sqrt{1 - \frac{\Delta H}{2}} = \left|\min c_{ph}^{(x)}\right| \tag{4.61}$$

Finally, observe that the zonal wavenumber K does not change much through the whole range of ΔH.

4.4 Physical interpretation

Here we provide some analytical considerations giving an important insight into the mechanism of hyper-reflection. Using substitution $\psi = F^{1/2}h$ we can rewrite Eq. (4.44) in its normal form

$$-\psi'' + P\psi = l^2\psi, \tag{4.62}$$

where the subscript $'-'$ was omitted from l_- and

$$P(y) = \frac{2FF'' - (F')^2}{4F^2} - \frac{k}{\omega + \mathrm{i}0 - kU}\frac{F'}{F} - \frac{1}{F} + k^2 + l^2. \tag{4.63}$$

The sign of $P(y) - l^2$ determines whether the solution oscillates or decays exponentially.

As outlined in §1.1.4, Eq. (4.62) can be perceived as the time-independent Schrödinger equation for a "quantum particle" with momentum l scattered by the "potential" $P(y)$. Note also that such analogy between quantum particles and oceanic waves has been has

been previously employed in the geophysical literature (see, *e.g.*, a recent paper by Le Dizès & Billant [49]).

Observe that potential $P(y)$ blows up at the singularities y_a and y_c as can be seen on Fig. 4.7. Typically, the jets given by (4.55) has potential $P(y)$ with two critical levels and two apparent singularities. Asymptotic behavior of $P(y)$ at an apparent singularity y_a is $\sim (y - y_a)^{-2}$. A singularity of this type in the potential acts as a strong barrier and impedes propagation of waves past the singularity (see Landau [48]). Most importantly, Fig. 4.7 illustrates that an *amplifying* critical level ($Q' > 0$, $W_h|_{y_c-0}^{y_c+0} > 0$) is located in-between two apparent singularities. Also, note that "wave amplitude" $|h(y)|$ reaches its maximum in this region. This indicates that waves are somewhat captured there.

These observations suggest the following interpretation of hyper-reflection: imagine a wave "oscillating" to and fro between two apparent singularities acting as barriers. Then, the wave undergoes multiple over-reflection at the amplifying critical level and its amplitude grows. Within the framework of this model, resonant over-reflection occurs if the amplification of the wave by the critical level compensates the loss of wave energy through the barriers. Note, however, that a certain restriction must placed on the phase of the "bouncing" wave after it went through one "to and fro" cycle. Otherwise the interference will weaken rather then strengthen it.

4.4.1 Resonance between two potentials

We discuss this idea in more details within the framework of a toy model presented on Fig. 4.10 and investigate the possibility of resonant over-reflection in this model. Two (regular) potential barriers with an amplifier in-between are supposed to act as a prototype for the original potential $P(y)$ (4.63)

$$\psi'' + k^2\psi = P_{\mathsf{toy}}(x)\,\psi + \mathrm{i}\,\Delta\,\delta(x)\,\psi, \tag{4.64}$$

where

$$P_{\mathsf{toy}} = P_1 + P_2, \tag{4.65}$$

and $P_{1,2}$ are functions with compact supports, $\left[x_1^-, x_1^+\right]$ and $\left[x_2^-, x_2^+\right]$, such that

$$x_1^- < x_1^+ < 0 < x_2^- < x_2^+; \tag{4.66}$$

$\Delta > 0$ characterise the strength of amplification.

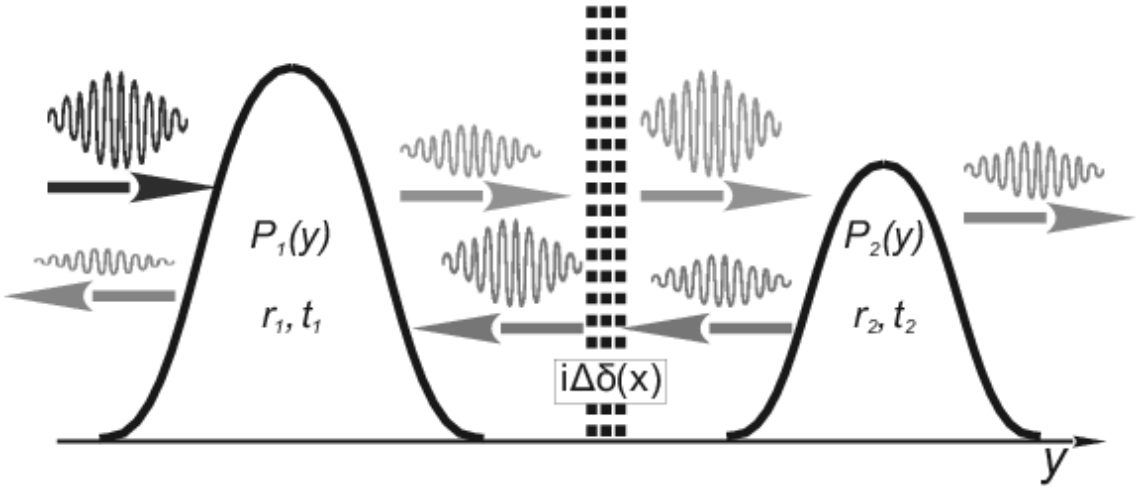

Figure 4.10: A schematic illustration of wave scattering by two potentials with compact non-overlapping supports P_1 and P_2 with an amplifier i $\Delta\,\delta\,(x)$ in-between. Transmission and reflection coefficients of the potentials $P_{1,2}$ are $t_{1,2}$ and $r_{1,2}$ respectively.

For both potentials $P_{1,2}$ we know the usual "from-left-to-right" scattering coefficients $r_{1,2}$ and $t_{1,2}$

$$-\psi_{1,2}'' + P_{1,2}\,\psi_{1,2} = l^2\,\psi_{1,2}, \tag{4.67}$$

$$\left.\begin{aligned} \psi_{1,2} &\to \mathrm{e}^{\mathrm{i}ly} + r_{1,2}\,\mathrm{e}^{-\mathrm{i}ly} \quad \text{for } y < x_{1,2}^-, \\ \psi_{1,2} &\to t_{1,2}\,\mathrm{e}^{\mathrm{i}ly} \qquad\qquad\quad \text{for } y > x_{1,2}^+. \end{aligned}\right\} \tag{4.68}$$

For the first jet, we introduce auxiliary "from-right-to-left" coefficients r_1', t_1',

$$-\psi_1'' + P_1\,\psi_1 = l^2\,\psi_1, \tag{4.69}$$

$$\left.\begin{aligned} \psi_2 &\to t_1'\,\mathrm{e}^{-\mathrm{i}ly} \qquad\qquad\quad \text{for } y < x_1^-, \\ \psi_2 &\to \mathrm{e}^{-\mathrm{i}ly} + r_1'\,\mathrm{e}^{\mathrm{i}ly} \quad \text{for } y > x_1^+. \end{aligned}\right\} \tag{4.70}$$

The global scattering coefficients r and t of the system in Fig. 4.10 can be found in terms of $r_{1,2}$, $t_{1,2}$ and Δ. The calculations involved are given in **Appendix E**, whereas here we shall only discuss the final result. The "no incident wave" condition (E.9) determines when the global scattering coefficients are infinite, *i.e.* when hyper-reflection occurs.

A reader familiar with quantum mechanics might associate the setting illustrated in Fig. 4.10 with the so-called *resonant tunneling* phenomenon. It was described by David Bohm in 1951 [7] who showed that for certain incident particles the transmission coefficient is equal to one, *i.e.* the double barrier is totally transparent for them. The situation that

could never happen for a single potential barrier.

However, we are looking for resonant over-reflection, *i.e.* solutions with infinite scattering coefficients. Hence, anticipating that singularities in the potential are a prerequisite we adjusted the setting by introducing an amplifier i $\Delta\,\delta\,(x)$ in the double-barrier potential. Indeed, if classical unitarity condition (1.24) holds for the potentials $P_{1,2}$

$$|r_{1,2}|^2 + |t_{1,2}|^2 = 1, \tag{4.71}$$

and $\Delta = 0$ then easy to check that "no incident wave" condition (E.9) is never be satisfied. Which implies that resonant over-reflection cannot exist.

The amplifying/absorbing term i $\Delta\ \delta\,(x)\,\psi$ in Eq. (4.64) can be "built into" the potentials $P_{1,2}$. Then no incident wave condition (E.12) can be written as

$$r_1' r_2 = 1, \tag{4.72}$$

where for the first barrier P_1 we used "right-to-left" r_1', t_1' scattering coefficients instead of "left-to-right" ones.

4.4.2 Discussion

Physically this result means the following. If we put a wave propagating to the right in-between two barriers, it will reach P_2 and a part of it will be reflected back. This reflected wave is then scattered by the first barrier P_1. So, condition (4.72) means that after two successive reflections from P_1 and P_2 the returning wave augmented by factor $r_1' r_2$ is identical to the original wave, *i.e.* phase and amplitude are unchanged.

Following this logic, having r_1' and r_2 such that

$$r_1' r_2 > 1 \text{ (real number)}, \tag{4.73}$$

results in a wave regaining its original phase and *increasing* its amplitude after two successive reflections. It is intuitively clear that the situation defined by (4.73) gives rise to an *exponentially growing* solution. Yet scattering coefficients remain finite in this case! Hence, we conjecture that the corresponding scattered wave solution with finite R and T coexists with a solution with imaginary ω and l (growing in time and decaying in space). Thus, the steady scattering component is likely to be virtually "invisible" against the background of growing unstable field. These ideas are elaborated in Chapter 6.

We shall also point out that:

- Hyper-reflection by a two-potential configuration never occurs if the potentials are mirror images of one another. In this case $r_1' = r_2$ – hence, condition (4.72) holds only if $r_1' = r_2 = \pm 1$. As a result, R and T remain finite according to (E.13) as the zero denominators are cancelled out by zero numerators.

- If the potentials have identical shapes (*i.e.* can be obtained from one another by translation along the y axis), the transmission coefficient T remains finite even if condition (4.72) does hold. In this case, it can be shown that

$$r_2 = -\frac{(r_1')^* \, t_1'}{(t_1')^*} \, \mathrm{e}^{\mathrm{i}lD},$$

  where D is the distance between the potentials. Then, (4.72) implies that

$$|r_1|^2 = 1,$$

  and formulae (E.13) show that T remains finite (but R can still be infinite).

As two barriers Q_1 and Q_2 come closer and finally merge together we return to our original problem with the potential from §4.4. Hence, condition (4.72) cannot be applied directly but we believe that it is the multiple over-reflection that drives resonant over-reflection. This interpretation resembles the concept of resonance. And, hence, the name of the phenomena acquires new meaning.

We will test the proposed explanation of the mechanism in the next chapter with help of a specifically constructed for this sake problem of Rossby wave scattering by a two-jet configuration on the QG beta-plane.

4.5 Summary

In this chapter a linear model is presented describing the scattering of small amplitude IGWs by a zonal jet in a two-layer rotating ocean. The results obtained within this rather simple model can give insight on how internal waves interact with strong surface currents that flow as a narrow zonal jet (in particular the eastward flowing Gulf Stream Extension, the Kuroshio Extension, the Agulhas Return Current and the Antarctic Circumpolar Current). Although, maybe with the exception of the latter, neither of these are strictly zonal, (in fact, the Gulf Stream and Kuroshio are classified as "western boundary currents") they

turn to mostly zonal for a part of their path. For example, the Gulf Stream separates from the US coast near Cape Hatteras, the Kuroshio Extension leaves the Japanese coast near $\sim 45°$N, and both become (meandering) eastward-flowing currents (see Ducet and Le Traon [23]).

Eq. (4.21) governing propagation of IGWs through the background flow contains apparent singularities (Boyd [9]) and critical layers (Booker & Bretherton [8]) where non-trivial interaction with the mean flow, *i.e.* absorption or over-reflection/over-transmission, can occur. We show that the sign of the jump in the wave flux across the critical layers is determined by the sign of the PV gradient according to Eq. (4.50). Thus, we derived the aggregate energy exchange condition (4.52) which determines whether the interaction results in absorption or over-reflection/over-transmission

In §4.3 we present the results of calculations of reflection and transmission coefficients as functions of two wavenumbers of the incident wave (k, l) for a two-parametric (ΔH, W) family of Bickley jets (4.55). Numerical integration of the singular scattering equation (4.21) was implemented in Matlab using an algorithm described in **Appendix C**. The scattering properties of a given jet can be succinctly shown on a 2D contour plot displaying isolines of the non-unitarity function.

The main results can be summarized as follows:

- In the (k, l) parameter plane 3 distinct regions are typically present (*e.g.* Fig. 4.5):
  - Incident waves with phase speeds satisfying $c_{ph}^{(x)} > \max_y U$ do not encounter any critical layers when it propagates across the jet and according to (4.54) in this case $S = 1$.
  - For sufficiently small l_- (when condition (4.26) is violated) the incident wave cannot penetrate the jet barrier and the transmitted wave does not exist $T = 0$. The reflection coefficient R, however, can still be computed but usually $S \sim 1$ there as the "non-propagating" region is conductive to complete reflection and the critical layers have no significant effect on the wave propagation.
  - Finally, the incident waves with parameters from the middle region on Fig. 4.5 typically have two apparent singularities interchanging with two critical level (an absorbing and an amplifying one, Fig. 4.4). Cases of significant over-reflection, over-transmission and absorption occur.
- For the first time, we found cases of *resonant over-reflection* within the framework of the RGRSW model as the calculations indicate that at a certain point on the

$(k,\, l)$ parameter plane reflection and transmission can be infinite. Dependence of the hyper-reflection wave vector (K, L_{-}) on the jet's width W and depth change ΔH was investigated (Figs. 4.8, 4.9).

- Generally, numerics suggest that linearly *stable* flows never over-reflect waves (*i.e.* $S \leq 1$) while *unstable* flows manifest over-reflection and even hyper-reflection. This important finding of the study will be further supported by analytical arguments in Chapter 6 where we show that a resonant over-reflected coexists with radiating instabilities.

In §4.4 a physical interpretation of the phenomenon of resonant over-reflection is given with help of transforming scattering Eq. (4.21) into its Schrödinger-type formulation (4.62). We argued that two apparent singularities act as containing barriers for the amplifying critical level in-between where multiple over-reflection can happen.

Chapter 5

Rossby Wave Scattering by Zonal Jets on the β-plane

In this chapter we consider the problem of scattering of small amplitude Rossby waves by jets on a barotropic β-plane governed by quasi-geostrophic (QG) equation Eq. (3.133). This classical model is traditionally applied to study planetary-scale Rossby waves and their interaction with surface currents and bottom topography. In particular, the critical layer theory is well-developed since early works by Dickinson & Clare [20], Lindzen & Tung [55], Yamada & Okamura [89] (see also a review article by [60]). Thus, we will concentrate on a special case where the mean flow is represented by two localized zonal jets. We will refer to this velocity profile as a *two-jet configuration*. This problem emerged as a testing ground for the double-barrier concept of resonance over-reflection proposed in §4.4.

Nevertheless, multiple zonal jets are widely found in geophysical systems. Double (multiple)-jet flows are known to be more persistent and less prone to fluctuation and meandering than single jets (Lee [51]). Antarctic Circumpolar Current provides an exelent example of a multiple-jet zonal flow in mid-latitudes (Sokolov and Rintoul [81]). Long-lived zonal jets are present in the Earth's tropical ocean and are ubiquitous in the atmospheres of Jupiter and Saturn. All this provides additional motivation for this problem.

Corresponding scattering equation (5.14) is somewhat similar to Eq. (4.21) studied in Chapter 4. Although, it is simpler and is essentially a slight modification of Rayleigh stability equation (*e.g.* Lin [52], Kuo [45]). The governing equation contains only critical layer singularities and no singularities of any other type. As discussed above critical layers lead to non-trivial interaction with the mean flow which results in over-reflection or absorption of waves. We solve the problem numerically and find the coefficients of

reflection and transmission as functions of wavenumbers and parameters of the jet.

As anticipated from the ideas presented in §4.4, we find that the two-jet configuration can hyper-reflect waves. The scattering coefficients of the hyper-reflected waves satisfy the theoretically derived condition (4.72). Hence, we assert the validity and generality of the results obtained in Chapter 4 which can be applied to any scattering problems regardless of the model.

5.1 Introduction

5.1.1 Two-jet configuration

Recall that many of ocean surface currents and atmospheric winds are roughly geostrophically balanced (see Chapter 1.1). Also note that solutions of the QG equation (3.131) (and its simplified version (3.133)) always represent a velocity field in geostrophic balance. But in particular, Eq. (3.131) supports a solution in the form

$$\psi = -\int U(y)\,\mathrm{d}y, \tag{5.1}$$

$$U(y) \to 0 \qquad \text{as } y \to \pm\infty, \tag{5.2}$$

which according to (3.131) represent a steady zonal flow with jet-like velocity profile $U(y)$.

Our goal is to consider a mean flow (5.1) that would give rise to a potential mimicking the one prescribed in §4.4.1. However, unlike its counterpart from Chapter 4, the equation governing scattering of Rossby waves on a barotropic β-plane does not involve apparent singularities. And our interpretation of resonant over-reflection discussed in §4.4 requires barriers trapping the wave.

As an alternative, we shall consider a two-jet configuration, where the wave can be "trapped" between the jets acting like containing barriers. Such a setting is also motivated physically, as two distinct well defined jets has been observed in the Antarctic Circumpolar Current by Gille [28], multiple jets also exist in the tropical part of the Earth's ocean, as well as on Jupiter and Saturn.

Fig. 5.1 illustrates the schematic of the scattering problem at hand and the configuration of the mean flow

$$U(y) = U_1(y) + U_2(y). \tag{5.3}$$

We assume that the jets's velocity profiles $U_{1,2}(y)$ are single-extremum functions with compact non-overlapping supports. We anticipate resonant over-reflection to occur when

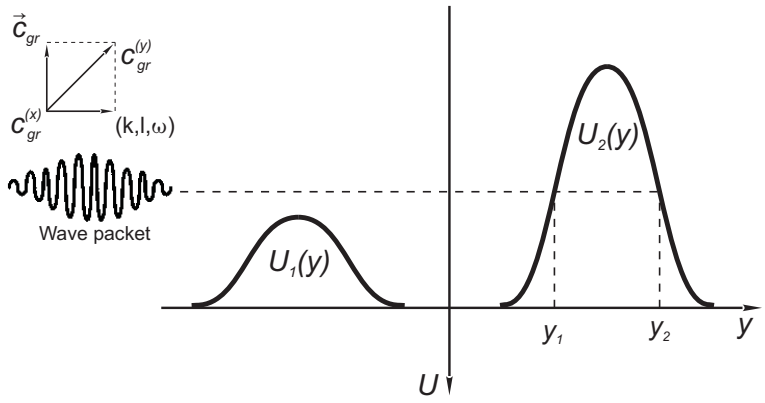

Figure 5.1: Formulation of the problem. Velocity profile $U(y)$ of the two-jet formation and a Rossby wave packet propagating with group speed $\vec{c}_{gr}$. The first jet $U_1(y)$ provides no critical layers while the wave encounters a pair of critical layer in the second jet $U_2(y)$.

the first jet with velocity profile $U_1(y)$ acts as a regular potential barrier while $U_2(y)$ provides both amplifying critical layers and the second barrier.

5.1.2 Free barotropic Rossby waves

We consider small amplitude solutions of the QG equation (3.133). The linearized equation is

$$\frac{\partial\left(\nabla^2\psi\right)}{\partial t}+\beta\frac{\partial\psi}{\partial x}=0, \tag{5.4a}$$

where the prime in β was omitted. We look for the solutions of Eq. (5.4a) in form of a harmonic wave

$$\psi_{k,l}=\mathrm{Re}\left[C_{k,l}\ \mathrm{e}^{\mathrm{i}kx+\mathrm{i}ly-\mathrm{i}\omega t}\right]. \tag{5.5}$$

Substituting (5.5) into (5.4a) we obtain the dispersion relation for free barotropic Rossby waves in the QG model

$$\omega=-\frac{\beta\,k}{k^2+l^2}, \tag{5.6}$$

where (k,l) is the horizontal wave vector and $\omega(k,l)$ is the wave frequency. The total fluctuation field $\psi(x,y,t)$ can be written as Fourier integral

$$h(x,y,t)=\mathrm{Re}\left(\int\int C_{k,l}\,\exp\left(\mathrm{i}\omega\left(k,l\right)t+\mathrm{i}kx+\mathrm{i}ly\right)\,\mathrm{d}k\,\mathrm{d}l\right). \tag{5.7}$$

The dispersion formula (5.6) yields the following formulae for Rossby wave group speed:

$$c_{gr}^{(x)} = \frac{\partial \omega}{\partial k} = \frac{\beta\left(k^2 - l^2\right)}{\left(k^2 + l^2\right)^2}, \qquad c_{gr}^{(y)} = \frac{\partial \omega}{\partial l} = \frac{2\beta\, k\, l}{\left(k^2 + l^2\right)^2}. \tag{5.8}$$

The equality

$$\operatorname{sign}\left(c_{gr}^{(y)}\right) = \operatorname{sign}\left(k\, l\right), \tag{5.9}$$

allows us to define whether the wave propagates towards or away from the mean flow based on its wavenumbers. Remarkably, the phase velocity of a Rossby wave in the zonal direction

$$c_{ph}^{(x)} = \frac{\omega}{k} = -\frac{\beta}{k^2 + l^2}, \tag{5.10}$$

is *always negative*. This proves that Rossby waves always travel westward.

5.2 Scattering equation

Here we consider scattering of free Rossby waves originating far from the jet and penetrating through the jet. A sketch of the problem and a typical velocity profile $U\left(y\right)$ of a westward current is outlined on Fig. 5.1. We shall look for the solution as a sum of the mean flow (5.1) and a small-amplitude wave $\tilde{\psi}$

$$\psi = -\int U(y)\,\mathrm{d}y + \tilde{\psi}. \tag{5.11a}$$

Following the usual linearization routine, with application to Eq. (3.133) one derives equation

$$\left(\frac{\partial}{\partial t} + U\frac{\partial}{\partial x}\right)\left(\nabla^2\tilde{\psi}\right) - U''\frac{\partial \tilde{\psi}}{\partial x} + \beta\frac{\partial \tilde{\psi}}{\partial x} = 0. \tag{5.12}$$

which supports harmonic wave solutions

$$\tilde{\psi} = \operatorname{Re}\left[\phi(y)\ \mathrm{e}^{\mathrm{i}kx - \mathrm{i}\omega t}\right]. \tag{5.13}$$

As the result, one obtains the following counterpart of IGW scattering equation (4.21) (Dickinson & Clare [20]):

$$-\phi'' + \left[\frac{k\left(\beta - U''\right)}{\omega + \mathrm{i}0 - kU} + k^2\right]\phi = 0, \tag{5.14}$$

where as before singularities are regularized with help of infinitesimal Rayleigh dissipation $\omega \to \omega + \mathrm{i}0$. Similarly to Eq. (4.21) studied in Chapter 4, Eq. (4.29) can contain critical layers y_c where

$$U(y_c) = c_{ph}^{(x)}. \tag{5.15}$$

Although, no singularities of any other type (*e.g.* apparent singularities) are present in this model. Observe that all eastward jets ($U > 0$) do not have critical layers because $c_{ph}^{(x)} < 0$ according to (5.10). Hence, only westward jets can effectively interact with Rossby waves.

Observe that the coefficients of (5.14) have equal limits as $y \to \pm\infty$ unlike the the coefficients of (4.21) (which involve a "step-like" function $H(y)$). In other words, the dispersion relation (4.10) is the same on both sides of the mean flow. As a result, a Rossby wave incoming from $y \to -\infty$ gives rise to a reflected wave propagating towards $y \to -\infty$ and transmitted wave at $y \to +\infty$ with identical meridional wavenumbers. Omitting the subscripts $'\pm'$, we write the corresponding boundary conditions (4.27) as

$$\left.\begin{aligned} &\phi \to \mathrm{e}^{\mathrm{i}ly} + r_{k,l}\,\mathrm{e}^{-\mathrm{i}ly} && \text{as } y \to -\infty, \\ &\phi \to t_{k,l}\,\mathrm{e}^{\mathrm{i}ly} && \text{as } y \to +\infty, \end{aligned}\right\} \tag{5.16}$$

The situation when we have a decay condition (such as (4.28)) instead of the transmitted wave is, hence, ruled out in this case. Eq. (5.14) together with (5.16) form a well-posed boundary-value problem which determines r and t together with the solution $\phi(y)$.

As mentioned in §2 this scattering problem has been examined by Dickinson & Clare [20], Lindzen & Tung [55], Yamada & Okamura [89] and Benilov, *et al.* [5]. Asymptotic representation of ϕ around critical layers, conditions for over-reflection and absorption, a unitarity condition can be found in these papers. Here we shall only state the main results which can also be readily obtained reapplying the procedure from Chapter 4 to Eq. (5.14).

The Wronksian $W_\phi = \mathrm{Im}\left(\phi'\phi^*\right)$ of the solution ϕ satisfies

$$(W_\phi)' = -\pi k Q' \left|\phi\right|^2 \delta(\omega - kU), \tag{5.17}$$

where $Q(y) = (1 + \beta\, y) - U'$ is the jet's potential vorticity (PV) within the barotropic β-plane model. Hence, again as in §4.2.3 wave energy is generated or dissipated at a critical layer depending on the PV gradient. The unitarity condition in this case is

$$T^2 + R^2 - 1 = \frac{\pi}{|l|} \sum_c \left[\frac{-Q'}{|U'|} \left|\phi\right|^2\right]_{y=y_c}, \tag{5.18}$$

where $R = |r_{k,l}|$ and $T = |t_{k,l}|$. The *non-unitarity coefficient* S

$$S^2(k, l_-) \equiv R^2 + T^2, \tag{5.19}$$

characterize the scattering properties of the mean flow as a whole. We will refer to the case when $S < 1$ as to absorption of waves and to $S > 1$ as to amplification (or over-reflection).

As discussed in §2.1 Over-reflection of waves can be clearly related to the necessary condition of barotropic instability (see Holton [34], Gill [27]). Stable ($Q' > 0$ or $\beta - U'' > 0$ everywhere) westward jets absorb Rossby waves. Hence, in this case resonant over-reflection is ruled out. On the other hand, potentially unstable jets ($Q' < 0$ or $\beta < U''$ somewhere in the flow) can over-reflect incoming Rossby waves.

Note, that Eq. (5.14) can be re-written in the "general" form (4.62), with help of the potential

$$P(y) = k^2 + l^2 + 1 - \frac{k\,(U'' - \beta)}{\omega + \mathrm{i}0 - kU}. \tag{5.20}$$

5.3 Numerical results

In this Section we present numerical evidence of waves hyper-reflected by the two-jet configuration (Fig. 5.2). We anticipate that such cases can be found based on our analytical considerations in §4.4.1. Condition (4.72) provides a clear criterion of hyper-reflection of waves between two localized potentials that our numerical results must comply with.

5.3.1 Multiple scattering and resonant over-reflection

We carry out calculations for the two-jet configuration composed of two Bickley jets as defined in (4.56) which shifted appropriately so that they can be perceived as non-overlapping with high accuracy. We choose U_2 so that expression $\beta - U_2''$ is negative somewhere to ensure that critical layers of amplifying type can occur. Critical layers in U_1 are not necessary for hyper-reflection to occur. The sole role of U_1 is to provide the second containing potential barrier.

One may wonder whether resonant over-reflection would occur if U_1 was replaced by a landmass acting as second (totally reflecting) barrier. Formula (4.72) indicates that, indeed, if a wave is reflected by U_2 with unitary reflection coefficient $r_2 = 1$ then it is a resonantly over-reflected wave. As mentioned in §2.2, this scenario was analyzed Lindzen and others [56]. Although, the studies were focused on a straightforward instability mechanism that exist in this case as the over-reflected wave with $r_2 > 1$ grows exponentially

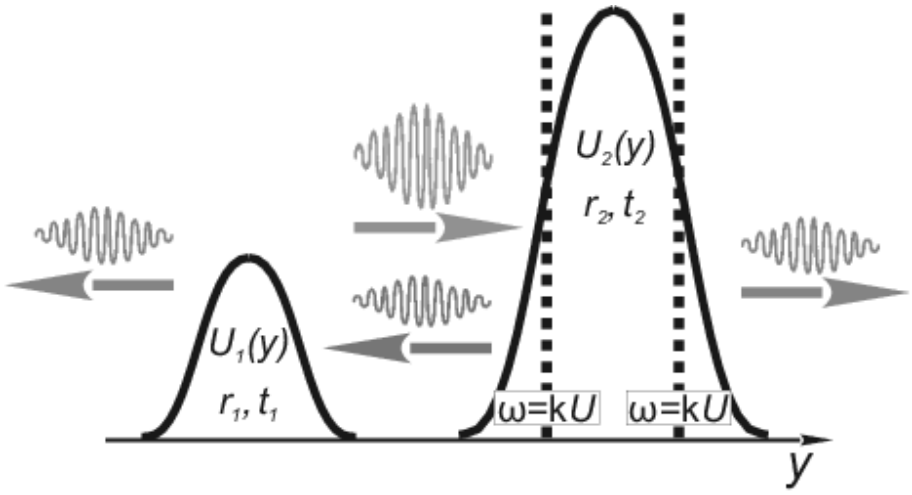

Figure 5.2: An illustration of the resonant over-reflection of a Rossby wave (k, l) by a two-jet configuration with no critical layers in jet $U_1(y)$ and a pair of critical layer in jet $U_2(y)$. Hence, $\max|U_1(y)| < c_{ph}^{(x)} < \max|U_2(y)|$.

when repeatedly reflected back by a rigid barrier.

We solve Eq. (5.14), (5.16) numerically using an algorithm analogous to the one applied in §4.3. The method integrates (5.14) using Runge–Kutta method implemented in Matlab. The integration contour steps around the singularities in the complex plain. We choose the path to lie in upper/lower complex half plane in agreement with the Rayleigh regularization $\omega \to \omega + \mathrm{i}0$ (see **Appendix C** for more details).

Individual scattering coefficients $r_{1,2}$ and $t_{1,2}$ of the two jets U_1 and U_2 were calculated alongside with the global reflection and transmission coefficients. Regions of over-reflection and absorption for U_1, U_2 (*e.g.* Fig. 5.3) and for the two-jet configuration as a whole were found (*e.g.* Fig. 5.4). These results are similar to those presented on Fig. 4.5 in §4.3.

The following remarks on the presented results should be put forth:

- Jet $U_1(y) = -0.7\,\mathrm{sech}^2(0.7y)$, Fig. 5.3a:
  - The flow is *stable* (the sufficient condition $\beta - U'' > 0$ holds everywhere). Hence, only absorption can occur and $S \leq 1$.
  - The waves with wave vectors (k, l) in the interior of the circle $\left|c_{ph}^{(x)}\right| > \max_y |U_1| = 0.7$ do not encounter any critical layers as they propagate across the jet. Hence, according to (5.18) – (5.19) $S \equiv 1$ there.
  - Rossby waves with wave vectors outside of this region are strongly attenuated.

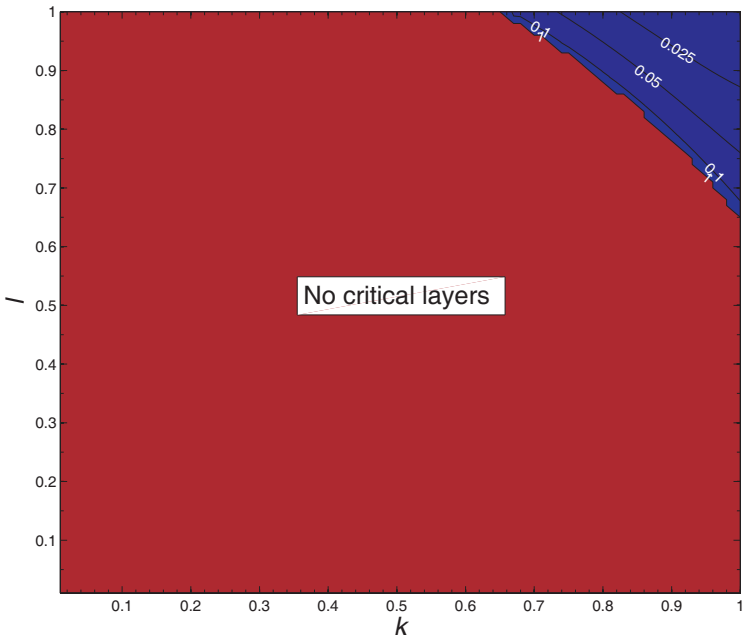

(a) By the Bickley jet $U_1(y) = -0.7\,\mathrm{sech}^2(0.7y)$.

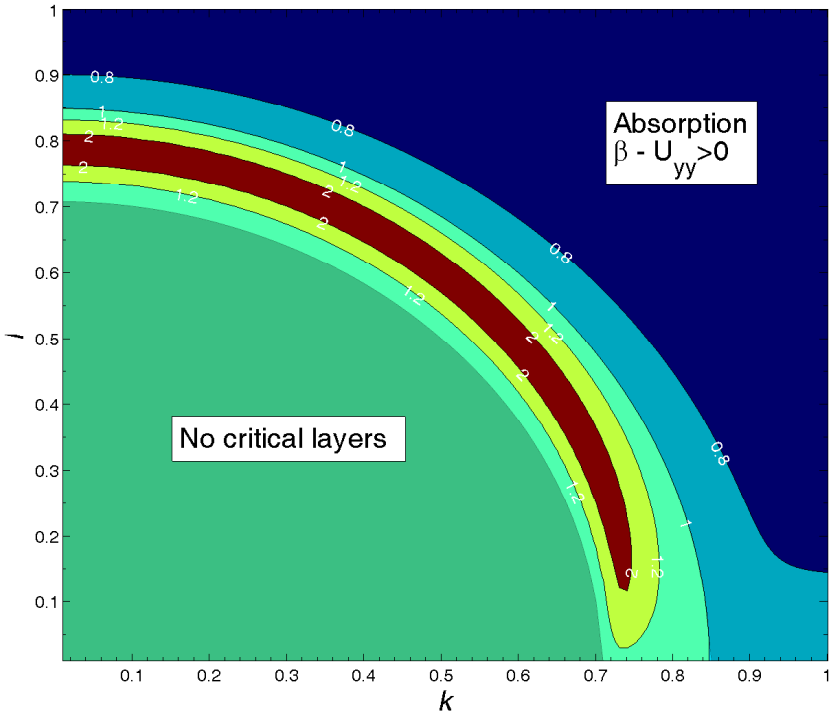

(b) By the Bickley jet $U_2(y) = -2\,\mathrm{sech}^2(2y)$.

Figure 5.3: Scattering of Rossby waves on the QG β-plane ($\beta = 1$) by individual jets. Filled contour plot displays isolines of non-unitarity coefficient $S(k, l)$.

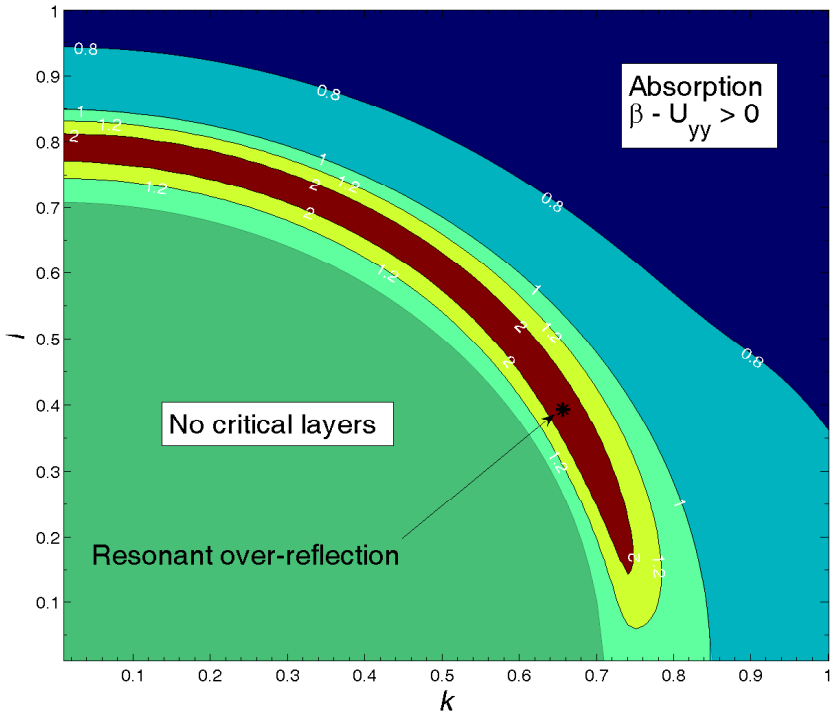

Figure 5.4: Scattering of Rossby waves on the QG β-plane ($\beta = 1$) by the two-jet configuration $U(y) = U_1(y) + U_2(y)$, where $U_{1,2}$ are equal to those in Fig. 5.3. The plot displays isolines of $S(k; l_-)$.

This result is in agreement with previous studies (*e.g.* Dickinson [19]) that showed almost complete absorption of incident waves that are much shorter than the width of the jet.

- Jet $U_1(y) = -2\,\mathrm{sech}^2(2y)$, Fig. 5.3b:
  - The flow is *unstable* ($\beta - U'' < 0$, when $-0.31 \lesssim y \lesssim 0.31$). Hence, when $c_{ph}^{(x)}$ is such that $y_c \notin [-0.31; 0.31]$ absorption occurs and if not, over-reflection occurs.
  - The waves satisfying condition $\left|c_{ph}^{(x)}\right| > \max_y |U_2| = 2$ do not have critical layers. Hence, inside of the corresponding circle on (k, l) plane $S \equiv 1$.
  - The region of over-reflection (the non-shaded region) is of primary interest to us. While the non-unitarity coefficient S remains finite there ($S \lesssim 8.5$, hyper-reflection is absent) we expect to find a hyper-reflected wave solution within this region when the two-jet configuration is considered.

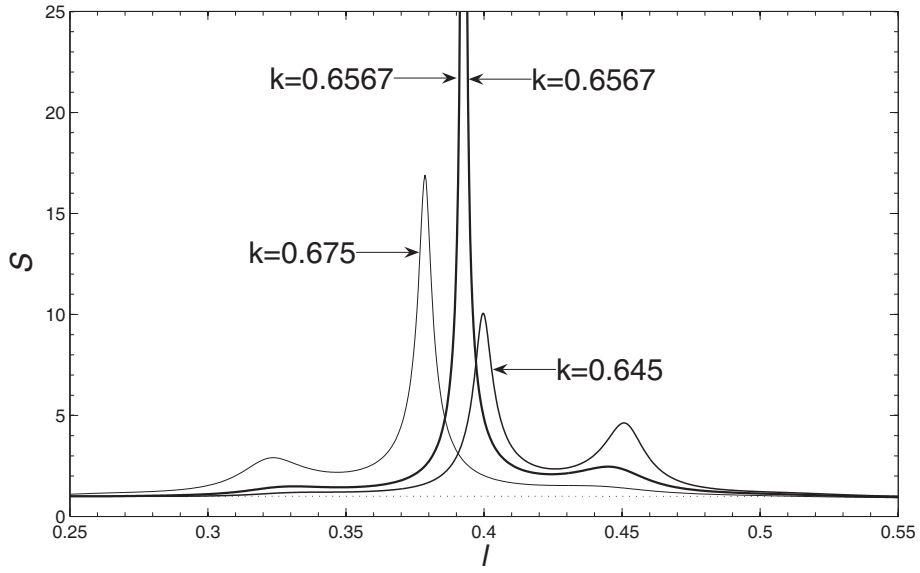

Figure 5.5: The dependence of the non-unitarity coefficient S on the meridional wavenumber l of the incident wave, for the two-jet configuration specified in Fig. 5.3. The latitudinal wavenumber k is fixed (the value indicated on for each curve).

- The two-jet configuration $U(y) = U_1(y + 20) + U_2(y - 20)$, Fig. 5.4:

  – At the first sight this plot does not differ much from Fig. 5.3b. And indeed, the regions of absorption ($S < 1$), over-reflection ($S > 1$) and neutral interaction ($S = 1$) remain exactly the same. However, the "containing" region between two jets is conductive to stronger over-reflection/absorption according to the predictions of §4.4.

  – We find a small region situated around $k \approx 0.65$ and $l \approx 0.39$, where over-reflection is anomalously high ($S \gtrsim 10$). Further computations specifically looking for the hyper-reflected wave solution (see §4.3.1 for the algorithm) were carried out within this region. Based on the results we conclude that for a certain value $k = K$ and $l = L$ the non-unitarity coefficient S is infinite – *i.e.* hyper-reflection occurs. The behavior of S as a function of l is plotted for 3 vertical (fixed k) sections of the region in Fig. 5.5.

    The computations were stopped when the non-unitarity coefficient reached values $S \sim 1500$ as further numerics would not be fully reliable. The wave vector for which hyper-reflection occurs for this two-jet configuration was found to be

$$K \approx 0.6567, \qquad L \approx 0.3926.$$

– Observe that the hyper-reflected wave (K, L) is scattered by the individual jets $U_{1,2}$ with (moderate) coefficients $r_{1,2}$, $t_{1,2}$ satisfying the no incident wave condition (E.10) (see §4.4.1).

5.3.2 Discussion

Hence, the mechanism of resonant over-reflection described in §4.4.1 is valid and present in problems of multiple scattering. Hence, we assert that the results obtained in Chapter 4 are general and can be applied to any scattering problems regardless of the model.

We shall also point out that:

- Mathematically, singularities associated with critical levels are not essential for hyper-reflection. Indeed, the "general" formulation of the problem through equation (4.62) shows that hyper-reflection can also occur if the potentials $P_{1,2}$ are analytical but *complex* functions. The latter property guarantees that over-reflection by a single jet may still occur – hence, so can hyper-reflection.

- In addition to hyper-reflection caused by trapping of Rossby waves between the jets on the β-plane described here, there are be cases of hyper-reflection of waves by a *single* Bickley jet when their critical levels are located at the jets' maxima (see Maslowe [61]). However, the corresponding singularities are *second*-order poles while both of the scattering problems we examined in this thesis (Chapters 4 and 5) involve *first*-order poles only. These two cases are very different because in the former case the conventional regularization of singularities with infinitesimal Rayleigh viscosity no longer works.

- The reason why hyper-reflection cannot occur for a *single* Bickley jet and not for a wave with a critical level located *at the jet's maximum* (described by Maslowe [61]), appears to be the *symmetry* in the governing Eqs. (5.14), (5.16) (about the middle of the jet's profile, *i.e.* $y = 0$). Recall that the scattering equations studied in Chapters 4 and 5 do not possess such symmetry due to variable layer thickness and two-jet profile respectively.

- One may wonder to what extent the analysis of this chapter relies on the presence of multiple jets. To address this we investigated what happens to the resonantly over-reflected wave when the velocity profiles merge with each other. As the distance between jets' maxima d is reduced there is no clear distinction between U_1 and U_2

and a single *asymmetric* emerges. We observed numerically how the parameters of the hyper-reflected wave smoothly adjusted to this and with the corresponding critical layer approaching the jet's maxima as d tends to 0 (in full agreement with the results in [61]). Hence, it is not the two-jet configuration but rather the asymmetry in the equations that is essential for the existence of resonant over-reflection.

5.4 Summary

We have examined linear scattering of barotropic Rossby waves by the background flow consisting of two localised zonal jets on a QG β-plane. The equation that describes the latitudinal structure of a propagating monochromatic wave was first derived about 60 years ago by Kuo [45] and is very well studied. As its counterpart from Chapter 4, it contains critical layers where absorption or over-reflection can occur depending on the sign of the PV gradient $Q' = \beta - U''$ there (Dickinson & Clare [20], Lindzen and Tung [55], Yamada and Okamura [89]).

It was not our intention to "re-invent the wheel" but rather to test and illustrate with an example the concept of hyper-reflection as a "resonance" between two containing barriers proposed in §4.4. So, we investigated numerically the scattering properties of two-jet flows with the individual profiles taken as Bickley jets (4.55). The main results were illustrated with help of contour plots displaying isolines of the non-unitarity function for each individual jet and the system as a whole (Fig. $5.3 - 5.4$).

We showed that while each individual Bickley jet cannot hyper-reflect waves (with an exception of waves with their critical levels at the jet's maxima [61]), the two-jet configuration manifests an example of hyper-reflection caused by trapping of waves between the individual jets playing the role of containing barriers. The cases of hyper-reflection occurred in full agreement with condition (4.72). Hence, we have successfully validated the results of §4.4 with this illustrative problem.

The presented results are also of interest on their own as they can be important in understanding dynamics of multiple-jet systems observed in the Antarctic Circumpolar Current, Earth's tropical ocean and in the atmosphere of Jupiter (see [81], and references therein).

Chapter 6

Resonant Over-Reflection as a Marginally Stable Disturbance

Linear homogeneous PDEs governing the dynamics of small-amplitude harmonic perturbations superimposed upon the mean flow on an unbounded domain can have two types of solutions. *Normal modes* which decay to zero at infinities make up the first type. They are typically studied in the context of linear instability problems in various models. In the context of RGRSW model such was examined by Paldor and Ghil [70] (and predecessors) and within the framework of a barotropic β-plane the earliest works were done by Kuo [45], Lin [52] and Dickinson and Clare [20]. Another type of solution can be found if the system has a restoring mechanism that supports wave motions at infinities. Such solutions are studied within the framework of corresponding scattering problem and represent the result of stationary interaction between an incoming wave and the mean flow. As we know, this wavy solutions do not vanish at infinities and can be decomposed there into the incident, reflected and transmitted waves.

In this section, we investigate the connection between the normal modes and scattered wave solutions. We show that hyper-reflection can be perceived as a borderline case of certain unstable normal modes (*radiating instabilities*). The idea is to examine what happens with a hyper-reflected wave when its wave vector or the parameters of the jet are perturbed. In §6.1 we keep our approach as general as possible, so that the results would be applicable to any scattering problem which can be formulated in terms of Schrödinger equation (4.62). Then, in §6.2 general results will be illustrated by the example of barotropic Rossby waves and jets of the QG β-plane.

6.1 General case

Typically, problems of scattering of small amplitude harmonic wave disturbances by a medium which properties vary in one direction only can be described by a single linear homogeneous ODE. The latter can be further simplified to be written in the form of the Schrödinger equation

$$-\phi'' + P\phi = l^2\phi, \tag{6.1}$$

as it has been done in §4.4. For simplicity we assume that

$$P(y) \to 0 \qquad \text{as } y \to \pm\infty.$$

Observe that this assumption holds for quasi-geostrophic jets (Chapter 5), but does not for ageostrophic ones (Chapters 4). However, the results obtained here can be readily extended to the latter case of "step-like" potentials ($P(y)$ has different limits as $y \to \pm\infty$).

To describe a hyper-reflected wave, we shall use the general equation (6.1) and the following boundary condition:

$$\left.\begin{array}{lll} \phi \to \bar{r}\,\mathrm{e}^{-\mathrm{i}ly} & \text{as} & y \to -\infty, \\ \phi \to \bar{t}\,\mathrm{e}^{\mathrm{i}ly} & \text{as} & y \to +\infty. \end{array}\right\} \tag{6.2}$$

Comparing (6.2) with the standard boundary condition for scattering, (4.27)/(5.16), one can see that the former describes reflected/transmitted waves without an incident one – which is what hyper-reflection essentially is.

However, we must ensure that Eq. (6.2) describes two outgoing waves rather than two waves coming from infinity and absorbed by the jet. To eliminate the latter possibility, we require for the energy flux to be outgoing:

$$c_{gr}^{(y)}(k_0, -l_0) < 0, \qquad c_{gr}^{(y)}(k_0, l_0) > 0, \tag{6.3}$$

where

$$\vec{c}_{gr} = \left(\frac{\partial\omega(k,l)}{\partial k}, \frac{\partial\omega(k,l)}{\partial l}\right),$$

is the waves' group velocity and (k_0, l_0) is the wave vector of a resonantly over-reflected wave.

Note also that the coefficients $\bar{r}$ and $\bar{t}$ can be related to the original scattering coefficients R and T by

$$\bar{r} = \lim_{(k,l)\to(k_0,L)} \frac{R}{\sqrt{|R|^2+|T|^2}}, \qquad \bar{t} = \lim_{(k,l)\to(k_0,l_0)} \frac{T}{\sqrt{|R|^2+|T|^2}},$$

where (k_0, l_0) is the wave vector of the hyper-reflected wave.

Equation (6.1) and boundary condition (6.2) form and eigenvalue problem, where ϕ is the eigenfunction and l is the eigenvalue. We shall distinguish two types of solutions: hyper-reflected waves ($\operatorname{Im} l = 0$) and "*trapped waves*" ($\operatorname{Im} l > 0$). Solutions with $\operatorname{Im} l < 0$, in turn, grow as $y \to \pm\infty$ [see (6.2)] and, thus, are meaningless physically.

Now, let

$$P = P_0 + \varepsilon P_1 + \varepsilon^2 P_2 + \cdots,$$

where P_0 is the unperturbed potential for which (k_0, l_0) is the wave vector of the hyper-reflected wave and ε is a small parameter. Note that P_0 (and hence P_1, P_2, *etc.*) has a number of singularities and the expansion is only applicable far from these points.

A perturbation of P should perturb the solution:

$$\phi = \phi_0 + \varepsilon\phi_1 + \varepsilon^2\phi_2 + \cdots, \qquad l = l_0 + \varepsilon l_1 + \varepsilon^2 l_2 + \cdots, \tag{6.4}$$

$$\bar{r} = \bar{r}_0 + \varepsilon\bar{r}_1 + \varepsilon^2\bar{r}_2 + \cdots, \qquad \bar{t} = \bar{t}_0 + \varepsilon\bar{t}_1 + \varepsilon^2\bar{t}_2 + \cdots. \tag{6.5}$$

In the next-to-leading order, the boundary-value problem (4.62), (6.2) yields

$$-\phi_1'' + P_1\phi_0 + P_0\phi_1 = l_0^2\phi_1 + 2l_0l_1\phi_0. \tag{6.6}$$

Recalling that

$$\left.\begin{aligned} \phi_0 &\to \bar{r}_0\,\mathrm{e}^{-\mathrm{i}l_0 y} \quad \text{as} \quad y \to -\infty, \\ \phi_0 &\to \bar{t}_0\,\mathrm{e}^{\mathrm{i}l_0 y} \quad \text{as} \quad y \to +\infty, \end{aligned}\right\}$$

one can readily show that the term involving ϕ_0 on the right-hand side of (6.6) causes ϕ_1 to grow linearly as $y \to \pm\infty$. As a result, expansion (6.4) is valid only for $|y| \ll \varepsilon^{-1}$ and should be treated as the *inner* solution of the problem.

The *outer* solution, in turn, is given by the boundary condition (6.2) – which represents the asymptotics of ϕ in the region where $|P| \ll 1$, *i.e.* for $|y| \gg 1$. The outer and inner solutions "overlap" for $1 \ll |y| \ll \varepsilon^{-1}$ – thus, for matching, the outer limit of ϕ_1 should

be equated to the inner limit of (6.2). This amounts to expanding (6.2) in ε, which yields

$$\left.\begin{array}{lll} \phi_1 \to \bar{r}_0\,\mathrm{e}^{-\mathrm{i}l_0 y}\,(-\mathrm{i}l_1 y) + \bar{r}_1\,\mathrm{e}^{-\mathrm{i}l_0 y} & \text{as} & y \to -\infty, \\ \phi_1 \to \bar{t}_0\,\mathrm{e}^{\mathrm{i}l_0 y}\,(\mathrm{i}l_1 y) + \bar{t}_1\,\mathrm{e}^{\mathrm{i}l_0 y} & \text{as} & y \to +\infty. \end{array}\right\} \tag{6.7}$$

The boundary-value problem (6.6) – (6.7) determines both ϕ_1 and l_1. The latter, however, is the more important characteristic, and it can be found without the former.

To find l_1, multiply (6.6) by ϕ_0 and integrate over a contour Γ in the complex plane that connects points $-Y$ and Y (where Y is an undetermined large number) and steps around the singularities as prescribed by the regularization (**Appendix C**). Integrating the term involving ϕ_1'' by parts twice and taking into account that ϕ_0 satisfies

$$-\phi_0'' + P_0\phi_0 = l_0^2\phi_0,$$

we obtain

$$\left(\phi_0'\phi_1 - \phi_0\phi_1'\right)_{y=Y} - \left(\phi_0'\phi_1 - \phi_0\phi_1'\right)_{y=-Y} + \int_\Gamma P_1\phi_0^2\,\mathrm{d}y = 2l_0l_1\int_\Gamma \phi_0^2\,\mathrm{d}y. \tag{6.8}$$

Observe that, in the limit $Y \to \infty$, the integral on the right-hand side of (6.8) diverges. Thus, at this stage, we let Y be large but not infinitely so, and re-arrange the first two terms in (6.8) using (6.7) – which yields

$$-\mathrm{i}l_1\left(\bar{t}_0^2 + \bar{r}_0^2\right)\mathrm{e}^{2\mathrm{i}l_0 Y} + \int_\Gamma P_1\phi_0^2\,\mathrm{d}y \to 2l_0l_1\int_\Gamma \phi_0^2\,\mathrm{d}y \qquad \text{as } Y \to \infty. \tag{6.9}$$

Next, introduce an auxiliary function

$$\hat{\phi}^2 = \begin{cases} \bar{r}_0^2\,\mathrm{e}^{-2\mathrm{i}l_0 y} & \text{if} \quad y \le 0, \\ \bar{t}_0^2\,\mathrm{e}^{2\mathrm{i}l_0 y} & \text{if} \quad y > 0, \end{cases} \tag{6.10}$$

in terms of which (6.9) can be re-written in the form

$$2l_0l_1\int_{-Y}^{Y}\hat{\phi}^2\,\mathrm{d}y - \mathrm{i}l_1\left(\bar{t}_0^2 + \bar{r}_0^2\right) + \int_{-Y}^{Y} P_1\phi_0^2\mathrm{d}y \to 2l_0l_1\int_{-Y}^{Y}\phi_0^2\,\mathrm{d}y \qquad \text{as } Y \to \infty.$$

Rearranging the integrals of $\hat{\phi}^2$ and ϕ_0^2 as a single integral of $\phi_0^2 - \hat{\phi}^2$ and taking now the

limit $Y \to \infty$, we obtain

$$\int_{-\infty}^{\infty} P_1 \phi_0^2 \, \mathrm{d}y = l_1 \left[2 l_0 \int_{-\infty}^{\infty} \left(\phi_0^2 - \hat{\phi}^2 \right) \mathrm{d}y + \mathrm{i} \left(\bar{t}_0^2 + \bar{r}_0^2 \right) \right]. \tag{6.11}$$

This equation is the final product of our derivation. It relates the perturbation l_1 of the eigenvalue to the perturbation P_1 of the potential. Observe that, if

$$P_1 = \mathrm{O}(y^{-1-\gamma}) \qquad \text{as } y \to \pm\infty,$$

where $\gamma > 0$, the integral on the left-hand side of (6.11) converges, and so does the integral on its right-hand side subject to a similar restriction imposed on P_0.

Most importantly, equation (6.11) is complex (as ϕ_0 is complex, and so are, generally, $\bar{r}_0$ and $\bar{t}_0$). Thus, for an arbitrary perturbation P_1, (6.11) yields either $\operatorname{Im} l_1 > 0$ (trapped wave), or $\operatorname{Im} l_1 = 0$ (hyper-reflected wave), or $\operatorname{Im} l_1 < 0$ (meaningless solution). We conclude that hyper-reflected waves are marginal to trapped ones.

Furthermore, one one should realize that trapped waves are all unstable, *i.e.* hyper-reflected waves are, in fact, marginally stable disturbances. This is somewhat of a conventional belief that decaying modes are always growing in time. Although, it is not necessarily true (*e.g.* a few analytical examples of neutral trapped modes on the barotropic β-plane are given in [61]). Hence, a rigorous proof is needed.

We can use the dispersion relation $\omega(k, l)$ defining the wave's frequency as a function of the wave vector, to write down the first-order correction to ω

$$\omega_1 = c_{gr}^{(x)}(k_0, l_0) \, k_1 + c_{gr}^{(y)}(k_0, l_0) \, l_1 + \hat{\omega}_1, \tag{6.12}$$

where $\hat{\omega}_1$ represents some other corrections due to the perturbation of other parameters in the the dispersion relation, such as, for instance, the ocean's depth.

Now recall that we deal with a conservative medium for which the dispersion relation is real, and hence, $\vec{c}_{gr}$ and $\hat{\omega}_1$ are both real too (as it results from perturbations of real parameters). Hence, (6.12) implies

$$\operatorname{Im} \omega_1 = c_{gr}^{(y)}(k_0, l_0) \operatorname{Im} l_1.$$

This equation shows that, since all "captured" (trapped) modes correspond to $\operatorname{Im} l_1 > 0$ and, according to (6.3), $c_{gr}^{(y)}(k_0, l_0)$ is positive, then $\operatorname{Im} \omega_1 > 0$, *i.e.* these modes are indeed

unstable. Note that in the context of hyper-reflection, conservative media are the only interesting ones, as dissipative media do not support propagation of waves without decay.

It is worth mentioning that captured modes are unstable due to wave generation at the critical levels (see [62], [49], and references therein) and the exponentially decreasing as $y \to \pm\infty$ "tails" of these modes can be interpreted as waves emitted at an earlier time, when the disturbance near the critical levels was exponentially weaker.

Finally, one may be alarmed by the fact that our analysis did not recover the scattered wave solutions and in the previous chapters we found resonance over-reflection as a part of the scattering problem. This apparent discrepancy is explained by the fact that boundary condition (6.2) does not allow for inward propagation of the energy flux and, hence, incoming waves. The described procedure can be modified to include an "incident-wave perturbation" in the boundary condition. In this case the perturbed solution can be obtained as a scattered wave with $\operatorname{Im} l_1 = 0$.

6.2 An example: waves and jets on the beta-plane

For illustrative purposes we present the results of the previous section to the problem from Chapter 5, *i.e.* a zonal jet (not necessarily a multi jet) in the QG β-plane model.

To prove that a hyper-reflected wave is marginally unstable, it is sufficient to perturb the zonal wavenumber

$$k = k_0 + \varepsilon k_1,$$

and then verify that one of the two possible signs of k_1 gives rise to an unstable trapped wave mode, whereas the other does not. The jet's shape $U(y)$ does not need to be perturbed.

Note also that, in this section, we do not necessarily imply that $U(y)$ represents a two-jet configuration. All we assume is that a hyper-reflected wave exists, and its wave vector is (k_0, l_0).

Perturbing the dispersion relation for barotropic Rossby waves (5.6) and formula for the scattering potential (5.20), we obtain

$$\omega_1 = -\frac{\beta k_1}{k^2 + l^2} + \frac{2\beta k_0 \left(l_0 l_1 + k_0 k_1\right)}{k^2 + l^2}, \tag{6.13}$$

$$P_1 = 2\left(l_0 l_1 + k_0 k_1\right)\left\{1 + \frac{k_0^2 \beta \left(U'' - \beta\right)}{\left[k_0 \beta - \mathrm{i}0 + k_0 U\left(k_0^2 + l_0^2\right)\right]^2}\right\}. \tag{6.14}$$

Substitution of (6.13) – (6.14) into the general formula (6.11) (where we need to replace ϕ with ψ) yields

$$l_1 = \frac{Ik_0k_1}{(J-I)\,l_0 + \frac{\mathrm{i}}{2}\left(\bar{t}_0^2 + \bar{r}_0^2\right)}, \tag{6.15}$$

where

$$I = \int\limits_{-\infty}^{\infty} \left\{ 1 + \frac{k_0^2\beta\,(U''-\beta)}{\left[k_0\beta - \mathrm{i}0 + k_0U\left(k_0^2+l_0^2\right)\right]^2} \right\} \psi_0^2\,\mathrm{d}y,$$

$$J = \int\limits_{-\infty}^{\infty} \left(\psi_0^2 - \hat{\psi}^2\right) \mathrm{d}y.$$

Again, there exists a trapped wave solution. It follows from (6.15) that, if a solution with $\mathrm{Im}\,l_1 > 0$ does not exist for $k_1 > 0$, it does so for $k_1 < 0$, and vice versa. One way or another, captured modes do exist; then it follows from (6.13) that $\mathrm{Im}\,l_1 > 0$ entails $\mathrm{Im}\,\omega > 0$ (instability).

Finally, observe that expression (6.13) can be re-written in the form

$$\omega_1 = c_{gr}^{(x)}\,(k_0,l_0)\,k_1 + c_{gr}^{(y)}\,(k_0,l_0)\,l_1, \tag{6.16}$$

where $c_{gr}^{(y)}$ and $c_{gr}^{(x)}$ are the meridional and zonal components of the group velocity of Rossby waves. Comparing (6.16) with the general expression (6.12) , one can see that $\hat{\omega}_1$ is zero in this case.

6.3 Summary and Discussion

In §6.1 we proved that hyper-reflected waves found within any scattering problem (that can be written as a Schrödinger equation (4.62)) are marginal to "trapped wave" modes, *i.e.* unstable disturbances that are usually referred in the literature as *radiating instabilities*. Then, in §6.2 we applied the result to the case of a zonal jet on the non-divergent barotropic β-plane. The example illustrates how a perturbation in the zonal wavenumber of a resonantly over-reflected wave gives rise to an unstable radiating mode.

Thus, we proved that the mean flow is linearly unstable when hyper-reflection is present. We emphasise that this new criterion for instability was obtained through the general approach based on the Schrödinger equation (4.62). Hence, it applies to all media that support over-reflection of waves: the ocean, atmosphere, plasma and many other physical settings. In particular, it is in agreement with the results of linear stability

analysis of problems examined by Lindzen [54], Maslowe [61], and Lott *et al.* [57] – in all of which hyper-reflected wave solutions are adjacent to radiating instabilities in the parameter space.

Recall that in §2.1 we discussed the prior results in the literature (two specific setting: vertical shear in Boussinesq fluid and zonal jet on the QG β-plane) indicate that necessary conditions for over-reflection and instability often coincide. It is now clear that the possibility of over-reflection can allow for the singular case, *i.e.* resonant over-reflection to appear, and the latter accompanies instabilities.

Although presence of unstable modes *does not* make the corresponding scattering problem and the obtained results irrelevant (see discussion in §7.2). *All* major currents in the Earth's ocean are essentially unstable. However, they are supported by external (climatic) forcing and the instabilities never make them disappear but only induce meanders and large fluctuations. Taking the time average in most cases produces a clear (smeared-out) mean flow. And even when the dynamics is dominated by the most unstable (trapped) modes, the resonantly over-reflected waves remain to be of great interest. Unlike non-radiating normal modes, hyper-reflected waves penetrate far away from the jet's core and, hence, constitute the main component of the solution in the far field.

Chapter 7

Conclusions

7.1 Summary and concluding remarks

It has been known for more than 120 years that the linearized equations for harmonic mode perturbations superimposed upon a mean flow involve critical layer singularities where the mean flow velocity equals the corresponding component of the wave's phase velocity (Rayleigh [74]). And more than 40 years ago it was established that waves penetrating a shear current or wind interact with the flow at the critical layers which can result in their absorption (Booker & Bretherton [8]) or amplification (Jones [40]). The latter case is best known as over-reflection (also as over-transmission), although their original definition is restricted to the case where the amplitude of the reflected (transmitted) wave exceeds that of the incident wave.

Based on these ideas, we examined scattering of small-amplitude internal gravity waves (IGWs) and Rossby waves by zonal jets in the ocean or atmosphere within the f-plane reduced gravity rotating shallow water (RGRSW) and quasi-geostrophic (QG) β-plane models respectively. Singularities of the corresponding governing equations (4.21) and (5.14) were studied analytically and non-unitarity conditions (4.52) and (5.18) describing the energy balance (hence, generation or dissipation of wave energy at the critical layers) were derived. An important finding of this study, is the fact that in both cases it is the sign of the derivative of the jet's potential vorticity (PV) that determines whether over-reflection (over-transmission) or absorption occurs.

Reflection and transmission coefficients were calculated numerically for the case of waves scattered by a Bickley jet and by a configuration consisting of two localised Bickley jets (§4.3 and §5.3). The numerics were carried out for a wide range of parameters which include two wavenumbers of the incident wave (k, l), the depth change across the jet

ΔH and the jet's width W. The integral picture of the scattering properties of a jet are succinctly shown on contour plots displaying isolines of the non-unitarity function (*e.g.* Fig. 4.5, 5.3, 5.4).

We find that jets can generate propagating wave instabilities where the "reflected" and "transmitted" waves are spontaneously emitted without the incident one. In other words, for the first time resonant over-reflection was found to occur within these two models. In §4.4 we proposed a plausible physical interpretation of the phenomenon after the governing equations (4.21) and (5.14) were transformed into a Schrödinger-type equation (4.62) with potentials (4.63) and (5.20) respectively.

1. For the f-plane RGRSW model, we argued that hyper-reflection occurs because an amplifying critical level is located in-between two apparent singularities. The latter act as containing barriers which can lead to multiple over-reflection and, hence, generation of propagating wave instabilities.

2. In case of a two-jet configuration on the QG β-plane, the individual jets themselves play the roles of barriers. Analytical "resonance" criterion (4.72) determining occurrence of hyper-reflection was applied and tested. According to it a wave trapped between the jets must regains its original amplitude and phase returning after two successive reflections of the jet-barriers.

3. We argued that in both cases over-reflection was *transformed* into hyper-reflection by an appropriate trapping mechanism (the double jet or apparent singularities).

The main result is, probably, the proof that resonantly over-reflected waves (*i.e.* neutral radiating modes) coexist with trapped unstable modes as shown in Chapter 6. We argued that a hyper-reflected wave is a marginally stable disturbance, a borderline case of radiating instabilities. Hence, in the spectral region the points corresponding to hyper-reflection form a part of the stability boundary curve. Moreover, its very existence is a criterion for linear instability of the mean flow.

Finally, note that the opposite statement is *not* correct: if a jet or another system is unstable, a hyper-reflected wave may not exist, nor be found on the neutral stability boundary. Firstly, the system which stability is under investigation must possess a restoring mechanism of certain nature (density stratification, planetary rotation, compressibility, *etc.*) to support radiating modes and, in particular, emission of waves. But even if present, resonant over-reflection may not occur.

For example, compare three analytical studies where scattering of IGWs incident upon a shear layer was examined within the Boussinesq model. Lott *et al.* [57] considered a general case with a hyperbolic tangent velocity profile and variable Brunt–Väisälä frequency N and found resonantly over-reflects IGWs. A specific case of this model with $N = \mathsf{const}$ was previously studied by Van Duin & Kelder [85] who showed that hyper-reflection is ruled out unless the width of the velocity "step" profile is 0. And in this (non-uniform) limit the profile approximates the Helmholtz profile and resonant over-reflection manifests itself for a whole range of wavenumbers (McKenzie [63], Lindzen [54]). Note, that the specific stratification that is smaller inside the shear layer than outside is the key explaining the difference in results of [57] and [85]. This outcome is compatible with our idea that a "trapping" mechanism (supported by the region of weak stratification in this case) is responsible for emergence of hyper-reflection.

The importance of the obtained results is related to investigation of spontaneous emission of waves by shear flows. As discussed in §2.2 propagating wave instabilities and resonant over-reflection provide a plausible source of waves in the ocean and atmosphere in general.

It is instructive to put the developed ideas in perspective of other theoretical interpretations of the phenomena of spontaneous emission of waves and radiating instabilities.

- First of all, throughout the thesis we extensively used the mathematical analogy between the scattering theory for waves in fluids, on the one hand, and particles in quantum mechanics, on the other hand (both governed by means of the *Schrödinger equation* equation). Recently, these long standing ideas have been actively promoted by Le Dizès and co-authors, who in a series of problems demonstrated that emission of internal waves from unstable mean flow can be analogous to the radioactive decay of nuclei in quantum mechanics ([49], and references therein). Their description of radiative instability, based on the WKB analysis for large cross-flow wavenumber, also allows for interpretation in terms of over-reflection.

- Another approach to understanding plane-parallel shear instabilities was proposed by Bretherton [13]. Specifically for the baroclinic instabilities in the two-layer QG model, he gave the following qualitative explanation. Instability is obtained in case of interaction between two counterpropagating Rossby waves, which are located in regions of different signs of the mean potential PV gradient and "locked on" to each other. The original approach was recently extended by Heifetz and co-authors, who also bring it in agreement with the over-reflection theory and rationalized the

latter in terms of PV thinking suggested by Bretherton. The two seemingly different paradigms illuminate very different aspects of the instability mechanism and, by relating them, deeper understanding is achieved.

- Finally, there is a concept of *negative energy waves*, which was developed and flourished in plasma physics, that gives insight into the linear (and nonlinear!) instability mechanisms. The approach was later adopted for hydrodynamic stability problems and used to explain instabilities in a number of systems (Cairns [16], Shrira *et al.* [80], and references therein). As one can show, after the appropriate definition, the negative energy waves can be found in the linearized system. However, its' establishment requires that energy is extracted from, rather than fed into the system. And, in contrast to the usual positive energy wave, their wave amplitudes increase when their "negative energy" is decreased (*e.g.* by damping). Observe that these ideas, *i.e.* growth of the wave energy at the expense of the mean state and the necessity of a dissipative process, clearly resemble those of the over-reflection. Generally, there is a link between the concepts that would be interesting to explore in context of the present work.

7.2 Limitations and future work

It is important to discuss the applicability and robustness of our results. The limitations stem from a multitude of approximations and assumptions which we were forced to adopt in order to make our models more tractable.

Here we shall list the introduced simplifications in the order they appear in the derivations in Chapters 4 and 5. We also propose that would help to validate the results and clarify the limits of their applicability.

1. In Chapters 4 & 5 the equations governing dynamics of fluctuations superimposed upon the mean flow were *linearized*. This is a crude assumption as finite amplitude wave dynamics is essentially nonlinear. Hence, as a natural extension of the present work it would be interesting to examine the phenomenon of resonant over-reflection within the weakly nonlinear theory (which retains cubic terms in the scattering equation). It may or may not rule out nonphysical infinite excitation of hyper-reflected waves. For example, Grimshaw [31], [32] developed the weakly nonlinear extension of extension of the model studied by McKenzie [63] and Lindzen [54] (within which the resonant over-reflection was found). He showed that the solution

develops a singularity in a finite time which confirmed existence of the phenomena even within the weakly nonlinear theory.

2. Following the standard practice for linear wave analysis we transformed the problem into the frequency-wavenumber domain (by taking Fourier transform in in zonal coordinate and time). As the result, explicit time dependence was removed from the equations and the steady-state problem was considered. However, to judge the importance of hyper-reflecion phenomenon, we need an estimate of the dynamical time scales involved. The initial problem solved for a single incident wave packet experiencing resonant over-reflection would greatly clarify the matters.

   McIntyre and Weissman [62] did this analytically (under certain assumptions) for hyper-reflection within Lindzen's vortex-sheet model. They found behaviour similar to that of a forced harmonic oscillator near resonance (*i.e.* the response exhibits linear growth in time). A more general situation (like ours) can be treated numerically but the overall result is expected to be similar.

   The numerical solutions of the time evolution of a wave packet experiencing over-reflected at a critical layer were obtained beforehand (*e.g.* in [83] for shallow water). Similar numerical simulations of the time-dependent 1D equations should be carried out for our problems (RSW and QG models). This can be done, *e.g.* with help of the shallow water module incorporated in COMSOL Multiphysics, a finite element package. The results could then be compared with the predictions of linear (and nonlinear, see below) models and high-resolution numerical simulations of the wave emission by unstable flows (such as in [87]). The numerics would also give some insight into the time-dependent and non-linear effects in the critical layers ([60], and references therein).

3. Throughout this thesis we approximated ocean currents with symmetric *zonal* jet-like velocity profiles, which constitutes an important limiting factor of this work. While there is no obvious reason to think that removing the symmetry assumption would greatly improve generality of the results, the situation is different with the assumption of zonality. Fig. 1.3 illustrates that (even after time-averaging) all major surface ocean currents are far from being zonal. Hence, it is extremely interesting to investigate the effect of nonzonality on the critical layer singularities in general, and the discovered examples of hyper-reflection in particular.

Some related work has already been done but is not presented in this thesis. For example, we showed that when meridional tilt is introduced into the quasi-geostrophic (QG) β-plane model, the logarithmic singularity in the solution at the critical layer $\sim x \ln(x)$ is replaced with oscillating singularity $\sim x^{1+i\alpha}$. Thus, the conventional regularization of singular points in the scattering equation is no longer applicable. However, as cited in §2.2, previous developments considering radiating instabilities generated by non-zonal currents on the quasi-geostrophic (QG) β-plane discovered the destabilizing effect of the meridional tilt and and resulting abundance of unstable radiating modes. Hence one may expect the hyper-reflection to exist as their limiting case.

Curiously, non-trivial wave-current interaction (*i.e.* absorption or amplification of the incident wave) is present even in absence of critical layer singularities because the coefficients in the governing equations are *complex-valued* (see 5.3.2). A special case of interaction between short barotropic Rossby waves and slow mean flow on the quasi-geostrophic (QG) β-plane was examined analytically with help of WKB approximation. The collective effect of Rossby-wave turbulence on the non-zonal jet and its resulting evolution was successfully modeled with a linear PDE. The effect was found to "smeared out" the initial mean flow profile. The solution approaches the limiting "stationary" profile as time tends to infinity.

Another non-trivial extension of the critical layer theory was done by Jones [39] and Grimshaw [29]. The latter introduced rotation about an axis inclined to the vertical into the Boussinesq model which corresponds to a non-trivial vertical component of the Coriolis force. And when the latter is strong enough, Grimshaw showed that the critical layers turns into more complicated singularities which effect is very different from that of the Booker & Brethertons critical layer [8]. Generally speaking, the question of what happens to the singularity associated with the critical layers (and, hence, our results) when the governing equations are perturbed by the introduction of of higher-order effects, requires deeper investigation.

4. In Chapter 6 we made a conclusion that resonant over-reflection necessarily entails instability. Hence the question arises as to how the (eventually nonlinear) *evolution of the current* due to unstable modes modify the results. What will happens to the singularities? How do the time scales of current evolution and the development of the resonant over-reflection compare? Nonlinear effects tend to alter the mean flow

in the vicinity of the critical layer ("nonlinear Landau damping" [60]). What will be the characteristic time scales and how do *these* compare to those of resonant over-reflection. What is the range of parameters and times where the developed theory could be applied as it is? These very complicated and, undoubtedly, important issues are far outside the scope of this work.

Note, that the information on wave-mean flow interaction in critical layers obtained from the scattering problems solved in Chapters 4 & 5 cannot be directly used to model the collective effect of waves on the mean flow similarly to how it was done in [5] and [53] (see §1.1.4). Hyper-reflected waves have infinite reflection and transmission coefficients and, hence, the influence of such incident wave on the flow is (unphysically) *infinitely* strong at the corresponding critical layers. Nevertheless, the example of scattering of IGWs by a shear layer of rotating stratified fluid considered by Van Duin & Kelder [85] illustrates that over-reflection does not necessarily imply hyper-reflection. Hence, the approach used by Benilov *et al.* [5] can be applied to model slow evolution of shear flows in Boussinesq fluid (and other models) due to the collective effect of a stochastic field. Generally, a system of nonlinear PDEs can be derived governing the evolution dynamics (which has been done for the model in Chapter 4).

In §2.3 we remarked that Ollers *et. al.* in [69] probably missed out hyper-reflected wave solutions within their model. This conjecture can be easily checked which would be another test for the ideas of resonance over-reflection elaborated in this thesis.

Finally, it would be interesting to carry out full linear stability analysis of Eqs. (4.21) and (5.14). Hence, to find all unstable normal modes (radiating and trapped ones) and construct the neutral stability boundary. The latter is expected to be quite complex and to be comprised of several neutral curves (corresponding to resonant over-reflection, neutral trapped modes, *etc.*) and to possibly forms cusps at the points of their intersection (Maslowe [61]).

Bibliography

[1] Acheson, D.J. 1976: On over-reflection. *J. Fluid Mech.,* **77**, 433-472.

[2] Afanasyev, Y.D., Rhines, P.B. & Lindahl, E.G. 2008: Emission of inertia-gravity waves by baroclinically unstable flows: laboratory experiments with Altimetric Imaging Velocimetry. *J. Atmos. Sci.,* **65**, 250-262.

[3] Balmforth, N.J. 1999: Shear instability in shallow water. *J. Fluid Mech.,* **387**, 97-127.

[4] Basovich, A.Ya. & Tsimring, L.Sh. 1984: Internal waves in a horizontally inhomogeneous flow. *J. Fluid Mech.,* **142**, 233-249.

[5] Benilov, E.S. Gnevyshev, V.G. and Shrira, V.I. 1992: Nonlinear interaction of a zonal jet and barotropic Rossby-wave turbulence: the problem of turbulent friction. *Dyn. Atmos. Oceans,* **16**, 339-353.

[6] Benilov, E.S. & Sakov, P.V. 1999: On the linear approximation of velocity and density profiles in the problem of baroclinic instability. *J. Phys. Oceanogr.,* **29**, 1374-1381.

[7] Bohm, D. 1951: *Quantum theory*, Prentice-Hall, New York, 646 pp.

[8] Booker, J.R. & Bretherton, F.P. 1967: The critical layer for internal gravity waves in a shear flow. *J. Fluid Mech.*, **27**, 513-539.

[9] Boyd, J.P.: 1976 Planetary waves and the semiannual wind oscillation in the tropical lower stratosphere. *Ph.D. thesis, Harvard University.*

[10] Boyd, J.P. 1978: The effects of latitudinal shear on equatorial waves. Part 1: Theory and methods. *J. Atmos. Sci.,* **35**, 2236-2258.

[11] Boyd, J.P. 1985: Complex coordinate methods for hydrodynamics instabilities and Sturm-Liouville eigenproblems with interior singularity. *J. Comput. Phys.*, **57**, 454-471.

[12] Bower, A.S., & Hogg, N.G. 1992: Evidence for barotropic wave radiation from the Gulf Stream. *J. Phys. Oceanog.,* **22**, 42-61.

[13] Bretherton, F.P. 1966: Baroclinic instability and the short wavelength cut-off in terms of potential vorticity. *Quart. J. Roy. Meteor. Soc.*, **92**, 335345.

[14] Case, K.M. 1960: Stability of inviscid plane Couette flow. *Phys. Fluids* **3**, 143-148.

[15] Chelton, D.B. & Schlax, M.G. 1996: Global observations of oceanic Rossby waves. *Science*, **272**, 234 - 238.

[16] Cairns, R.A. 1979: The role of negative energy waves in some instabilities of parallel flows. *J. Fluid Mech.*, **92**, 1-14.

[17] Davis, P.A. & Peltier, W.R. 1980: Resonant Parallel Shear Instability in the Stably Stratified Planetary Boundary Layer, *J. Atmos. Sci.,* **33**, 1287-1300.

[18] Davis, P.A. & Peltier, W.R. 1980: Some characteristics of the Kelvin Helmholtz and over-reflection modes of shear Row and of their interaction through vortex pairing, *J. Atmos. Sci.,* **36**, 2394-2412.

[19] Dickinson, R.E. 1970: Development of a Rossby wave critical level. *J. Atmos. Sci.,* **27**, 627-633.

[20] Dickinson, R.E. & Clare, F.J. 1983: Numerical study of the unstable modes of a hyperbolic-tangent barotropic shear flow. *J. Atmos. Sci.,* **30**, 1035-1049.

[21] Drazin, P.G. 1958: The stability of a shear layer in an unbounded heterogeneous inviscid fluid. *J. Fluid Mech.,* **4**, 214-224.

[22] Dritschel, D.G & Vanneste, J. 2006: Instability of a shallow-water potential-vorticity front. *J. Fluid Mech.,* **561**, 237-254.

[23] Ducet, N. & Le Traon, P.Y. 2006: A comparison of surface eddy kinetic energy and Reynolds stresses in the Gulf Stream and the Kuroshio Current systems from merged TOPEX/Poseidon and ERS-1/2 altimetric data. *J. Geophys. Res.*, **106**, 16603-16622.

[24] Dunkerton, T.J. 1990: Eigenfrequencies and horizontal structure of divergent barotropic instability originating in tropical latitudes. *J. Atmos. Sci.,* **47**, 1288-1301.

[25] Eltayeb, I.A. & McKenzie, J.F. 1975: Critical-level behaviour and wave amplification of a gravity wave incident upon a shear layer. *J. Fluid Mech.,* **72**, 661-671.

[26] Fantini, M. & Tung, K.K. 1987: On radiating waves generated from barotropic shear instability of a western boundary current. *J. Phys. Oceanogr.,* **17**, 1304-1308.

[27] Gill, A.E., 1981: *Atmosphere-Ocean Dynamics,* Academic Press, New York, 662 pp.

[28] Gille, S.T. 1994: Mean sea surface height of the Antarctic Circumpolar Current from GEOSAT data: methods and application. *J. Geophys. Res.* **99**, 18255-18273.

[29] Grimshaw, R.H.J. 1975: Internal gravity waves: critical layer absorption in a rotating fluid. *J. Fluid Mech.,* **70**, 287-304.

[30] Grimshaw, R.H.J. 1976: The reflection of internal gravity waves from a shear layer *Q. J. Mech. Appl. Math.,* **29**, 511-525.

[31] Grimshaw, R.H.J. 1979: On resonant over-reflection of internal gravity waves from a Helmholtz velocity profile. *J. Fluid Mech.,* **90**, 161-178.

[32] Grimshaw, R.H.J. 1981: Resonant over-reflection of internal gravity waves from a thin shear layer. *J. Fluid Mech.,* **109**, 349-366.

[33] Harnik, N. & Heifetz, E. 2007: Relating Overreflection and Wave Geometry to the Counterpropagating Rossby Wave Perspective: Toward a Deeper Mechanistic Understanding of Shear Instability. *J. Atmos. Sci.*, **64**, 2238-2261.

[34] Holton, J.R. 1972: *An Introduction to Dynamic Meteorology.* Academic Press, New York, 319 pp.

[35] Howard, L.N. 1961: Note on a paper of John W. Miles. *J. Fluid Mech.,* **10**, 509-512.

[36] Hristova, H.G., Pedlosky J. & Spall, M.A. 2008: Radiating instability of a meridional boundary current. *J. Phys. Oceanogr.,* **38**, 2294-2307.

[37] Ivanov, Y.A. & Morozov, Y.G. 1974: Deformation of internal gravity waves by a stream with horizontal velocity shear. *Oceanology,* **14**, 457-461.

[38] Jacobs, G.A., Hurlburt, H.E., Kindle, J.C., Metzger, E.J., Mitchell, J.L., Teague W.J. & Wallcraft, A.J. 1994: Decade-scale trans-Pacific propagation and warming effects of an El Niño anomaly. *Nature,* **370**, 360-363.

[39] Jones, W.L. 1967: Propagation of internal gravity waves in fluids with shear flow and rotation. *J. Fluid Mech.,* **30**, 439-448.

[40] Jones, W.L. 1968: Reflection and stability of waves in stably stratified fluids with shear flow: a numerical study. *J. Fluid Mech.,* **34**, 609-624.

[41] Kamenkovich, I.V. & Pedlosky J. 1996: Radiating Instability of Nonzonal Ocean Currents. *J. Phys. Oceanogr.,* **13**, 972-987.

[42] Kessler, W.S. 1990: Observations of long Rossby waves in the northern tropical Pacific. *J. Geophys. Res.,* **95**, 5183-5217.

[43] Killworth, P.D. & McIntyre, M.E. 1985: Do Rossby-wave critical layers absorb, reflect, or over-reflect? *J. Fluid Mech.,* **161**, 449-492.

[44] Knessl, C. & Keller, J.B. 1995: Stability of linear shear flows in shallow water. *J. Fluid Mech.,* **303**, 203-214.

[45] Kuo, H.L. 1949: Dynamic instability of two-dimensional nondivergent flow in a barotropic atmosphere. *J. Meteor.,* **6**, 105-122.

[46] Kwasniok, F. & Schmitz, G. 2003: Radiating instabilities of internal inertia-gravity waves. *J. Atmos. Sci.,* **60**, 1257-1269.

[47] Lalas, D.P. & Einaudi, F. 1976: On the characteristics of gravity waves generated by atmospheric shear layers, *J. Atmos. Sci.,* **33**, 1248-1259.

[48] Landau, L.D. & Lifshitz, E.M. 1981: *Quantum Mechanics Non-Relativistic Theory*, 3rd Edn., Butterworth-Heinemann.

[49] Le Dizès, S. & Billant, P. 2009: Radiative instability in stratified vortices. *Phys. Fluids,* **21**, 096602 (8 pages).

[50] Le Blond, P.H., & Mysak, L.A. 1978: *Wavesin the Ocean*, Elsevier. 602 pp.

[51] Lee S. 1997: Maintenance of multiple jets in a baroclinic flow *J. Atmos. Sci.*, **54**, 1726-1738.

[52] Lin, C.C. 1955: *The Theory of Hydrodynamic Stability,* Cambridge University Press, 155 pp.

[53] Lindzen, R.S. & Holton J.R. 1968: A theory of the quasi-biennial oscillation. *J. Atmos. Sci.,* **25**, 1095-1107.

[54] Lindzen, R.S. 1974: Stability of a Helmholtz velocity profile in a continuously stratified infinite Boussinesq fluid - applications to a clear air turbulence. *J. Atmos. Sci.,* **31**, 1507-1514.

[55] Lindzen, R.S. & Tung K.K. 1978: Wave over-reflection and shear instability. *J. Atmos. Sci.,* **35**, 1626-1632.

[56] Lindzen, R.S. 1988: Instability of plane parallel shear flow (toward a mechanistic picture of how it works), *Pageoph.,* **126**, 103-121.

[57] Lott, F., Kelder, H. & Teitelbaum H. 1992: A transition from Kelvin-Helmholtz instabilities to propagating wave instabilities. *Phys. of Fluids (A - Fluid Dyn.) ,* **4**, 1990-1997.

[58] Lovegrove, A.F., Read, P.L. & Richards, C.J. 2000: Generation of inertia-gravity waves in a baroclinically unstable fluid. *Quart. J. R. Met. Soc.,* **126**, 2940-2950.

[59] Malanotte-Rizzoli, P., Haidvogel, D.B. & Young, R.E. 1987: Numerical Simulation of Transient Boundary-Forced Radiation. Part I: The Linear Regime. *J. Phys. Oceanogr.,* **17**, 1439-1457.

[60] Maslowe, S.A. 1986: Critical layers in shear flows. *Ann. Rev. Fluid Mech.* **18**, 405-432.

[61] Maslowe S.A. 1991: Barotropic instability of the Bickley jet. *J. Fluid Mech.,* **229**, 417-426.

[62] McIntyre, M.E. & Weissman, M.B. 1978: On radiating instabilities and resonant over-reflection. *J. Atmos. Sci.,* **35**, 1190-1196.

[63] McKenzie, J.F. 1972: Reflection and amplification of acoustic gravity waves at a density and velocity discontinuity. *J. Geophys. Res.,* **77**, 2915-2926.

[64] McPhaden, M.J. & Yu X. 1999: Equatorial waves and the 1997-98 El Nino. *Geophys. Res. Lett.,* **26**, 2961-2964.

[65] Mied, R.P. & Dugan, J.P. 1975: Internal wave reflection by a velocity shear and density anomaly. *J. Phys. Oceanog.,* **5**, 279-287.

[66] Miles, J.W. 1961: On the stability of heterogeneous shear flows. *J. Fluid Mech.,* **10**, 496-508.

[67] Muller, P. 1976: On the diffusion of momentum and mass by internal gravity waves. *J. Fluid Mech.,* **77**, 789-823.

[68] Muller, P. 1977: Spectral features of the energy transfer between internal waves and a larger-scale shear flow. *Dyn. Atmos. Oceans,* **2**, 49-72.

[69] Ollers, M.C., Kamp, L.P.J., Lott F., et al. 2003: Propagation properties of inertia-gravity waves through a barotropic shear layer and application to the Antarctic polar vortex. *Quart. J. Royal Meteorol. Soc.,* **129**, 2495-2511.

[70] Paldor, N. & Ghil, M. 1997: Linear instability of a zonal jet on an f-plane. *J. Phys. Oceanog.,* **27**, 2361-2369.

[71] Pedlosky J. 1987: *Geophysical Fluid Dynamics,* Springer-Verlag New York, 710 pp.

[72] Pedlosky J. 2002: The destabilization of Rossby normal modes by meridional baroclinic shear. *J. Phys. Oceanogr.,* **32**, 2418-2423.

[73] Ripa, P. 1983: General stability conditions for zonal flows in a one-layer model on the β-plane or the sphere. *J. Fluid Mech.,* **126**, 463-489.

[74] Rayleigh, Lord 1883: The form of standing waves on the surface of running water. *Proc. Lond. Math. Soc.* **15**, 69-78.

[75] Romanova, N.N. & Yakushkin, I.G. 1995: Internal gravity waves in the lower atmosphere and sources of their generation (review), (in Russian). *Izv. Akad. Nauk, Fiz. Atmos. Okeana,* **31**, 163-184.

[76] Rosenthal, A.J., Lindzen, R.S. 1958: Instabilities in a stratified fluid having one critical level. Part II: Explanation of gravity wave instabilities using the concept of over-reflection, *J. Atmos. Sci.,* **40**, 521-529.

[77] Satomura, T. 1981: An investigation of shear instability in a shallow water. *J. Met. Soc. Japan,* **59**, 148-167.

[78] Schmitz, W.J., Jr., Holland, W.R. & Price, J.F. 1983: Mid-latitude mesoscale variability. *Rev. of Geophys. and Space Phys.,* **21**, 1109-1119.

[79] Shakina, N.P. 1990: *Hydrodynamical Instability in the Atmosphere,* Gidrometeoizdat, Leningrad, USSR, 309 pp.

[80] Shrira, V.I., Voronovich, V.V. & Kozhelupova N.G. 1997: Explosive Instability of Vorticity Waves. *J. Phys. Oceanogr.*, **27**, 542-554.

[81] Sokolov, S., Rintoul, S.R. 2007: Multiple jets of the Antarctic circumpolar current South of Australia. *J. Phys. Oceanogr.*, **51**, 3261-3280.

[82] Sutherland, B.R., Caulfield, C.P. & Peltier, W.R. 1994: Internal wave generation and hydrodynamic instability. *J. Atmos. Sci.,* **37**, 1394-1412 .

[83] Takehiro, S.-I. & Hayashi, Y.-Y. 1992: Over-reflection and shear instability in a shallow-water model. *J. Fluid Mech.,* **236**, 259-279.

[84] Talley, L.D. 1983: Radiating Barotropic Instability. *J. Phys. Oceanogr.,* 1**3**, 972-987.

[85] Van Duin, C.A. & Kelder, H. 1982: Reflection properties of internal gravity waves incident upon a hyperbolic tangent shear layer. *J. Fluid Mech.*, **120**, 505-521.

[86] Vladimirov, V.S. 1971: *Equations of Mathematical Physics,* New York: Dekker, 418pp.

[87] Viúdez A. & Dritschel D.G. 2006: Spontaneous generation of inertia-gravity wave packets by balanced geophysical flows. *J. Fluid Mech.,* **553**, 107-117.

[88] Williams, P.D., Haine, T.W.N. & Read, P.L. 2008: Inertia-gravity waves emitted from balanced flow: observations, properties, and consequences. *J. Atmos. Sci.,* **65**, 3543-3556.

[89] Yamada, M. & Okamura M. 1984: Over-reflection and over-transmission of Rossby waves. *J. Atmos. Sci.,* **41**, 2531-2535.

[90] Zakharov, V.E. 1974: The Hamiltonian Formalism for waves in nonlinear media having dispersion. *Radiophys. and Quantum Electron.,* **17**, 326-343.

[91] MetEd (by UCAR). Web course on *Introduction to Ocean Currents*. Online at `www.meted.ucar.edu`.

[92] Wikipedia. Entry for *Kuroshio Current*. Online at `upload.wikimedia.org`.

[93] Windows to the Universe (by UCAR). Entry for *Water: The Hydrosphere*. Online at `www.windows2universe.org`.

[94] Visible Earth (by NASA). Entry for *Atmospheric gravity waves and internal waves off Australia*. Online at `visibleearth.nasa.gov`.

[95] Earth Observatory (by NASA). Entry for *Internal Waves in the Indian Ocean*. Online at `earthobservatory.nasa.gov`.

[96] NOCS. Notes on *Circulation of the Atmosphere*. Online at `www.noc.soton.ac.uk`.

[97] Hunter College (CUNY). Notes on *Introduction to Rossby waves*. Online at `www.geography.hunter.cuny.edu`.

[98] RSMAS. *Ocean Surface Currents*. Online at `www.oceancurrents.rsmas.miami.edu`.

[99] OSCAR (by NOAA). *Realtime Ocean Surface Currents Analyses*. Online at `www.oscar.noaa.gov`.

Appendix A

Asymptotic Solution around a Critical Layer

Here we derive asymptotic solutions of Eq. (4.21) around a critical layer $y = y_c$, where by definition $\Omega(y_c) = 0$. So, we develop coefficients of Eq. (4.21) $F(y)$ and $\Omega(y)$ as Taylor series at the vicinity of y_c

$$\Omega(y_c + \eta) = \left(\Omega'\right)^c \eta + O\left(\eta^2\right), \tag{A.1}$$

$$F(y_c + \eta) = F^c + \left(F'\right)^c \eta + O\left(\eta^2\right), \tag{A.2}$$

where superscript $'c'$ denotes that the function is evaluated at y_c and $\eta = y - y_c$.

We apply Frobenius method to get two linearly independent solutions. One smooth solution of Eq. (4.29) can be found in the form

$$\phi_1 = \eta \sum_{n=0}^{\infty} c_n \eta^n, \qquad c_0 = 1 \tag{A.3}$$

Substituting (A.3) into Eq. (4.29) yields an infinite system of linear equations which determines coefficients c_n. In particular,

$$c_1 = \frac{1}{2} \frac{(F')^c}{F^c} \left(\frac{1 - (U')^c}{(U')^c} \right). \tag{A.4}$$

We derive the second linearly independent solution when we apply Liouville's theorem to Eq. (4.21) which states

$$\frac{\mathrm{d}\phi_1}{\mathrm{d}\eta}\phi_2 - \phi_1 \frac{\mathrm{d}\phi_2}{\mathrm{d}\eta} = F^c F^{-1} \tag{A.5}$$

From that we acquire:

$$\phi_2 = -F^c\phi_1 \int F^{-1}\phi_1^{-2} d\eta = \\ = -F^c\phi_1 \int \left((F^c)^{-1} - \left(F'\right)^c \eta + \cdots \right) \eta^{-2} \left(1 + c_1\eta + \cdots\right)^{-2} d\eta = \\ = 1 + \left(\frac{F'}{FU'}\right)^c \left(\eta \ln\eta + \frac{1}{2}\left(1 - \left(U'\right)^c\right)\eta \right) + \mathrm{O}\left(\eta^2 \ln\eta\right) + ..., \quad \text{(A.6)}$$

where all the terms denoted as $'...'$ are proportional to η and are regular; $\zeta(\eta)$ is a smooth function. Thus, while the solution itself is continuous at the critical point its derivative has an essential discontinuity there. Hence, Eq. (A.6) shows that the critical layer singularity give rise to a logarithmic branch point in the solution of Eq. (4.21).

Two asymptotic solutions (A.3) and (A.6) allow to rederive Eq. (4.50) in a more natural way compared to how it was done in §4.2.2. By doing so we verify correctness of formula (4.50) and obtain better understanding of its nature. So, we calculate the value of the jump in momentum flux across the critical layer

$$W_h|_{y_c-0}^{y_c+0} = \mathrm{Im}\left(Fh'h^*\right)\big|_{y_c-0}^{y_c+0} = \frac{\left(F'\right)^c}{\left(U'\right)^c} |G_2|^2 \,\mathrm{Im}\left(\ln\eta\right)|_{-0}^{+0}. \quad \text{(A.7)}$$

In §4.2.2 we discussed that infinitesimal Rayleigh wave dissipation $\omega \to \omega + \mathrm{i}0$ should be introduce to regularise the solutions. Critical layer singularities, defined by equation $\omega + i\alpha - kU = 0$, are shifted off the real axis into complex plane. With no great loss of generality, velocity profile $U(y)$ is assumed to be analytically continued into a small complex strip around real axis. Then, for sufficiently small α when $kU_y(y_c) > 0$ (< 0) the singularities are located in the upper (lower) half-plane. These points converge to the real axis while staying at their half-plane as α becomes small. Hence, the contour along which the solution of inviscid problem (4.21) shall be continued is chosen so that critical layer singularities of the viscous problem do not intersect the contour as α tends to 0. The latter specifies a choice of the logarithmic branch in (A.6). Hence,

$$\mathrm{Im}\left(\ln\eta\right)|_{-0}^{+0} = \mathrm{sign}\left(k\left(U'\right)^c\right)\pi. \quad \text{(A.8)}$$

Finally, substituting (A.8) into (A.7) and keeping in mind the equality $\mathrm{sign}(k) = \mathrm{sign}(U^c)$ we obtain formula (4.50) again

$$W_h|_{y_c-0}^{y_c+0} = \mathrm{sign}\left(U^c\right)\pi \frac{\left(F'\right)^c}{\left|\left(U'\right)^c\right|} |G_2|^2 = \mathrm{sign}\left(U^c\right)\pi \left(\frac{F'}{|U'|}|h|^2\right)\Big|_{y=y_c}. \quad \text{(A.9)}$$

Here we used the fact that $\phi_1(y_c) = 0$ and $\phi_2(y_c) = 1$ and that

$$\left(|h|^2\right)\Big|_{y=y_c} = |G_2|^2 . \tag{A.10}$$

Appendix B

The Unitarity Condition (4.52)

Multiplying (4.44) by h^* (where the asterisk denotes complex conjugate), taking the imaginary part, and integrating along the y-axis we obtain

$$\mathrm{Im}\int\limits_{-\infty}^{\infty}\left(Fh'\right)'h^*\mathrm{d}y+\int\limits_{-\infty}^{\infty}\mathrm{Im}\left(\frac{kF'}{\omega+\mathrm{i}0-kU}-k^2F\right)|h|^2\,\mathrm{d}y=0, \tag{B.1}$$

where F is given as in (4.45). With help of integration by parts and the boundary conditions (4.27), the first term simplifies to

$$\mathrm{Im}\int\limits_{-\infty}^{\infty}\left(Fh'\right)'h^*\mathrm{d}y=\frac{l_+H_+T^2+l_-H_-\left(R^2-1\right)}{\omega^2-1}-\int\limits_{-\infty}^{\infty}\mathrm{Im}\left(F\right)\left|h'\right|^2\mathrm{d}y. \tag{B.2}$$

where $R=|r_{k,l}|$ and $T=|t_{k,l}|$.

Only singular points y_c and y_a can give non-zero contribution to the integrals in (B.1) and (B.2). To evaluate it we shall use the formulae

$$\mathrm{Im}\,\frac{1}{f(y)\pm\mathrm{i}0}=\mp\pi\delta[f(y)]=\mp\pi\sum_n\frac{\delta(y-y_n)}{|f'(y_n)|},$$

$$\int\limits_{-\infty}^{\infty}\delta[f(y)]\,G(y)\,\mathrm{d}y=\sum_n\frac{G(y_n)}{|f'(y_n)|},\qquad\int\limits_{-\infty}^{\infty}\delta'[f(y)]\,G(y)\,\mathrm{d}y=-\sum_n\frac{G'(y_n)}{|f'(y_n)|},$$

where y_n are the roots of the equation $f(y)=0$. Applying the above formulae to the

integrals in (B.1) and (B.2), we obtain

$$\frac{l_+H_+\left|T\right|^2+l_-H_-\left(\left|R\right|^2-1\right)}{\omega^2-1}=\pi k\sum_c\left(\frac{F'\left|h\right|^2}{\left|kU'\right|}\right)^c$$
$$-\pi\sum_a\left[H^a\,\mathrm{sign}\left(\Omega^a\right)\frac{\left(\left|h'\right|^2+\left(\frac{k\left|h\right|^2}{\Omega}\right)'+k^2\left|h\right|^2\right)^a}{\left|A'\right|^a}\right], \quad \text{(B.3)}$$

where indices are also used $'c'$ and $'a'$ to number the critical layers and apparent singularities respectively; Ω and A are as defined in (4.30).

Using all these we show that at y_a

$$\left(\left|h'\right|^2+\left(\frac{k\left|h\right|^2}{\Omega}\right)'+k^2\left|h\right|^2\right)^a = \left(\left|h'\right|^2+\frac{k}{\Omega}\left(\left|h\right|^2\right)'-\frac{k\left(\Omega'\right)}{\left(\Omega\right)^2}\left|h^a\right|^2+k^2\left|h^a\right|^2\right)^a =$$
$$= \left|\left(h'\right)^a\right|^2-p\left(\left(\left|h\right|^2\right)'\right)^a+p^2\left|h^a\right|^2=\left|\left(h'\right)^a-ph^a\right|^2,$$

where we used the definition of p in (4.37) and the definition of the apparent singularity in the form (4.38) The latter is identically zero at y_a as the asymptotics (4.41) and (4.35) of the solution as $y\to y_a$ show. Finally,

$$\left[\left|h'\right|^2+\left(\frac{k\left|h\right|^2}{\omega-lU}\right)'+k^2\left|h\right|^2\right]_{y=y_a}=0.$$

And as a result, the second term on the right-hand side of (B.3) vanishes, and (B.3) reduces to (4.52) as required.

Appendix C

The Numerical Method for Problem (4.21),(4.27)/(4.28)

Without loss of generality we describe the numerical scheme for a scattering problem where the incident waves propagates towards the zonal jet from $y = -\infty$. Integration starts from large positive values of y ($y \to +\infty$) towards $y \to -\infty$ using the boundary condition corresponding to a transmitted wave of unit amplitude

$$h \to \mathrm{e}^{\mathrm{i}l_+ y} \qquad \text{as } y \to +\infty, \tag{C.1}$$

or a decaying wave

$$h \to \mathrm{e}^{-|l_+| y} \qquad \text{as } y \to +\infty, \tag{C.2}$$

instead of the original condition as in (4.27) / (4.28). Then Eq. (4.21) is integrated backwards along the y-axis using a $7-8$ order Runge–Kutta algorithm implemented in Matlab. The step size is automatically reduced to keep the desired accuracy.

In absence of singular points, a sufficiently large negative y can be reached where the solution can be decomposed uniquely into an incident and a reflected wave of amplitudes a and b respectively

$$h \to a\,\mathrm{e}^{\mathrm{i}l_- y} + b\,\mathrm{e}^{-\mathrm{i}l_- y} \qquad \text{as } y \to -\infty. \tag{C.3}$$

Then, using linearity of Eq. (4.21) we normalize the incident wave to unity and find reflection and transmission coefficients as

$$r_{k,l} = \frac{b}{a}, \qquad t_{k,l} = \frac{1}{a}. \tag{C.4}$$

However, Eq. (4.21) supports two types of singularities y_a and y_c. Hence, we need to modify the simple approach described above to account for it. We introduce two modifications based on the regularization discussed in §4.2.2 and in **Appendix A** in order to integrate past the singular points.

The first method introduces a small imaginary component into the wave frequency $\omega \to \omega + \mathrm{i}\varepsilon$, $\varepsilon = 10^{-8}$ which acts as a small linear Rayleigh damping. So, the singularities are shifted off the real axis which enables integration. It can be shown that this approximation for Eq. (4.44) entails error of order $O\left(\sqrt{\varepsilon}\right)$ in the solution $h\left(y\right)$ as well as the scattering coefficients r and t. Further decrease in ε brings the correction term in ω^2 down to the order of the machine epsilon $\left(10^{-16}\right)$ and makes results of the regularization unreliable.

A more accurate modification lies in stepping around singular points in the complex plain. Mathematically it implies analytical continuation of the coefficients and solutions of Eq. (4.21) into the plane of complex y and modifying the integration contour so that it "misses" the singular points. This approach was initially used by Boyd [11] for a Chebyshev collocation method and by Benilov & Sakov [6] for the Runge–Kutta method (as in this work).

One would still have to keep the endpoints fixed, and also make sure that the modified path can be moved back to the real axis without touching any of the critical levels (the apparent singularities are unimportant in this case, as the solution is regular there). This would that the solution would arrive at its final destination with the correct value.

For a given incident wave we resolve equations $A = 0$ and $\Omega = 0$ with respect to y. Typically, four singular points arise for the jets given by (4.55) or similar: two critical levels and two apparent singularities. Then, we construct the integration contour consisting of straight line segments along the y-axis and semicircles of an appropriate radius.

The integration path (Fig. C.1) must satisfy the following requirements:

- Therefore, the semicircles around critical layers y_c are located in in the *upper* half-plane when $kU_y^c < 0$ and in the *lower* half-plane when $kU_y^c > 0$. can only be moved *downwards* and *upwards*, respectively. This guarantees that the modified path can be moved back to the real axis without touching any of the critical levels. Because the term i0 in the equation (4.32) moves critical layer singularities just *above* and just *below* the real axis for for $kU'(y_c) > 0$ and $kU'(y_c) < 0$ respectively.

- The choice of how apparent singularities are stepped around can be *arbitrary* as the solution is regular there (see §4.2.2). We fix semicircles to lie in the upper half-plane.

- The analytical continuation of coefficients of (4.21) can have additional non-physical singularities at complex values of y. We need to make sure that the modified path can be moved back to the real axis without touching them. The Bickley jet (4.55), for example, is singular at

$$y = \tfrac{1}{2}\mathrm{i}\pi W, \;\; \pm\tfrac{3}{2}\mathrm{i}\pi W, \;\; \pm\tfrac{5}{2}\mathrm{i}\pi W ...$$

  Note that these are easily avoided by keeping the path of integration close to the real axis (radius of semicircles $r \sim 10^{-3}$ was used).

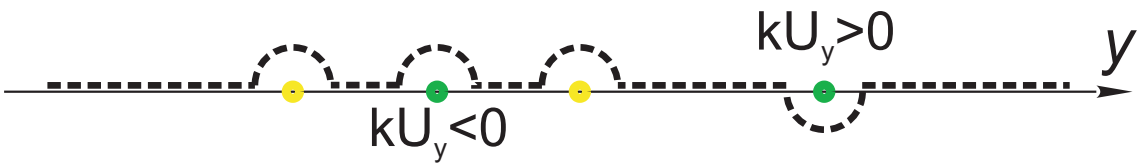

Figure C.1: Typical integration contour. As before, apparent singularities are represented by yellow circles; critical layers by green circles.

Both solvers underwent all usual numerical testing such as change of input parameters, integration limits (as the integration interval $(-\infty; +\infty)$ is replaced with $[-y_{\mathrm{inf}}; y_{\mathrm{inf}}]$), relative and absolute tolerances specified in Runge–Kutta algorithm (and hence, the step of integration), *etc.* Several numerical solutions of the same problem obtained with the two above-mentioned methods were compared and the difference $\mathrm{O}\left(10^{-4}\right)$ is observed. It is consistent with the error estimate for the first method $\left(\sqrt{\varepsilon} = 10^{-4}\right)$. While the second method is exact and the discretization error in Runge–Kutta algorithm was set to be 10^{-8}.

For waves short compared to the meridional scale of the jet ($k^2 \to \infty$), WKB approximation for the solution of Eq. (4.21) can be found far from singular and so-called *turning* points or in their absence (see **Appendix D**). We compared numerical result for short waves ($k \gg 1$ and $\left|c_{ph}^{(x)}\right| > |U|$ so that critical layers are ruled out) with WKB asymptotic solutions and found them to be in good agreement.

Finally, numerical solutions have all the features predicted by the theory described in §4.2. For instance, the solution remains regular around y_a singularities and does not depend on the location of the bypass contour (when the second method is used). The derivative of the solution h' blows up around y_c singularities and Wronskian W_h, which is constant elsewhere, undergoes a jump. If the bypass around critical layers is incorrectly chosen to lie in the wrong complex half-plane then the jump in Wronskian W_h changes

sign.

Therefore, the ability of the numerical methods to integrate the boundary-value problem (4.21) , (4.27) / (4.28) is well tested and the results are reliable. The results obtained using the more accurate complex bypass approach were reported throughout this work.

Appendix D

WKB Solution of Eq. (4.21)

Here we shall derive WKB approximation for two linearly independent solutions of Eq. (4.21) for the case y-scale of the mean flow is much longer than x-wavelength of an incident wave (or equivalently $k \to \infty$). We rewrite Eq. (4.21) in a form explicitly containing small parameter in front of the highest derivative

$$\frac{1}{k^2}\left(\tilde{F}h'\right)' + \left(\frac{\tilde{F}'}{k^2\left(c_{ph}^{(x)} - U\right)} - \tilde{F} + 1\right)h = 0, \tag{D.1}$$

where $\tilde{F} = k^2 F = \frac{H}{\left(c_{ph}^{(x)} - U\right)^2 + \frac{1}{k^2}(U'-1)}$. Making the substitution

$$h(y) = \exp\left(k\left(\sum_{n=0}^{\infty} \frac{1}{k^n} S_n(y)\right)\right) \tag{D.2}$$

Eq. (D.1) yields

$$\tilde{F}\left(\left(\sum_{n=0}^{\infty} \frac{S_n'}{k^n}\right)^2 + \frac{1}{k}\sum_{n=0}^{\infty} \frac{S_n''}{k^n}\right) + \frac{\tilde{F}\prime}{k}\left(\sum_{n=0}^{\infty} \frac{S_n''}{k^n}\right) + \frac{1}{k^2}\frac{\tilde{F}\prime}{\left(c_{ph}^{(x)} - U\right)} + \left(1 - \tilde{F}\right) = 0. \tag{D.3}$$

Developing $\tilde{F}$ and $\tilde{F}'$ as series in $\frac{1}{k^2}$ and assembling equal-order terms we obtain an infinite chain of first-order differential equations for functions $S_n(y)$. We are mostly interested in $S_0(y)$ and $S_1(y)$ because, as usual, the former corresponds to the fast oscillatory motion when the latter represents the leading amplitude term. When those two are known, two

linearly independent solutions of (D.1) are obtained in the form

$$h_{1,2}(y) = \left[\tilde{F}_0\left(1-\tilde{F}_0\right)\right]^{-1/4} \exp\left(\pm \mathrm{i}k \int \sqrt{\frac{1}{\tilde{F}_0} - 1}\mathrm{d}y\right), \tag{D.4}$$

where $\tilde{F}_0$ denotes $\tilde{F}\Big|_{k=\infty} = \frac{H}{(c_{ph}^{(x)}-U)^2}$. This WKB approximation is irrelevant in the vicinity of critical points of Eq. (4.21) as well as near the turning points.

Appendix E

The Scattering Coefficients for a Two-Jet Configuration

Our goal here is to derive global scattering coefficients t and r of the system shown on Fig. 4.10 given the transmission and reflection coefficients $t_{1,2}$ and $r_{1,2}$ of the potentials $P_{1,2}$ (see Eq. (4.67)) and amplification characteristic $\Delta > 0$.

First of all, we investigate how the $\mathrm{i}\,\Delta\,\delta\,(x)\,\psi$ term alter free wave solution $\left[x_1^+; x_2^-\right]$ between the potentials. Suppose

$$\begin{aligned} \Psi &= A\,\mathrm{e}^{\mathrm{i}kx} + B\,\mathrm{e}^{-\mathrm{i}kx} \qquad \text{if } x_1^+ < x < 0, \\ \Psi &= C\,\mathrm{e}^{\mathrm{i}kx} + D\,\mathrm{e}^{-\mathrm{i}kx} \qquad \text{if } 0 < x < x_2^-, \end{aligned} \tag{E.1}$$

where A, B, C and D are undetermined constants. Integrating Eq. (4.64) from $-\varepsilon$ to $+\varepsilon$ and taking the limit $\varepsilon \to 0$ yields

$$\Psi\,(+0) = \Psi\,(-0)\,, \qquad \Psi'\,(+0) - \Psi'\,(-0) = \mathrm{i}\,\Delta\,\Psi\,(0)\,.$$

With help of (E.2) coefficients A and B can be found in terms of C and D

$$\begin{aligned} A &= \tfrac{\Delta}{2k} D + \left(1 + \tfrac{\Delta}{2k}\right) C, \\ B &= -\tfrac{\Delta}{2k} C + \left(1 - \tfrac{\Delta}{2k}\right) D. \end{aligned} \tag{E.2}$$

Lets construct the incident and reflected waves that correspond to the transmitted

wave $t_2\,\mathrm{e}^{\mathrm{i}kx}$. Potential P_2 works in agreement with

$$\begin{aligned} \Psi &= t_2\,\mathrm{e}^{\mathrm{i}kx} && \text{if} \quad x > x_2^+, \\ \Psi &= \mathrm{e}^{\mathrm{i}kx} + r_2\,\mathrm{e}^{-\mathrm{i}kx} && \text{if} \quad 0 < x < x_2^-, \end{aligned} \tag{E.3}$$

Then, with help of (E.1), (E.2) for a solution satisfying (E.3) one can find the solution left of the amplifier

$$\Psi = (1+\Delta')\,\mathrm{e}^{\mathrm{i}kx} + (r_2 - \Delta')\,\mathrm{e}^{-\mathrm{i}kx} \quad \text{if} \quad x_1^+ < x < 0, \tag{E.4}$$

where notation $\Delta' = \frac{\Delta}{2k}\,(1+r_2)$ was introduced.

We shall find the solution of the scattering problem with $P_1\,(y)$ which give rise to (E.4) in the region $x_1^+ < x < 0$. Using linearity of Eq. (4.64) and reality of its coefficients (which implies that Ψ^* is a solution as long as Ψ is) we deduce two auxiliary solutions

$$\begin{aligned} \Psi &= (1+\Delta')\,\mathrm{e}^{\mathrm{i}kx} && \text{if} \quad x_1^+ < x < 0, \\ \Psi &= \tfrac{1}{t_1}\,(1+\Delta')\,\mathrm{e}^{\mathrm{i}kx} + \tfrac{r_1}{t_1}\,(1+\Delta')\,\mathrm{e}^{-\mathrm{i}kx} && \text{if} \quad x < x_1^-, \end{aligned} \tag{E.5}$$

$$\begin{aligned} \Psi &= (r_2 - \Delta')\,\mathrm{e}^{-\mathrm{i}kx} && \text{if} \quad x_1^+ < x < 0, \\ \Psi &= \tfrac{r_1^*}{t_1^*}\,(r_2 - \Delta')\,\mathrm{e}^{\mathrm{i}kx} + \tfrac{1}{t_1^*}\,(r_2 - \Delta')\,\mathrm{e}^{-\mathrm{i}kx} && \text{if} \quad x < x_1^-. \end{aligned} \tag{E.6}$$

Their sum provides the matched solution

$$\begin{aligned} \Psi &= I\,\mathrm{e}^{\mathrm{i}kx} + H\,\mathrm{e}^{-\mathrm{i}kx} && \text{if} \quad x < x_1^-, \\ \Psi &= t_2\,\mathrm{e}^{\mathrm{i}kx} && \text{if} \quad x > x_2^+, \end{aligned} \tag{E.7}$$

where

$$\begin{aligned} I &= \tfrac{1}{t_1}\,(1+\Delta') + \tfrac{r_1^*}{t_1^*}\,(r_2 - \Delta'), \\ H &= \tfrac{1}{t_1^*}\,(r_2 - \Delta') + \tfrac{r_1}{t_1}\,(1+\Delta'). \end{aligned} \tag{E.8}$$

Therefore, the requirement that the media spontaneously radiates waves $I = 0$ is equivalent to

$$(t_1^* + r_1^* t_1 r_2) + \Delta'\,(1+r_2)\,(t_1^* - r_1^* t_1) = 0. \tag{E.9}$$

The amplifying/absorbing represented by term $\mathrm{i}\,\Delta\,\delta\,(x)\,\psi$ in Eq. (4.64) can be "built into" the potentials $P_{1,2}$. Then no incident wave condition (E.9) simplifies to

$$t_1^* + t_1 r_1^* r_2 = 0. \tag{E.10}$$

Also, the global scattering coefficients can be obtained in a simple form

$$r = \frac{t_1^* r_1 + t_1 r_2}{t_1^* + t_1 r_1^* r_2}, \qquad t = \frac{|t_1|^2 t_2}{(t_1^* + t_1 r_1^* r_2)} \tag{E.11}$$

Note that similar calculations can be done when we use "from-right-to-left" coefficients r_1', t_1', for the first barrier P_1 (see (4.70)) instead of the standard "left-to-right" ones r_1, t_1. In this case no incident wave condition (E.10) transforms into

$$r_1' r_2 = 1, \tag{E.12}$$

and the global scattering coefficients are

$$r = \frac{t_1' \left(r_2 - (r_1')^*\right)}{(t_1')^* \left(1 - r_1' r_2\right)}, \qquad t = \frac{t_2 \left(1 - |r_1'|^2\right)}{(t_1')^* \left(1 - r_1' r_2\right)}. \tag{E.13}$$